Novel kinases play an essential role during asexual proliferation of *Plasmodium falciparum* parasites
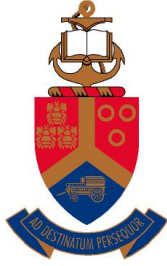
by

Henrico Langeveld

Submitted in partial fulfilment of the requirements for the degree

Magister Scientiae
(Specialisation in Biochemistry)

Faculty of Natural and Agricultural Sciences
Department of Biochemistry, Genetics and Microbiology
University of Pretoria
South Africa

SUBMISSION DECLARATION

I, Henrico Langeveld, declare that the dissertation, which I hereby submit for the degree *Magister Scientiae* in the Department of Biochemistry, Genetics and Microbiology at the University of Pretoria, is my own work and has not previously been submitted by me for a degree at this or any other tertiary institution.

SIGNATURE: _____

DATE: ____08 / 02 / 2022_____
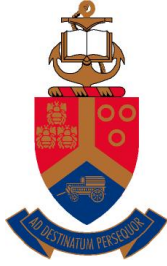
UNIVERSITEIT VAN PRETORIA
UNIVERSITY OF PRETORIA
YUNIBESITHI YA PRETORIA

<u>DECLARATION OF ORIGINALITY</u>

University of Pretoria
Faculty of Natural and Agricultural Sciences
Department of Biochemistry, Genetics and Microbiology
Division of Biochemistry

Full names of student: Henrico Langeveld

Student number: 16253622

Declaration:

1. I understand what plagiarism is and am aware of the University's policy in this regard.
2. I declare that this dissertation is my own original work. Where other people's work has been used (either from a printed source, Internet, or any other source), this has been properly acknowledged and referenced in accordance with departmental requirements.
3. I have not used work previously produced by another student or any other person to hand in as my own.
4. I have not allowed and will not allow anyone to copy my work with the intention of passing it off as his or her own work.

SIGNATURE: _____

DATE: _08 /02 /2022_____

Acknowledgements

I would just like to express my gratitude to all my friends and family for their support and input throughout this amazing MSc degree journey.

Specifically, I want to thank my parents, Hennie, and Lizette Langeveld for always being ready and eager to sit and listen to me express my passion for science, and I would like to thank them for teaching me to always keep moving forward even if some days and some experiments seem like train smash, there is always light at the end of the tunnel.

Then I would also like to show my appreciation to my close friends and lab partners, Daniel Opperman and Shante da Rocha. Thanks for all the insightful "science" discussion we had during lunch times and for all the advice and input when science was being science.

Then to all the members from the M^2PL laboratory, thank you for all the advice and help during my project. I could not have asked for a better group of talented and experienced scientists to learn from.

Finally, I would like to show my utmost appreciation to my supervisor and mentor Prof. Lyn-Marié Birkholtz. I am incredibly thankful for all the remarkable guidance and advice during my project, she has truly helped me become a better more well-rounded scientist. Thanks for believing in me and providing me with amazing opportunities, I could not have asked for a better mentor during this time. She is truly and inspiration and a science role model I look up too, thanks Prof.

"Without the love of research, mere knowledge and intelligence cannot make a scientist."
Irène Joliot-Curie

Summary

Novel antimalarial drug targets, and drugs and that target the causative agents for malaria in humans, *Plasmodium falciparum* parasites, are constantly needed due to the emergence of drug-resistant malaria parasite strains. Within unexplored biological avenues of the parasite, unique and essential proteins can be identified and studied as potential drug targets. One of these processes is the unique and atypical cell cycle of the *P. falciparum* parasite and the largely unexplored regulatory mechanisms and essential role players governing these mechanisms. Three genes (*pf3d7_0105800, pf3d7_1112100* and *pf3d7_1364400*), encoding uncharacterised protein kinases with unknown functions within the parasite, were identified from transcriptome analyses of the switch between states of cell cycle arrest to cell cycle re-entry. This study aimed to functionally validate the essential nature of these putative kinases within the parasite life cycle through genetic manipulation, exposing potential novel targets in the kinase drug target space.

The essentiality of the putative kinases was determined by successfully cloning the 5'-gene-encoding fragments of each gene, namely *pf3d7_0105800*, *pf3d7_1112100* and *pf3d7_1364400*, into a specialised targeted gene disruption system. This generated truncated versions of each protein, with only ~140–282 N-terminal residues remaining. These gene disruptions resulted in each of the three investigated putative kinase proteins (PF3D7_0105800, PF3D7_1112100 and PF3D7_1364400) indicated as having essential functions during parasite asexual proliferation, as parasites were not able to survive without the full, intact proteins. To gain more in-depth understanding of the function of the selected putative kinase proteins, alternative inducible systems were subsequently evaluated. The 3'-fragment of each gene was successfully cloned to allow displacement of the proteins from their site of action (knock sideways). The data from these inducible systems indicated that two of the kinases (PF3D7_0105800 and PF3D7_1112100) were found to localise to the cytoplasm of asexual parasites, but that insufficient displacement occurred to infer functionality with the knock sideways system. Parasites utilising an alternative system, gene knockdown (*glmS* ribozyme), were therefore also generated for future exploration.

Collectively, novel putative antimalarial drug targets were described that are essential to the cell cycle regulation of *P. falciparum* parasites. This expands our knowledge of the unique kinome of *P. falciparum* parasites and reveals new potential role players in the parasite's atypical cell cycle.

Table of contents

List of figures

List of tables

Abbreviations

ACT	Artemisinin-based combination therapies
AdoMetDC	*S*-adenosylmethionine decarboxylase
AGC	cAMP-dependent, cGMP-dependent and protein kinase C
ARK	Aurora-related kinase
Amp	Ampicillin
ApiAP2	*Apicomplexan* APETALA2 domain protein
ART	ATM and Rad 3-related
ATc	Anhydrotetracycline
ATM	Ataxia-telangiectasia mutated
BSD	Blasticidin S deaminase protein
BUB	Budding uninhibited by benzimidazole
CAK	CDK-activating kinase
CaMK	Calcium/calmodulin-dependent kinases
CDK	Cyclin-dependent kinase
CDPK	Calcium-dependant protein kinase
Chk	Checkpoint kinase
CK	Casein kinase
CKI	CDK inhibitor
CKS	Cyclin-dependent regulatory subunit
CLK	Cyclin-dependent-like kinases
CRK	Cyclin-related kinases
DFMO	α-Difluoromethylornithine
DIC	Differential interference contrast
E2F	Transcription factor 2
ePK	Eukaryotic protein kinase
FIKK	Phenylalanine-Isoleucine-Lysine-Lysine motif
FKBP	FK506 binding protein 12
FRB	FKBP12-rapamycin-binding
gDNA	Genomic DNA
GFP	Green fluorescent protein
GlcN	Glucosamine
glmS	Glucosamine-6-phosphate riboswitch ribozyme
GSK	Glycogen synthase kinase
hDHFR	Human dihydrofolate reductase
HEPES	4-(2-hydroxyethyl)-1-piperazineethanesulfonic acid
hpi	Hours post invasion
IDC	Intraerythrocytic development cycle
IRS	Indoor residual spraying
LLINs	Long-lasting insecticide-treated nets
MAD	Mitotic arrest-deficient
MAPKs	Mitogen-activated protein kinases
MCC	Mitotic checkpoint complex
MMV	Medicines for Malaria Venture
Neo-R	Neomycin resistance marker

NIMA/Nek	Never-in-mitosis A
PBS	Phosphate buffered saline
PBS-T	1x Iso-PBS with 0.1 % (v/v) Tween-20
PCR	Polymerase chain reaction
PK	Protein kinase
R-point	Restriction point
Rb	Retinoblastoma proteins
SLI	Selection-linked integration
SPB	Spindle pole body
TCP	Target candidate profiles
TGD	Targeted gene disruption
TK	Tyrosine kinase
TKL	Tyrosine kinase-like
TPP	Target product profiles
WHO	World Health Organisation

Chapter 1: Literature review

1.1. Malaria; a disease burden

Malaria is one of the most devastating parasitic diseases, which has an economic and socio-economic impact on various countries worldwide. The most severely impacted countries are found in sub-Saharan Africa, parts of Asia, Central and South America (Figure 1-1). According to the World Health Organisation (WHO), malaria resulted in 229 million cases worldwide in 2019. Of the 87 countries that were malaria endemic in 2019, 29, mainly located within the WHO African region, accounted for 95 % of malaria cases globally with Nigeria (27 %), the Democratic Republic of the Congo (12 %), Uganda (5 %), Mozambique (4 %) and Niger (3 %) accounting for approximately 51 % of all cases globally [9].
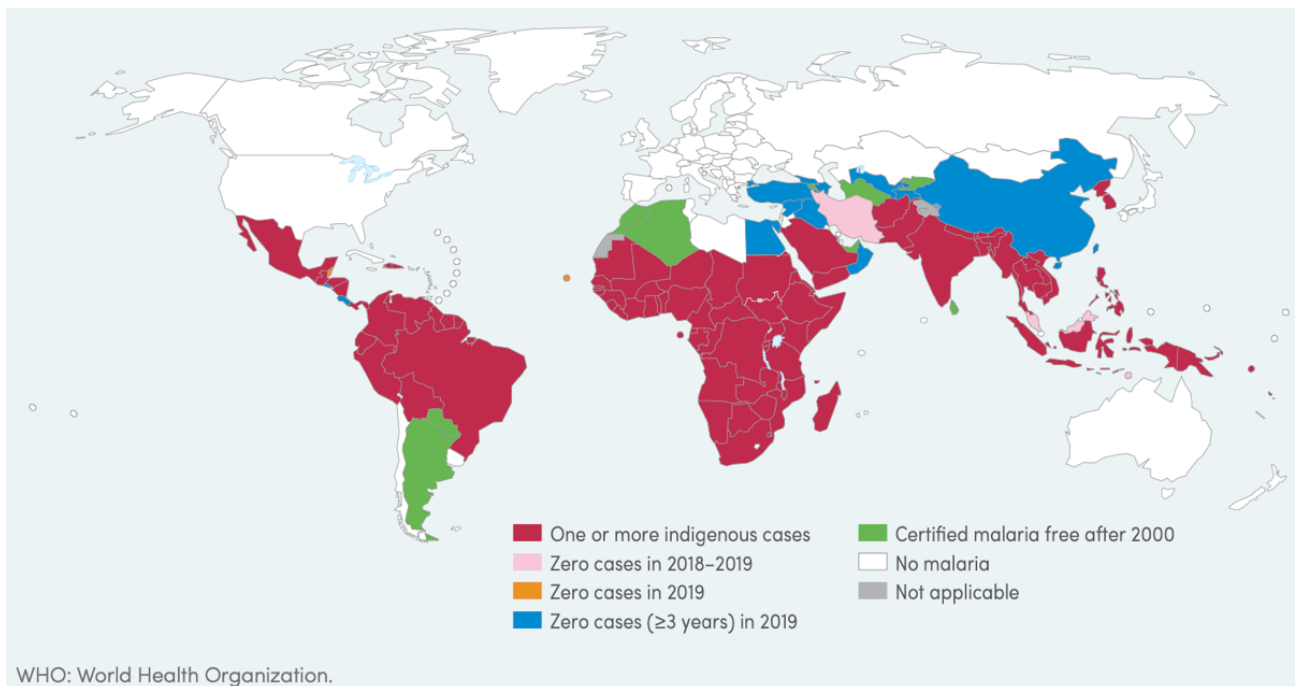
Figure 1–1: Global overview of malaria incidence. Geographical distribution of malaria incidence with indigenous cases in 2000 and their status by 2019. Countries that have had zero indigenous cases for the past three consecutive years are considered malaria free. China and El Salvador reported zero indigenous cases for the second consecutive year, while Iran, Malaysia and Timor-Leste reported zero indigenous cases for the first time in 2019. Image adapted from the WHO malaria report 2020 [9].

There has been a global decline in malaria mortality rate, with an estimated death toll of ~409 000 in 2019 compared to ~594 000 in 2010 [9]. Most deaths were localised to the 32 countries in the WHO African Region and India. In Africa, 51 % of those deaths were distributed between six countries; Nigeria (23 %), the Democratic Republic of the Congo (11 %), the United Republic of Tanzania (5 %), Burkina Faso (4 %), Mozambique (4 %) and Niger (4 %) and children under the age of five years still contribute ~274 000 (67 %) of all malaria related deaths [9]. It is therefore evident that developing countries bear the brunt of the disease burden and the impact of malaria poses a substantial additive strain on the already struggling health care systems of these countries.

Malaria can be divided into asymptomatic, uncomplicated, or severe (complicated) disease courses, based on the severity. The disease outcome depends on multiple environmental factors and human host factors, as well as the *Plasmodium* species involved. The first noticeable symptoms of malaria are non-specific, and include headache, fever, chills, nausea and vomiting, but the characteristic factor is that these symptoms present in a 36-72 h cycle [10, 11]. Early diagnosis is key in controlling the disease outcome, especially cerebral malaria, severe anaemia and acute renal failure, which may lead to death if left untreated [11].

Parasites of the *Plasmodium* genus are responsible for causing malaria and are transmitted to humans by the female *Anopheles* mosquito. There are numerous species of *Anopheles* mosquito, which act as vectors for *Plasmodium* parasites. [12]. Five species of *Plasmodium* infect humans: *Plasmodium falciparum*, *Plasmodium ovale*, *Plasmodium malariae*, *Plasmodium vivax*, and *Plasmodium knowlesi* [13]. *P. falciparum* is the most serious of all malaria-causing *Plasmodium* species, causing most malaria-related deaths and contributing more than 65 % of malaria cases.

1.2. *P. falciparum* life cycle

Each of the different *Plasmodium* species that infect humans have complex and diverse life cycles. The life cycle of *P. falciparum* consists of a asexual stages that occur within the human host and sexual stages that occur across the human host and female *Anopheles* mosquito [13] (Figure 1-2). Once a female *Anopheles* mosquito feeds on the blood of a human host, hundreds of sporozoites are released into the bloodstream of the human host (Figure 1-2A). Once in the blood stream the sporozoites migrate to the liver and infect hepatocytes. Within the hepatocytes the sporozoites undergo exo-erythrocytic schizogony (Figure 1-2B), where asexual replication occurs over 6-16 days, producing thousands of haploid hepatic merozoites (1N) which, upon rupture of the hepatic schizont, are released in parasite-filled vesicles called merosomes [12, 14, 15] (Figure 1-2C). The asexual intra-erythrocytic development cycle (IDC, Figure 1-2D) is established once a merozoite successfully invades a host erythrocyte.

During the asexual IDC, a single merozoite, enclosed within a parasitophorous vacuole separating the merozoite from the erythrocyte cytoplasm, develops into a morphologically characterised ring-stage parasite within ~6 hours after erythrocyte invasion [16] (Figure 1-2D). The ring-stage parasite subsequently develops into a highly metabolically active trophozoite stage. This is the period during the asexual IDC where cellular growth and erythrocyte modification occurs, as well as the formation of new permeability pathways [17]. These new pathways allow for substrate uptake from the surrounding nutrient-rich medium and the efflux of metabolic waste products [16-18]. Haemoglobin found within the erythrocyte is broken down into various amino acids (except for isoleucine) through proteolysis in an acidic digestive vacuole, which are utilised in protein synthesis, as the parasite has limited capacity for de novo amino acid synthesis [18, 19]. During the proteolysis of haemoglobin the haem complex, which is toxic to the parasite, is released and, through polymerization of the free haem into a haemozoin

crystal, is detoxified, resulting in pigmentation of trophozoite-stage parasites [15, 18]. Approximately 33–36 hours post-invasion (hpi), the trophozoite parasite transitions to a schizont stage, where the parasite undergoes a series of nuclear divisions in a process known as schizogony. During early schizogony, 4–6 rounds of asynchronous and endomitotic cell division cycles results in a polynucleated (>4N) schizont, followed by a final round of karyokinesis occurring synchronously and simultaneously with cytokinesis, resulting in the formation of 16–32 haploid nuclei (1N) [17, 20]. Finally schizogony is concluded with segmentation of the nuclei and formation of structural inner membrane complexes and plasma membranes around each daughter merozoite [20]. Upon rupture of the parasitophorous vacuolar membrane and then the erythrocyte plasma membrane, the merozoites are released to infect other erythrocytes. It is this cyclical, coordinated rupturing of the erythrocytes that causes malaria symptoms [21] (Figure 1-2).
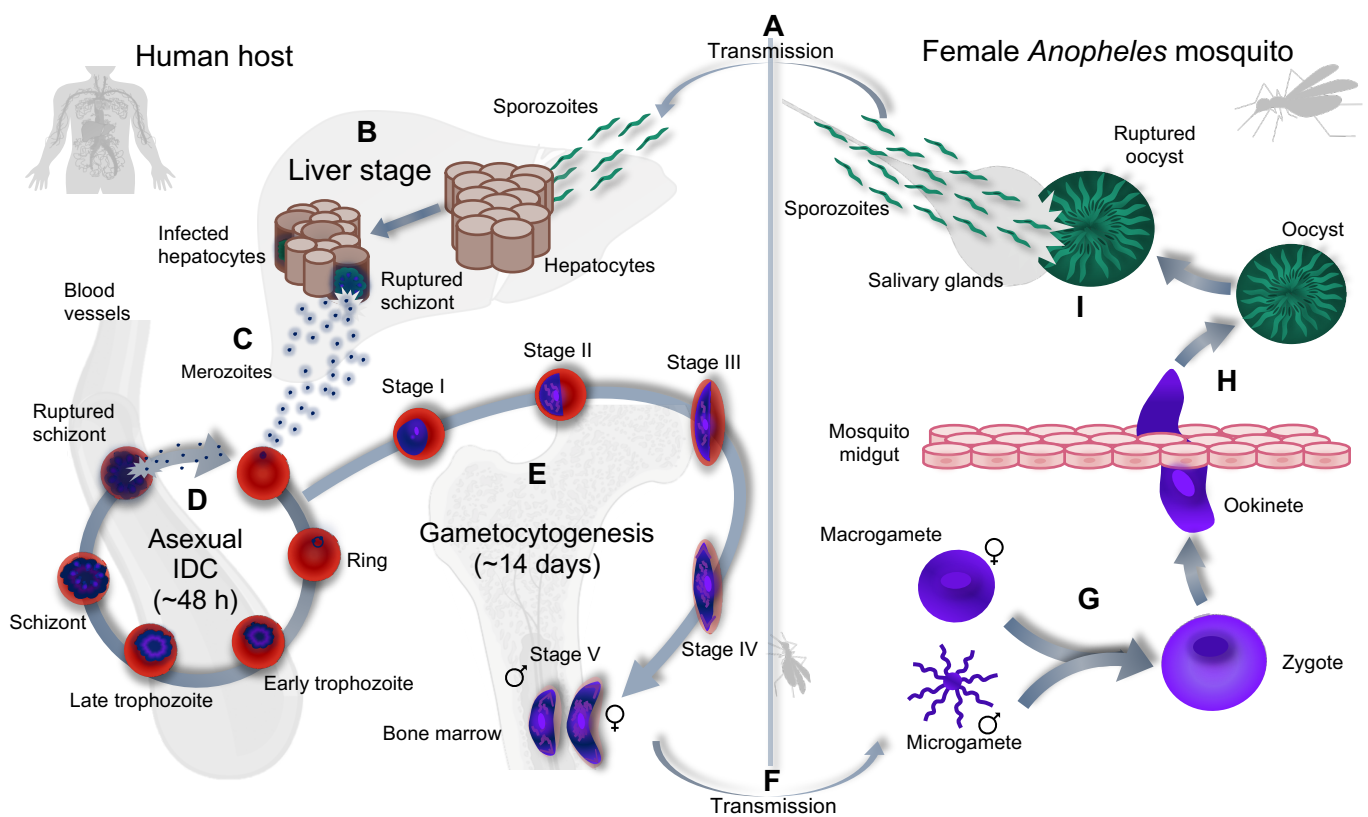
Figure 1–2: The life cycle of the *P. falciparum* parasite. **(A)** The parasite life cycle begins when an infected female *Anopheles* mosquito transmits sporozoites to a human host when feeding on the human's blood. **(B)** Sporozoites enter the bloodstream and infect healthy hepatocytes, replicating asexually within these cells. **(C)** A schizont is formed by multiple rounds of asexual replication and, upon rupturing, releases multiple merozoites back into the bloodstream which themselves infect healthy erythrocytes. **(D)** The merozoites sequentially differentiate into different morphological stages accompanied by multiple rounds of asexual replication to produce more merozoites. **(E)** A portion of the merozoites released differentiate into male or female gametocytes through a process called gametocytogenesis. **(F)** The mature stage V gametocytes are taken up by a female mosquito feeding on the infected human's blood. **(G)** The stage V gametocytes differentiate into gametes which fuse to form a zygote. This zygote matures into an ookinete. **(H)** The ookinete moves across the midgut where it forms an oocyst containing multiple sporozoites. **(I)** Once the oocyst ruptures, sporozoites are released and migrate to the salivary glands of the mosquito.

From each completed asexual IDC, a proportion (<10 %) of the asexual parasites diverge and differentiate into sexual stage gametocytes, a process known as gametocytogenesis [21]. During

gametocytogenesis (Figure 1-2E), parasite development occurs over five distinct morphological stages (I-V) a developmental characteristic unique to *P. falciparum* sexual-stage parasites (Figure 1-2E). Similarly to asexual parasites, early-stage gametocytes (stage I–III) degrade haemoglobin and form hemozoin deposits within individual digestive vacuoles structures but, in contrast to asexual IDC parasites, early-stage gametocytes do not undergo any DNA replication or nuclear division, hence the gametocytes remain haploid (1N) throughout gametocytogenesis [22]. The transition from a stage I gametocyte to stage II is marked by the formation of the inner membrane complex and a dense network of microtubules underneath the parasite plasma membrane, initiating the morphological changes to the gametocyte [22]. By stage III, the gametocytes adopt a "D" shape where the parasite has an average length that is twice its width, and elongation continues to occur until stage IV, where the parasites reach a maximum length leading to the unique falciform shape [22, 23]. Stage I–IV gametocytes sequester within the host bone marrow and spleen and do not circulate in the bloodstream. After ~10–12 days of development, mature male and female transmissible stage V gametocytes are released back into the bloodstream due to a decrease in membrane rigidity, and subsequently migrate towards the skin capillaries [24].

When an uninfected female *Anopheles* mosquito ingests mature male and female gametocytes (Figure 1-2F), the mature gametocytes sense a change in the microenvironment (pH, temperature, and exposure to xanthurenic acid) in the mosquito midgut. This triggers differentiation into male (micro-) and female (macro-) gametes. The male gametocyte undergoes three rounds of DNA replication within 15–20 min to produce eight mature flagellated microgametes This process is one of the fastest known DNA-replication events [3, 24]. Single haploid micro- and macrogametes fuse within the midgut lumen to form a haploid (2N) zygote (Figure 1-2G), which matures into a motile ookinete. The ookinete migrates through the midgut lining and develops into an oocyst (Figure 1-2H). The oocyst undergoes multiple rounds of nuclear division to produce thousands of haploid sporozoites that are released and migrate to the salivary glands of the mosquito (Figure 1-2I), whereupon the entire cycle starts again [24, 25].

The parasite has a complex life cycle with multiple developmental stages during the cycle, each of which may be targeted by existing treatments, or by compounds that are in the developmental process.

1.3. Malaria control and treatment

Due to the adverse effects of malaria on public health and economic growth, particularly in African countries, various control strategies are used to control different aspects of the disease, including vector control and parasite-specific strategies. Vector control strategies are aimed at decreasing the number of *Anopheles* mosquitos that can transmit the parasite, thus disrupting the transmission of parasites between humans and mosquitoes. Use of long-lasting insecticide-treated nets (LLINs) and indoor residual spray (IRS) with insecticides like dichlorodiphenyltrichloroethane and pyrethroid-based

compounds resulted in a significant improvement in the control of mosquitoes and a decrease in malaria transmission [9]. The use of IRS has been one of the most effective means of vector control, causing a decrease in the mosquito population [26]. LLINs prevent transmission of the parasite to humans by placing a physical barrier between the infected female *Anopheles* mosquito and the human [26]. Unfortunately, the effectiveness of insecticide-based vector control strategies is threatened due to insecticide-resistant *Anopheles* mosquito strains [27].

The development of a vaccine-based strategy against malaria has been attempted, without any high efficacy observed beyond a ~30–40 % protection in children under the age of 5 years [28]. Chemoprophylactic and chemotherapeutic compounds are the primary tools used to prevent parasite-infection and decrease parasitaemia, thereby relieving a patient of malaria symptoms [9]. The most effective treatments against all malaria-causing *Plasmodium* species in current use are artemisinin-based combination therapies (ACTs) [29]. However, parasites resistance to ACTs, that was first identified on the Thai-Cambodia border region [30, 31], have now been shown to be present in multiple different African countries, threatening the sustained use of these frontline antimalarials [32-36]. This situation is concerning and stresses the need for the discovery of new antimalarial drugs against *P. falciparum* parasites [37].

For new antimalarial drugs to be effective in the fight against the disease, these will have to target multiple stages of the parasite life cycle to not only treat and cure a patient of malaria symptoms, but additionally prevent transmission of the parasite. The Medicines for Malaria Venture (MMV), whose main goal is to develop and distribute affordable antimalarial drugs across the world, have created criteria for target candidate profiles (TCPs), and target product profiles (TPPs), where each TPP addresses multiple biological activities. This would require antimalarial drugs to be dual-active against the asexual blood stage parasites (TCP-1) for elimination of symptom-causing asexual stages and against gametocytes (TCP-5) and vector stages (TCP-6) for transmission-blocking activity. Novel drug targets, playing a crucial role during various stages of the parasite life cycle, first need to be identified to be able to develop novel and dual-active antimalarial drugs. To identify such drug targets, the unique biological pathways associated with parasite development need to be explored. It is evident that *P. falciparum* parasites vary the rate at which they progress through each life cycle stage, which points to the complexity and flexibility of the mechanisms that govern these processes.

1.4. Mammalian cell cycle model

For mammalian cells to successfully replicate and produce daughter cells, the cell cycle, divided in to four distinct phases, need to be completed successfully (Figure 1-3) [38]. The mammalian cell cycle starts with the interphase, which accounts for the largest part of the cell cycle and is divided into different sub-phases, namely the gap 1 (G_1), synthesis (S), and gap 2 (G_2) phases [38]. During the early stage of the G_1 phase, the cell is mitogen dependent and growth factors are required for the cell to progresses

further into the cell cycle. The cell begins to increase in size and synthesise mRNA and proteins required for commencement of the S phase, where DNA replication occurs [38, 39]. After DNA replication has been completed, the cell enters a relatively short G2 phase where the cell further increases in size and produces organelles and proteins required for the mitotic (M) phase. The M phase is separated into four different stages; prophase, metaphase, anaphase and telophase [38]. During prophase, metaphase, and anaphase, the chromosomes condense, mitotic spindle bodies form, and sister chromatids divide to form two daughter nuclei. During telophase, the cell divides into two identical daughter cells with uncondensed daughter nuclei, followed by nuclear envelope reconstruction together with cytokinesis. The progression from one cell cycle phase to the next is tightly regulated by multiple surveillance pathways which ensure correct and adequate copies of genetic material are passed on to the daughter cells.

In mammalian cells, these surveillance pathways are referred to as cell cycle checkpoints. There are four well-defined cell cycle checkpoints situated throughout the cell cycle (Figure 1-3). The mechanisms coordinating and regulating the transition through these checkpoints are coordinated by the interplay of various proteins, with kinase proteins playing a central role. Amongst the various kinases are a specific class of serine/threonine kinases called cyclin-dependent kinase proteins (CDKs), which are the master regulators of the cell cycle. Depending on the availability and active status of a specific CDK, the cell will be able to pass through a specific checkpoint. CDKs are only able to perform their regulatory functions within the cascade once activated by a cyclin protein, so named due to cyclic expression throughout the cell cycle [40]. Cyclins (cyc) bind to and phosphorylate a target residue of the specific CDK partner, in turn allowing these CDKs to regulate the activities of multiple other proteins involved in phosphorylation-dependent cascades [40-42].

The first checkpoint within the cell is the restriction point (R checkpoint) or G_1 checkpoint, during which the cell growth phase is controlled (cells must have reached a specific cell size) and the availability of a nutrient-rich favourable environment is evaluated. If favourable, a mitogen-dependent cascade of events is triggered, which leads to the expression of CDK4/6 and CycD (Figure 1-3). This checkpoint is very well characterised in yeast and is referred to as START [43]. The R-point is also the point at which a cell exits the cell cycle into a quiescent (G_0) state if conditions are not favourable. Activation of CDK4/6 by CycD promotes cell cycle progression past the R-point through phosphorylation, and thereby inactivation of Rb proteins (so called due to their first discovery in retinoblastoma). This prevents Rb from inhibiting eukaryotic transcription factor 2 (E2F), a transcription factor family responsible for transcription of multiple genes required for the S phase [41, 44]. After the R-point has been passed, the cell will fully commit to cell cycle progression, even in the absence of growth factors, entering a mitogen-independent stage of the cell cycle. The second checkpoint is the G_1/S checkpoint, which occurs just before the cell enters the S phase. Before the cell progresses through this checkpoint, DNA integrity is evaluated by specialised kinase proteins known as ATM (ataxia-telangiectasia mutated) and ART (ATM and Rad 3-related) (Figure 1-3) [45].

6
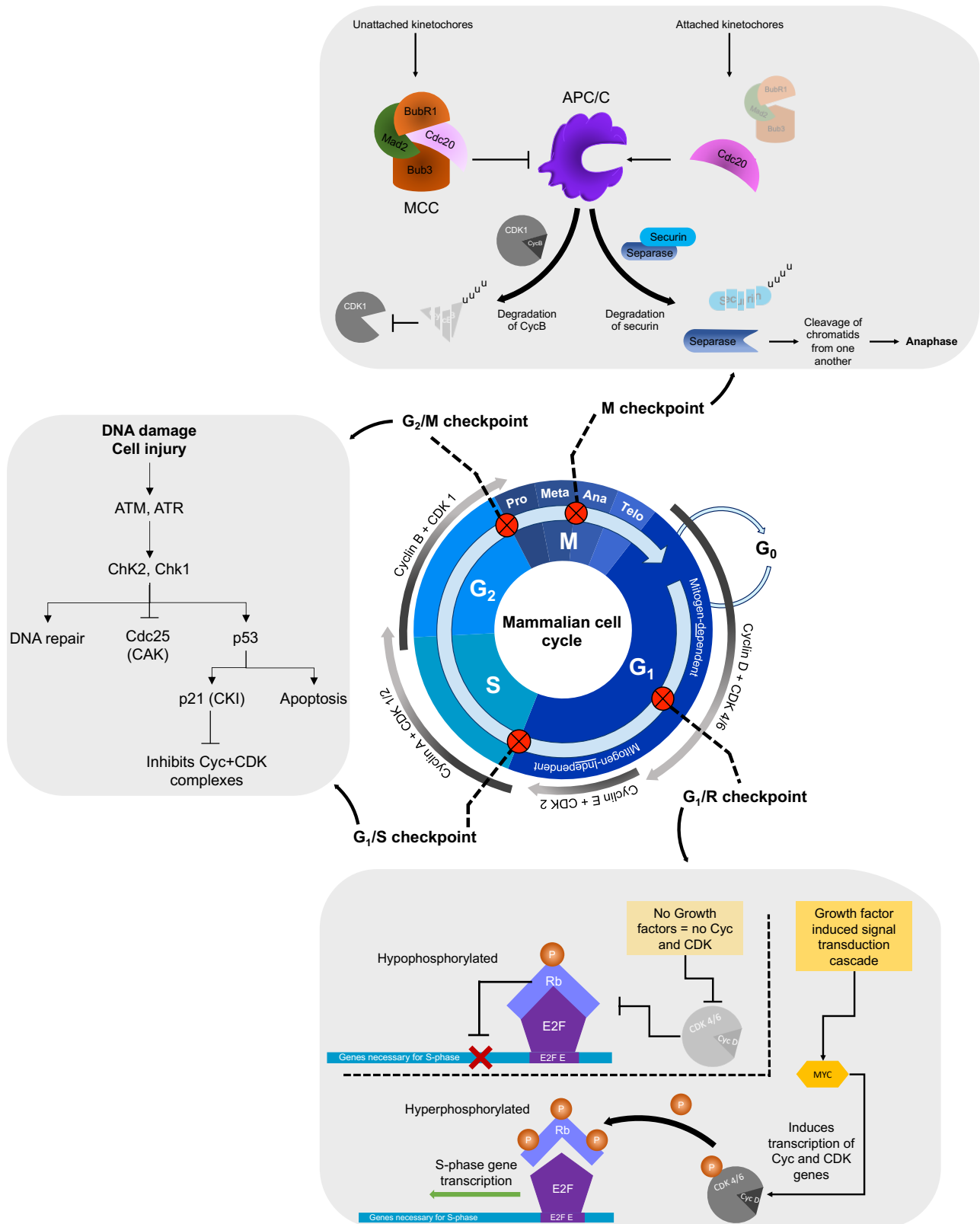
Figure 1–3: Schematic representation of a mammalian cell cycle and the regulatory mechanisms at different checkpoints. The canonical mammalian cell cycle model consists of four cell cycle phases, starting with the G_1 phase, progressing through the S and G_2 phases and ultimately reaching the M phase, which is divided into a further four subphases. The progression from one cell cycle phase to the next is regulated by cell cycle checkpoints (⊗). Specialised cascades of various proteins govern these checkpoints, of which cyclins and CDKs are the master regulators. At the first checkpoint (G_1/R), CDK4/6 and cyclin D transcription is induced in the presence of growth factors. CDK4/6 and cyclin D then activate downstream cascades required to enter the S phase. During the second and third checkpoint, G_1/S and G_2/M, the cell evaluates DNA or cell damage with the help of specialised proteins known as ATM and ATR. If DNA or cell damage is detected, ATM and ATR activate a series of protein cascades leading to various cellular responses including a halt in cell cycle progression. A final checkpoint is located within the M phase between metaphase and anaphase, where kinetochore attachment is evaluated. In its absence, the cell cycle is halted due to the mitotic checkpoint complex binding to and inhibiting the activity of the APC/C complex, in turn preventing it from inducing degradation of CycB and securin.

7

If DNA damage is detected, ATM and ART phosphorylate Chk1 and Chk2, which then in turn phosphorylate and activate p53, a tumour suppressor and transcription factor. p53 leads to an increase in transcription of the CDK inhibitor (CKI) p21, blocking G1 phase CDK-cyclin complexes [45]. In addition, Chk1 and Chk2 phosphorylates a CDK-activating kinase (CAK) Cdc25, subsequently inhibiting G1 phase CDKs (Figure 1-3) [41, 45]. The G_2/M checkpoint is regulated by the same ATM and ART mechanisms regulating the G_1/S checkpoint transition (Figure 1-3). During the G_2/M checkpoint, the cell ensures DNA replication is complete and that no DNA damage has occurred, in addition to ensuring adequate size is reached for cell division to occur within the M phase [40, 46].

The last well-defined checkpoint within the mammalian cell cycle is the M checkpoint, present just before the cell enters anaphase within the M phase. This checkpoint ensures complete spindle assembly and chromosome attachment at the metaphase plate has occurred [40, 41]. During the prophase (early in the M phase), if any of the chromatids are not attached to kinetochores, this will lead to the formation of the mitotic checkpoint complex (MCC). The MCC is composed of BubR1, Bub3, Mad2 and Cdc20. This complex will bind to and prevent the activation of APC/C. If kinetochores are attached to all sister chromatids, the MCC is not formed and Cdc20 is able to activate APC/C, which will thus result in degradation of securin and CycB by means of ubiquitination. Once securin is degraded, separase is liberated and in turn allows the separation of the sister chromatids (Figure 1-3) [47-49].

If the cellular conditions are not adequate for the cell to pass through these dedicated checkpoints due to, for example, a lack of vital metabolic precursors or growth factors required for cellular processes or DNA damage, the cell will exit the cell cycle and enter a quiescent state (G_0 phase). During this arrested phase, the cell will await extracellular or intracellular signals to verify that the cell is able to re-enter the cell cycle. In mammalian cells, if DNA or cell damage is too severe, the cell will undergo programmed cell death (apoptosis) to prevent the cell from becoming cancerous [40, 41, 46].

1.5. *P. falciparum*'s atypical cell cycle

The cell cycle of *P. falciparum* has many aspects that differ from that of the conventional mammalian cell cycle model. The cell cycle of asexual *P. falciparum* is coupled to the asexual IDC of the parasite (Figure 1-4). Merozoites (with a 1N DNA copy number) invading erythrocytes are typically in a G_0-like, non-replicative state with condensed chromatin [50]. During the transition of ring to early trophozoite, (~2–20 hpi), decondensing of chromatin, increases in cell size and in RNA and protein content occur, similar to the processes occurring during the transition of the G_1A to G_1B phase in the mammalian cell cycle [51, 52] (Figure 1-4). The S phase is initiated during the late trophozoite stage (2N) at ~24 hpi, where the first round of DNA replication occurs over a period of 4–6 h, after which 3–4 rounds of continuous DNA synthesis occurs, alternating with mitotic phases with no clear G_2 phase (either briefly after the last M phase or completely absent) [52, 53]. The latter is the major point by which the

P. falciparum cell cycle deviates from the known mammalian cell cycle model (Figure 1-4). During 3–4 rounds of alternating DNA synthesis and mitosis, cytokinesis does not occur, leaving the nuclear envelope intact. This is also known as closed mitosis, resulting in a multi-nucleated (>16–32N) mature schizont (~44 hpi) [52].
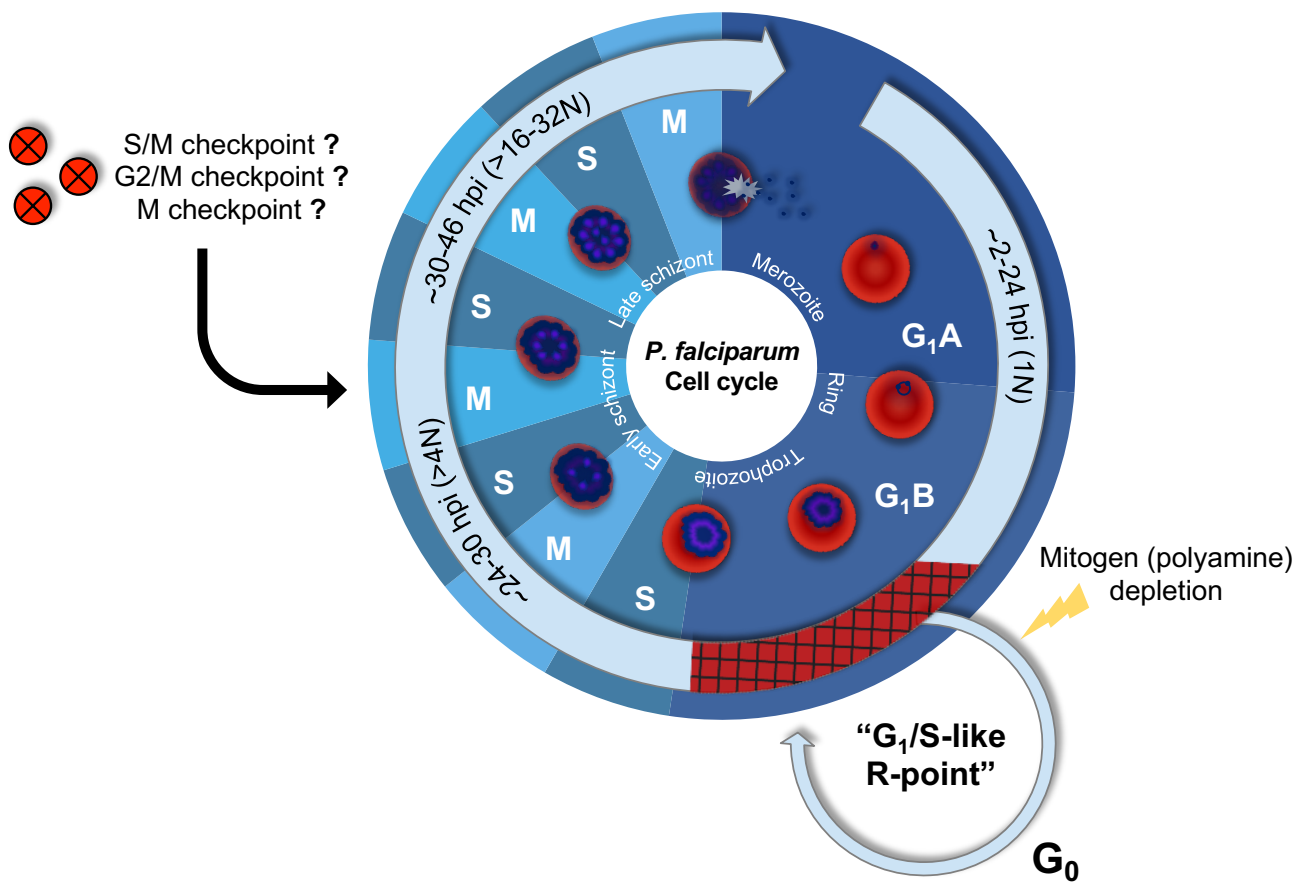
Figure 1–4: Schematic representation of the atypical *P. falciparum* cell cycle. The corresponding morphological parasite stages are overlapped with the proposed cell cycle phases. Merozoites released from a ruptured schizont are in a quiescent, non-replicative G_0 phase (light blue). Ring-stage parasites during the G_1A-phase (dark blue) develop to a G_1B-phase early trophozoite-stage. The S-phase (grey-blue) is initiated during the mature trophozoite stage (~24 hpi). Alternating S- and M-phases (medium blue) occur during schizogony resulting in a multi-nucleated schizont (>16–32N) at ~46–48 hpi. A proposed cell cycle checkpoint (▦) include an R-like or G_1/S-like checkpoint due to polyamine starvation. Data for figure were compiled from [1-8].

As described for the mammalian cell cycle, the M phase is divided into four sub-phases where the chromatin decondenses during the prophase. However, in contrast, the chromatin of *P. falciparum* stays condensed during the alternating S– and M phases, with spindles remaining intact within the nuclear envelope. During the last round of mitosis (~46–48 hpi), synchronous nuclear division occurs followed by segmentation and a single cytokinesis event yielding 16–32 daughters merozoites per schizont [53, 54] (Figure 1-4).

The cell cycle checkpoints regulating transition from one phase to the next are largely uncharacterised in *P. falciparum*. A G_2 checkpoint is completely absent [52, 55], and detecting and describing a possible S/M-like checkpoint within the alternating S and M phase has proven difficult due to variation in the genome replication speeds at different life cycle stages [56]. However, the presence of an R-point-like

checkpoint has been suggested to be present during the ring stage of the parasite, since the parasite is able to halt life cycle progression when subjected to nutrient starvation, presumably by entering a dormancy state similar to that of a G_0-phase [57]. Conclusive evidence of a mitogen-activated R-point was further evident by the restriction of polyamines as mitogens (Figure 1-4). Polyamines are known as important mitogenic regulators of mammalian cell cycle progression [58], enabling tight cell cycle synchronization at the G_1/S transition point. Restriction of polyamines can be affected by inhibition of the rate-limiting biosynthetic enzyme, ornithine decarboxylase, by its exclusive suicide inhibitor DL-α-difluoromethylornithine (DFMO). Although this reversible R-like checkpoint induced in *P. falciparum* has many hallmarks of a eukaryotic G_1/R checkpoint, it does show divergence as many canonical effectors involved in the eukaryotic G_1/R checkpoint is absent [8] (Figure 1-4). Therefore, the exact molecular role players governing the atypical cell cycle, and its proposed checkpoints in *P. falciparum*, are largely understudied. However, cyclin and CDK-related kinases (CRK) along with other candidate kinases, have been identified within the parasite, as will be presented below.

1.6. *P. falciparum*'s kinome and their role as cell cycle regulators

1.6.1. The *P. falciparum* kinome

Eukaryote protein kinases (ePKs) as a class consists of 518 proteins, distributed within seven main families: CK1 (casein kinase 1), CMGC (**C**DK [cyclin-dependent kinases], **M**APK [mitogen-activated protein kinases], **G**SK [glycogen synthase kinase] and **C**LKs [CDK-like kinases]), TKL (tyrosine-kinase-like), AGC (PKA [cyclic-adenosine-monophosphate-dependent protein kinase A], PKG [cyclic-guanosine-monophosphate-dependent protein kinase G], PKC [protein kinase C] and related proteins), CamK (calcium/calmodulin-dependent kinases), STE (PKs acting as regulators of MAPKs) and TyrK (tyrosine kinases) [2, 5, 59, 60]. By contrast, the *P. falciparum* genome contains a much smaller set of genes (105) encoding for protein kinases (PKs) or PK-related proteins (Figure 1-5) [2]. A total of 65 of these *Pf*PKs do show similarity to the classical eukaryotic PKs including proteins which fall within the ACG, CMGC, TKL, TKL and RGC families.
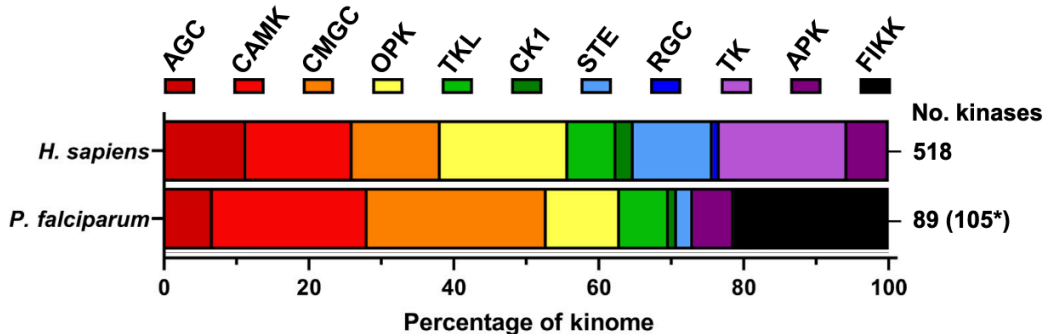
Figure 1–5: Comparison of kinome composition of *Homo sapiens* and *P. falciparum*. The kinase families which are represented within the *P. falciparum* kinome included here are tyrosine kinase-like kinases (TKLs), PKA, PKG and PKC (AGC), dual specificity tyrosine-regulated kinases and the CDK-like kinases (CMGCs), calcium/calmodulin-dependent kinases (CaMK), casein kinase 1 (CK1), orphan protein kinases (OPKs) and lastly an apicomplexans-specific group known as the (FIKK) kinases and atypical protein kinases (APKs). While receptor guanylyl cyclases (RGCs) and tyrosine kinases (TKs) families are seemly absent in *P. falciparum*. The asterisk (*) indicates the revised number of kinase proteins. Image adapted from [2].

However, thus far, there is no indication of proteins in *P. falciparum* which show homology to those proteins within the eukaryotic TyrK or RGC families [2, 5, 60-63] (Figure 1-5). The bulk of the remaining *Pf*PKs are phylogenetically distinct from known ePK families and are termed atypical *Pf*PKs (APK) and orphan kinases (OPK) (Figure 1-5). The APK and OPKs are a small set of *Pf*PKs that exhibit limited or no sequence similarity to known ePKs, but nevertheless possess kinase catalytic activity. Additionally, there is a large novel family which are exclusively found within *Apicomplexa,* consisting of 20 proteins containing a conserved Phe-Ile-Lys-Lys motif found within subdomain II of the catalytic domain, known as the FIKK kinases [5, 62] (Figure 1-5)*.* Nearly all of the FIKK proteins identified within the parasite have variable N-terminal regions but contain a conserved vascular transport signal and/or a *Plasmodium* export element (PEXEL) and localize to various areas within the infected erythrocyte, indicating a possible role in sensing or protein transport [64].

FIKK proteins have been implicated in the remodelling of the erythrocyte membrane cytoskeleton, which is a vital part of the virulence of the parasite. However, it has been demonstrated that majority of the kinase proteins are not essential to parasite survival [65]. Interestingly, this group is much larger in *P. falciparum* compared to other species within the *Plasmodium* genus [4, 60, 62].

1.6.2. Association of *Pf*PKs and the *P. falciparum* life cycle and cell cycle

Several studies have attempted to associate *Pf*PKs with function in the *P. falciparum* life cycle and associated cell cycle [2, 3, 63, 66]. This includes either chemical interference of specific kinases or genetic manipulation (e.g., gene knockout) to prove the function of a specific kinase. Thus far, 36 kinases that have been subjected to gene knock out studies have been found to be critical role players within the asexual proliferation and the asexual cell cycle, while 26 kinases were found not to be essential to these developmental phases [2, 67]. The *Pf*PKs essential to asexual proliferation and the cell cycle includes kinases important to host cell invasion, egress, and motility – thereby excluding them as potential cell cycle regulators (Figure 1-6).

To date only three proteins have been identified which cluster to the ACG family: cGMP-dependent kinase (*Pf*PKG), cAMP-dependent kinase (*Pf*PKA) and *Pf*PKB [62]. *Pf*PKA associates with and phosphorylates *Pf*AMA1, which is essential in merozoite invasion [6, 68]. Similarly, *Pf*PKB has been shown to be essential during merozoite invasion by phosphorylating *Pf*GAP45 and interacting with the motor complex in the presence of calcium/calmodulin (CaM) [69]. *Pf*PKG is the most well-characterised protein kinase within the *P. falciparum* AGC family and has an essential role throughout the parasite life cycle, such as in merozoite egress [70, 71] and invasion [71, 72] (Figure 1-6). These ACG kinases have been linked to regulatory interactions with calcium-dependent protein kinases (CDPK) by maintaining calcium Ca^{2+}-homeostasis [6, 72].

The CDPK proteins are a group of several proteins that have no orthologues within mammals, but rather within plants, protists, oomycetes and green algae [62, 73]. The several *Pf*CDPKs (*Pf*CDPK1–7) identified thus far have been found to be essential for multiple biological processes as regulators in Ca^{2+}-mediated signalling [73]. Of the seven *Pf*CDPKs identified, only *Pf*CDPK1, 2 and 5 have been found to be essential during asexual proliferation, specifically during merozoite invasion and egress [74-77] (Figure 1-6). However, neither of the kinase proteins identified within the ACG or CDPK group have been implicated within the cell cycle thus far.
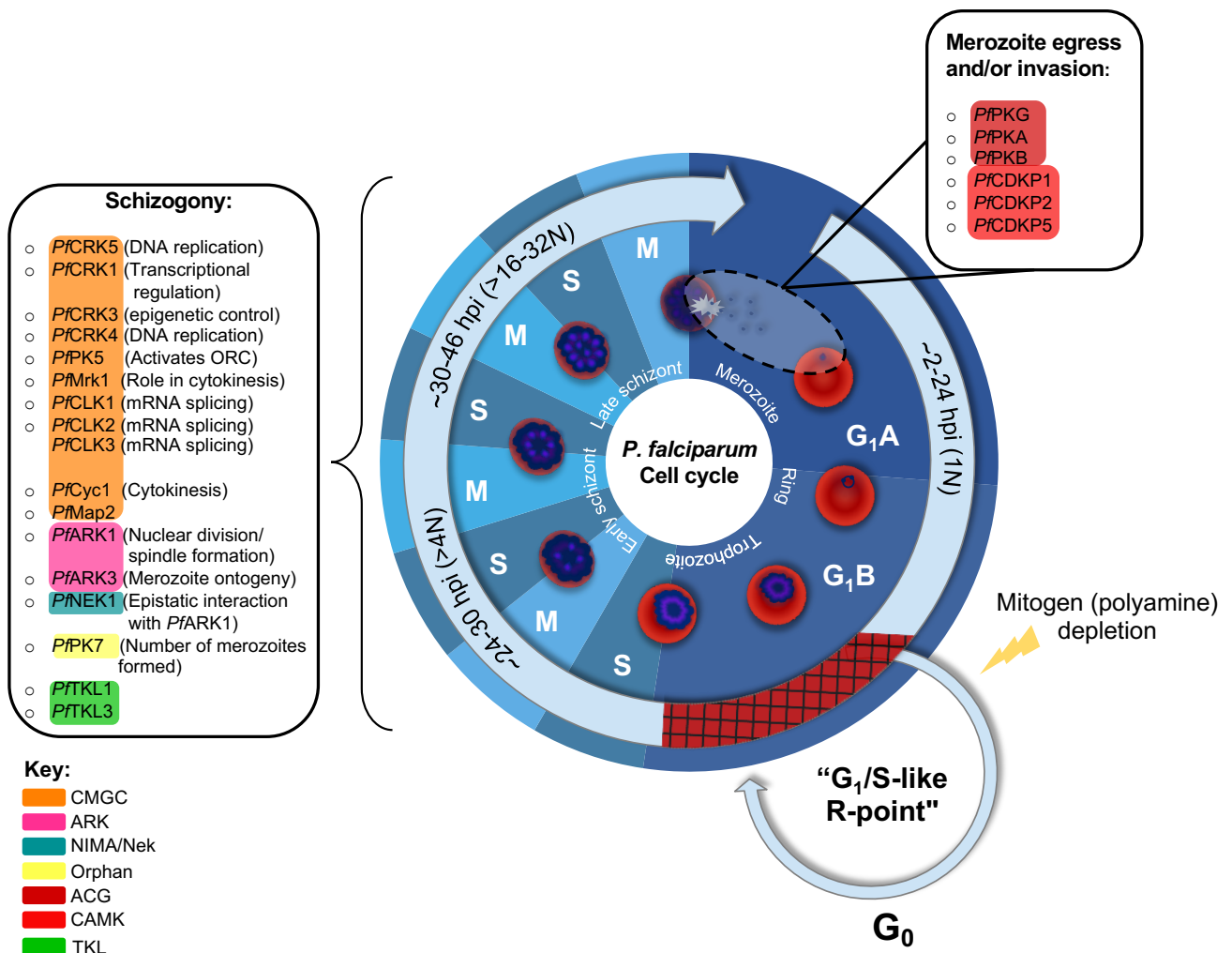
Figure 1–6: Schematic representation of the atypical *P. falciparum* cell cycle and known kinase regulators. PKG, PKA and PKB which cluster in the ACG family, have all been implicated in merozoite invasion and egress, along with three CDPK family members; CDPK1, CDPK2 and CDPK5. Protein kinases that are mainly clustered within the CMGC family have been found to play important functions during schizogony (multiple rounds of asynchronous and endomitotic cell division cycles) along with several members of the ARK, NIMA/Nek, TKL and orphan kinase families. These kinase proteins have been linked to various functions ranging from DNA replication machinery, mRNA splicing to spindle formation. Data compiled from [1-8].

Canonical mammalian cell cycle CDKs and related kinase proteins, amongst other regulators, have been identified within the *P. falciparum* CMGC family [2]. Amongst these canonical proteins were three cyclin-like proteins, *Pf*Cyc1, *Pf*Cyc3 and *Pf*Cyc4, which unexpectedly did not phylogenetically cluster with the G_1 or S-phase, or with mitotic cyclins of plants or animals, and are ubiquitously expressed, unlike the cyclical expression pattern found within the mammalian cell cycle model [3, 78]. In addition to the three cyclin-like proteins, seven CRKs were also identified within *P. falciparum* [2, 66, 79].

Of these, protein kinase 5 (*Pf*PK5, a putative homologue of the mammalian Cdk1 and Cdk5) and *Pf*Mrk1 (a putative homologue of mammalian Cdk7) have been shown to associate with, and be regulated by, *Pf*Cyc1, *Pf*Cyc3 and *Pf*Cyc4 [80-82]. *Pf*PK5 is implicated as an essential cell cycle regulator due to the phosphorylation and activation of origin of replication control components during schizogony [83]. Furthermore, *Pf*Mrk1 and *Pf*Cyc1 form a complex during schizogony, and knockdown of *Pf*Cyc1 causes a stage-specific arrest after nuclear division [84]. In addition to the important roles of *Pf*PK5, *Pf*Mrk1 and *Pf*Cyc1 within the parasite cell cycle, *Pf*Crk1 and 3–5 have been implicated in various biological roles linked to the cell cycle, for instance in DNA replication, epigenetic control and transcriptional regulation [3] (Figure 1-6). Four cyclin-dependent-like kinases (CLK) have been identified within *P. falciparum* namely *Pf*CLK1–4 [1, 62, 85]. Within mammalian cells, CLKs are important regulators in mRNA splicing through phosphorylation. Of these, *Pf*CLK1–3 have been found to essential in IDC schizogony, with a likely function in phosphorylation of serine/arginine-rich splicing factors during mRNA splicing and shuttling [7, 85, 86] (Figure 1-6).

Furthermore two MAPK protein homologues, *Pf*Map1 and *Pf*Map2, have been identified within the parasites kinome [87, 88]. Only *Pf*Map2 has been shown to be essential during schizogony, while *Pf*Map1 is dispensable. However, this raised the notion that *Pf*Map2 could fulfil *Pf*Map1 function [89, 90]. Interestingly, seemingly no member of the MAPKK group has been identified within the *P. falciparum* kinome, although a TKL protein, *Pf*TKL3, is suggested to be a potential MAP3K candidate [91]. Within eukaryotes, the TKL families such as RAF and MLK, are MAP3Ks, which form core modules of the MAPK cascade pathway, ultimately playing a role in cell cycle regulation. In addition to *Pf*TKL3, three other *Pf*TKLs have been identified, *Pf*TKL1, *Pf*TKL2 and *Pf*TKL4. However, limited studies aimed at uncovering the role of these proteins within the parasites have been conducted. Both *Pf*TKL1 and *Pf*TKL3 have been shown to cluster more closely and, through the use of genetic disruption methods, were shown to play an essential role in IDC schizogony [1, 91] (Figure 1-6).

Apart from *Pf*MAPK and *Pf*TKL, there is a lack of proteins that play roles in MAPK signalling pathway, which lead to a proposed view of atypical MAPK regulation by members of NIMA/Nek (never-in-mitosis) kinases [87, 92]. Within *P. falciparum* four similar proteins (*Pf*Nek1–4) have been identified which are similar to the NIMA/Nek family within eukaryotes [62, 63]. The NIMA/Nek family is mainly involved in a variety of roles in cell cycle regulation as well as mitosis and meiosis within eukaryotes [93, 94].

*Pf*Nekl1 is the only protein out of the four which is an orthologue to known eukaryotic Nek kinases, having clustered with human Nek2, which is involved in microtubule organization and mitotic spindle assembly [88]. Therefore, it was proposed that *Pf*Nek1 is involved in mitotic events within the parasite, and the increased expression of *Pf*Nek1 during late trophozoite/early schizont stages just as DNA replication is initiated, only further supports this proposed function [88, 95]. Additionally, genetic disruption of *Pf*Nek1 indicated essentiality of the protein during the asexual IDC [96, 97] (Figure 1-6). *Pf*Nek3 has also been suggested to have a role as an atypical MAPK, with studies showing *Pf*Nek3

interacting with and phosphorylating *Pf*Map2 [98]. *Pf*Nek2 and *Pf*Nek4 are predominantly expressed during sexual stages of the parasite with no apparent essential role during asexual IDC, but rather fulfilling essential roles during meiotic transition and gametocytogenesis [95, 98, 99].

In addition to the NIMA/Nek family, the *P. falciparum* genome encodes for three aurora kinase homologues, *Pf*ARK1–3 [98]. Aurora kinases are serine/threonine kinases that play pivotal roles in the control of cell division within eukaryotes, and *Pf*ARK1–3 have all been found to be essential for the IDC of the parasite [97, 98, 100, 101] (Figure 1-6). Interestingly, *Pf*ARK2 is present only in *Plasmodium* species, while *Pf*ARK1 and *Pf*ARK3 are conserved across all Apicomplexans. Localisation studies have demonstrated co-localisation of *Pf*ARK1 with intra-nuclear microtubule spindles, which suggests that this protein plays a role during early spindle pole body formation [102].

1.7. Identification of novel kinase proteins during cell cycle re-entry

In addition to these well-described kinases, several other proteins within the *P. falciparum* genome have kinase or kinase-like annotations. Considering the limited nature of the *P. falciparum* kinome, and the fact that ~60 % of the genome remains unannotated and contains uncharacterised genes that encode for proteins which fulfils essential functions, exploring the parasite's genome for additional kinases is of importance.

A previous study evaluated changes in gene expression around the mitogen-induced G_1/S R-point in *P. falciparum* [8]. Comparison of the gene expression profiles of several gene families, including kinases and potential kinase-related proteins, indicated differential expression of these genes between the mitogen-induced cell cycle arrested state and three different points of cell cycle re-entry (at RE1 (3 h), RE2 (6 h) and RE3 (12 h)) [8]. Of the genes with differential expression, implying either functionality in or dependence on cell cycle progression, 228 individual transcripts were allocated to kinases and phosphatases. This includes differential expression of several kinases known to play essential roles in proliferation/cell division, which included *ark2*, *nek1*, the *clk1-3, crk3-5* and *pk5* (Figure 1-7).
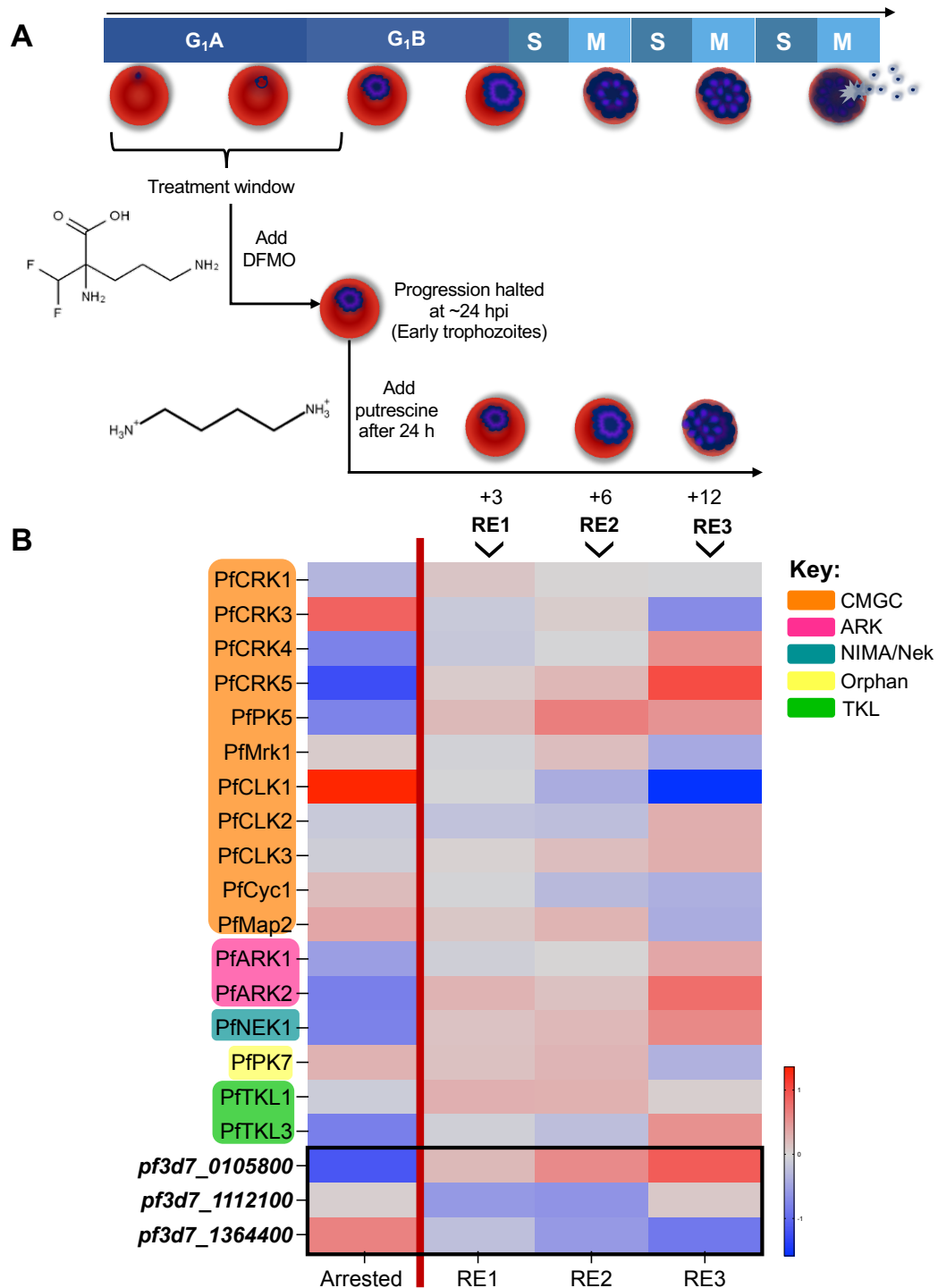
Figure 1–7: The transcriptional profiles of essential kinase proteins during cell cycle arrest and re-initiation. (A) *P. falciparum* parasite development was arrested at the ring-/early trophozoite-stage (22 hpi) with DFMO and sampled 24 h (Arrest) post-treatment. The cell cycle arrest was reversed by addition of putrescine (a mitogen), and parasites were sampled at three time points during re-entry: 3 h (RE1), 6 h (RE2) and 12 h (RE3) post-putrescine treatment. **(B)** The transcriptome profile of known kinase proteins which have been shown to be essential to schizogony are indicated during cell cycle arrested as well as during the re-entry of the cell cycle at specific time points (RE1-3). The uncharacterised kinase-encoding genes selected to be evaluated are shown in bold. Data obtained from [8].

However, in addition to these known kinase-encoding genes, three uncharacterised putative kinase genes (*pf*3d7_*0105800, pf*3d7_*1112100* and *pf*3d7_*1364400*) were present during the re-entry of the cell cycle as early and intermediate responders (Figure 1-7). During re-entry of the parasite's cell cycle, *pf*3d7_*0105800* was upregulated, whereas *pf*3d7_*1364400* and *pf*3d7_*1112100* were suppressed [8].

15

While *pf*3d7_*1112100* was found to be downregulated, it was co-expressed with other genes which were up-regulated, indicating that *pf*3d7_*1112100* could have a repressive function during this period [8]. Based on the presence and transcriptional profile of the uncharacterised putative kinase proteins during cell cycle arrest and throughout re-entry, and the need to functionally evaluate potential kinases with proposed importance to the cell cycle, it would be of value to determine the function and essentiality of these kinase candidates in *P. falciparum* and potentially gain insight into the dynamics of the parasite cell cycle and regulation thereof.

1.8.   Genetic manipulation tools used in *P. falciparum*

Genome editing has been a widely used tool in characterising and functionally validating uncharacterised proteins including kinase proteins. Several kinase proteins have been shown to be essential using conventional knockout systems, which has also led to a better overall understanding of the functional roles of kinase proteins within the parasite life cycle using inducible systems.

A variety of conditional strategies have been developed within the field and used to uncover the function and essentiality of different genes within the *P. falciparum* parasite. This includes, for example, conditional DNA editing techniques like the site-specific recombinase Cre/LoxP knockout system where LoxP sites are introduced flanking the target DNA sequence and once induced, results in the excision of this sequence [67, 103]. Targeted gene deletion can also be achieved by targeting a truncated N-terminal region of the gene of interest into the genome to displace the full-length gene through a single homologous recombination event. This leads to the translation of a truncated, non-functional protein [67, 103].

Gene expression can also be altered post-transcriptionally at the mRNA level, based on inducible Tet repressor protein (TetR) aptamer and *glmS* systems. The TetR aptamer system is based on the binding and dissociation of TetR to the TetR-binding RNA aptamers located in the 5' UTR of a target gene. In the absence of anhydrotetracycline (ATc), TetR binds to the aptamer and prevents translation of the mRNA while in the presence of ATc, but dissociates from the aptamer in its absence, allowing mRNA translation and protein synthesis to proceed [67, 104]. The *glmS* system affects the transcript abundance (mRNA level) of the target gene rather than targeting a gene directly. This system has been shown to be very effective for inducible knockdown of gene expression in *P. falciparum* [106, 107]. This system relies on the activation of a *glmS* ribozyme element, which is a natural ribozyme originating from Gram-positive bacteria and requires glucosamine-6-phosphate for catalytic activity. In this system, the ribozyme sequence is introduced in the 3'UTR of a gene of interest, leading to the expression of a chimeric mRNA containing the ribozyme element, and can be induced by the addition of glucosamine (GlcN), leading to instability and degradation of the chimeric mRNA [67, 108] (Figure 1-8). An advantage of this system is that the degradation of the target mRNA is controllable to a certain extent, as the level of self-cleavage can be adjusted by varying the concentration of GlcN added. To ensure the findings

observed for the knockdown experiments are in fact due to the activation of the *glmS* ribozyme, an inactive version of the *glmS* ribozyme, M9 (-mut), which contains a single point mutation that abrogates autocatalytic activity, is used as a suitable control [67, 108].
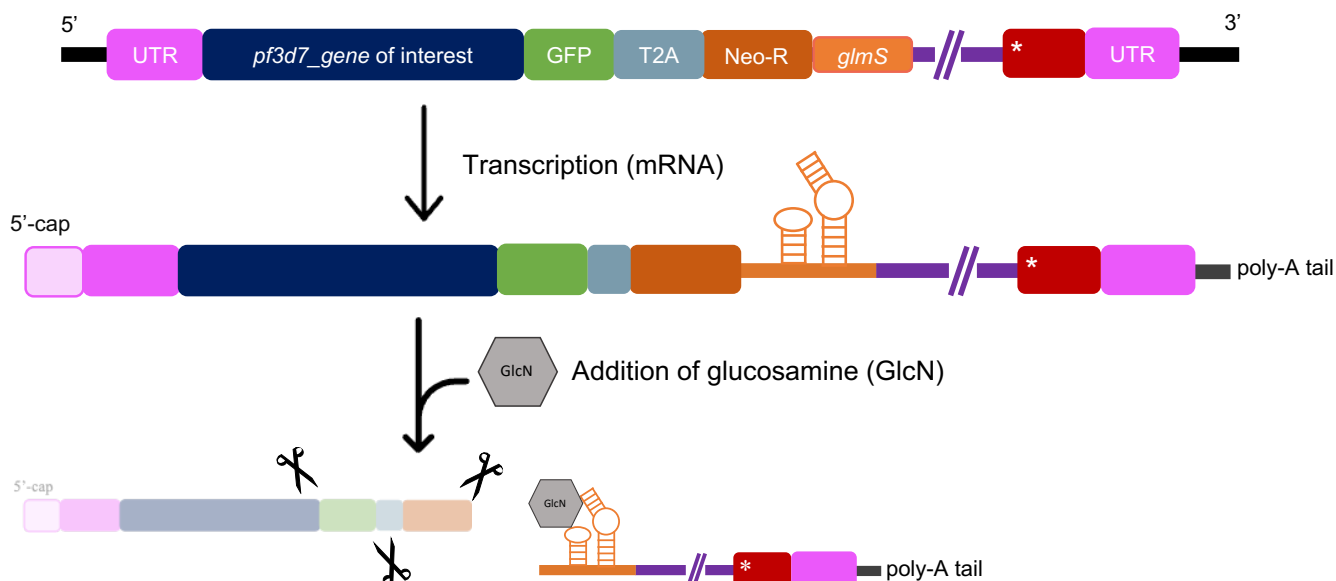
Figure 1–8: Schematic representation of the *glmS* ribozyme conditional knockdown tool. The ribozyme is inserted at the 3'-UTR of the gene of interest. The addition of glucosamine, which binds and activates the ribozyme, results in self-cleavage of the RNA and subsequently knockdown of protein expression. ***glmS***: glucosamine-6-phosphate riboswitch ribozyme. **GlcN**: glucosamine-6-phosphate.

In addition to conditional DNA and mRNA level-based systems, there are systems that influence protein stability, for instance the FK506 binding protein 12 (FKBP)-destabilisation domain system. This system decreases protein stability in the absence of the rapamycin-derived ligand Shield (Shld-1) due to the destabilisation domain of the FKBP, fused to the N- or C-terminus of the target protein However, the FKBP system can also be used to displace proteins from their normal cellular site of function to, e.g., the nucleus or plasma membrane. This knock sideways interferes with the function of the target protein by altering its location within the cell and, in so doing, theoretically removing it from its predicted site of action, preventing it from fulfilling its intended function [103]. The mislocalisation of the target protein relies on the tight and specific dimerisation of FKBP and FKBP12-rapamycin-binding (FRB) domains induced by the addition of rapamycin (Figure 1-9). The protein of interest is tagged with multiple FKBP domains, encoded by the SLI-sandwich plasmid, which will be expressed in a transgenic parasite line, while the FRB domain is expressed episomally from an additional mislocaliser plasmid. The FRB domain is fused to a targeting signal allowing for localisation to a specific compartment (nucleus or plasma membrane). Addition of rapamycin allows for the dimerisation of the FKBP and FRB domains (the 'sandwiching' of the protein) and induces relocalisation of the FKBP-tagged protein to the target site and depletion at its normal site of action (Figure 1-9).
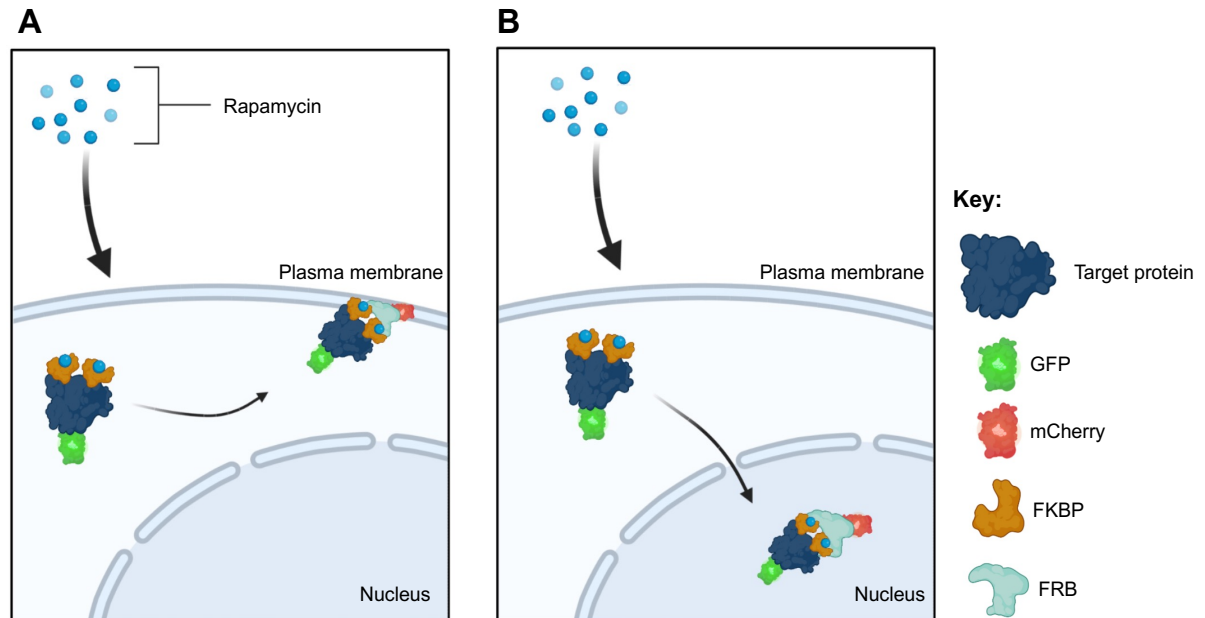
Figure 1–9: Schematic representation of the knock sideways sandwich tool. The knock sideways strategy relies on two components; an FKBP tag appended to a protein of interest and a mislocaliser protein fused to FRB and containing targeting motifs to a specific cellular compartment. In the presence of rapamycin, FKBP binds to FRB, resulting in sequestration of the protein of interest in the target compartment for mislocalisation. **(A)** Plasma membrane mislocalisation and **(B)** Nuclear mislocalisation. Images were designed using BioRender.

Various limitations and factors have made it challenging to introduce these manipulation systems into the parasite genome, for example the shortage of robust selection markers to allow for consecutive genetic manipulations on the same parasite, as well as poor transfection efficiency [105]. However, selection-linked integration (SLI) [106] uses a double selection system to rapidly select for episomal uptake of DNA constructs using one selection marker (human dihydrofolate resistance, hDHFR) followed by homologous recombination and integration through a promoter-less targeting region linked to a second selection marker (neomycin resistance gene, Neo-R). This combination has been found to increase the speed and success rate in producing transgenic lines [106].

This dissertation therefore aims to characterise the three putative kinase protein-encoding genes, *pf3d7_0105800, pf3d7_1112100* and *pf3d7_1364400,* identified during mitogen-induced cell cycle arrest and re-entry, using genetic manipulation. SLI-mediated integration was used and a TGD system was applied to determine essentiality of these genes to the parasite. Additionally, knockdown (SLI-*glmS*) and knock sideways (SLI-sandwich) systems were generated for future characterisation of evaluation of protein functionality for those genes found to be essential. By uncovering the essentiality and biological function of these putative kinases to cell cycle regulation, we will expand our current understanding of *P. falciparum* parasite biology and regulatory mechanisms. These findings could serve as a basis for future interrogation of these proteins as potential drug targets, contributing towards the goals of malaria control and elimination.

Hypothesis

The putative kinases *pf3d7_0105800, pf3d7_1112100* and *pf3d7_1364400* play an essential role during asexual proliferation of *P falciparum* parasites.

Aim and Objectives

1.9. Aim

To determine the function and essentiality of selected putative kinases during asexual proliferation of *P. falciparum* parasites using complimentary genetic tools

1.10. Objectives

1.10.1. Construct recombinant SLI-sandwich and SLI-*glmS*/*glmS*-mut plasmids for all three putative kinase genes under investigation.

1.10.2. Generate transgenic parasite lines for TGD, knock sideways and knockdown of all three kinases.

1.10.3. Elucidate the function and essentiality of the selected putative kinase proteins in the transgenic lines using phenotypic analyses.

1.11. Research outputs

Langeveld H., Birkholtz LM. Novel kinase proteins play a pivotal role during the life cycle progression of *Plasmodium falciparum* parasites 6th South African Malaria Research Conference. Oral presentation, Pretoria, August 2021.

Langeveld H., Birkholtz LM. Novel kinase proteins play a pivotal role during the life cycle progression of *Plasmodium falciparum* parasites SASBi-SC/SAGS 2021 Virtual Student Symposium. Oral presentation, Virtual (Stellenbosch), September 2021.

Langeveld H., Birkholtz LM. Novel kinase proteins play a pivotal role during the life cycle progression of *Plasmodium falciparum* parasites. Johns Hopkins' Future of Malaria Research Symposium. Oral presentation, Virtual (USA), November 2021.

Chapter 2: Experimental procedures

2.1. Ethics statement

All experiments were carried out in the Malaria Parasite Molecular Laboratory (M²PL) biosafety level 2-(BSL2) certified facility (registration number 39.2/University of Pretoria-19/160) in which *P. falciparum* parasites were cultivated for this study. All *in vitro* experiments involving human blood holds ethics approval from the University of Pretoria Research Ethics Committee of the Health Sciences Faculty (506/2019) and the *in vitro* cultivation of human malaria parasites is covered by an umbrella ethics approval (NAS ethics approval no: 180000094) for the SARChI program under Prof. Lyn-Marié Birkholtz.

2.2. *In silico* analysis of selected putative kinase genes

2.2.1. Protein domain predictions of PF3D7_0105800, PF3D7_1112100 and PF3D7_1364400

InterPro (https://www.ebi.ac.uk/interpro/, accessed Nov 2021) was used to predict conserved domains within the PF3D7_0105800, PF3D7_1112100 and PF3D7_1364400 putative kinase proteins to provide information about the superfamily/family type to which these putative proteins may belong to. The protein architecture, such as structural motifs, low complexity regions and transmembrane regions, were identified with SMART (http://smart.embl-heidelberg.de/, accessed Nov 2021).

2.2.2. Protein–protein interactions of putative kinase proteins

The protein-protein interactions of the selected putative kinase proteins were predicted using STRING (version 11.5) network algorithm (https://string-db.org/, accessed Nov 2021). This summarises the network of predicted associations for a particular protein. The lines connecting the different proteins represent the predicted functional associations. These interactions are based either on proteins with similar functions in different species, proteins with similar metabolic functions, or co-expression of genes. The STRING network parameters were set to include protein-protein interactions for PF3D7_1364400 with a minimum required interaction score of medium confidence (0.4), while for PF3D7_0105800 and PF3D7_1112100 the interaction score was set to high confidence (0.7) and a maximum of 10 interacting proteins.

2.3. *In vitro* cultivation of asexual *P. falciparum* parasites and synchronisation

An NF54 (drug-sensitive) *P. falciparum* parasite strain was cultured under aseptic conditions. Parasites were cultivated in fresh human erythrocytes (various blood types) in RPMI-1640 culture medium supplemented with 23.81 mM sodium bicarbonate, 0.024 mg/mL gentamycin (Hyclone, USA), 25 mM

HEPES pH 7.5 (Sigma Aldrich, USA), 0.2 % (w/v) D-glucose and 0.2 mM hypoxanthine (Sigma Aldrich, USA) and 5 g/L Albumax II (Invitrogen, USA, a human serum alternative). Parasite cultures were incubated at 37 °C under hypoxic conditions (90 % N_2, 5 % O_2 and 5 % CO_2, AFROX, South Africa). Whilst shaking at ~60 rpm to aid parasites invasion, parasitaemia was routinely determined with Rapi-Diff staining (Merck, South Africa) of a thin blood smear and visualised under a light microscope (Nikon, Japan) at 1000x magnification. Parasitaemia was defined as the percentage of parasite-infected erythrocytes and was determined by counting 500–1000 individual erythrocytes.

Parasite cultures were synchronised to obtain parasites in the same developmental stage. Cultures comprised of mostly ring-stage parasites were incubated in 5 % (w/v) D-sorbitol (Sigma-Aldrich, Germany) for 15 min at 37 °C. This permitted the selective elimination of the more permeable trophozoite and schizont parasitic stages due to the membrane structure of erythrocytes infected with these stages being more permeable to sorbitol, causing an increase of osmatic water entry into the parasites and causing the parasites to swell and burst [107, 108]. After incubation, the culture was centrifuged at 3500 *xg* for 3 min, and the supernatant was aspirated. The remaining sorbitol was washed out twice using fresh RPMI medium (without Albumax II) and the parasites were resuspended in fresh medium (containing Albumax II) and erythrocytes to adjust the culture to a 5 % haematocrit.

2.4.   Cloning strategy for generation of recombinant SLI-sandwich plasmids

To functionally analyse the selected putative kinase proteins throughout the different parasite developmental stages, the knock sideways system was employed, which results in displacement of the protein under investigation from its hypothesised site of action through FKBP-mediated protein-protein interactions (sandwich). Gene fragments of ~600–1100 bp in sizes corresponding to the 3'-region of the coding strand for each selected putative kinase were PCR amplified and directionally cloned into the SLI-sandwich plasmid using *Not*I and *Avr*II restriction enzymes (REs) (Figure 2-1). The SLI-sandwich plasmid was kindly provided by Dr. Tobias Spielmann's lab (Bernhard Nocht Institute for Tropical Medicine, Hamburg, Germany).

2.4.1. Genomic DNA isolation from NF54 asexual *P. falciparum* parasites

Genomic DNA (gDNA) isolation was performed on intraerythrocytic *P. falciparum* NF54 parasites to be used in downstream PCR amplification experiments. The Quick-gDNA Blood Miniprep kit (Zymo Research, USA) was used to extract gDNA from a blood sample (>3 % parasitaemia and >50 % trophozoite stage parasites) as per the manufacturer's instructions.
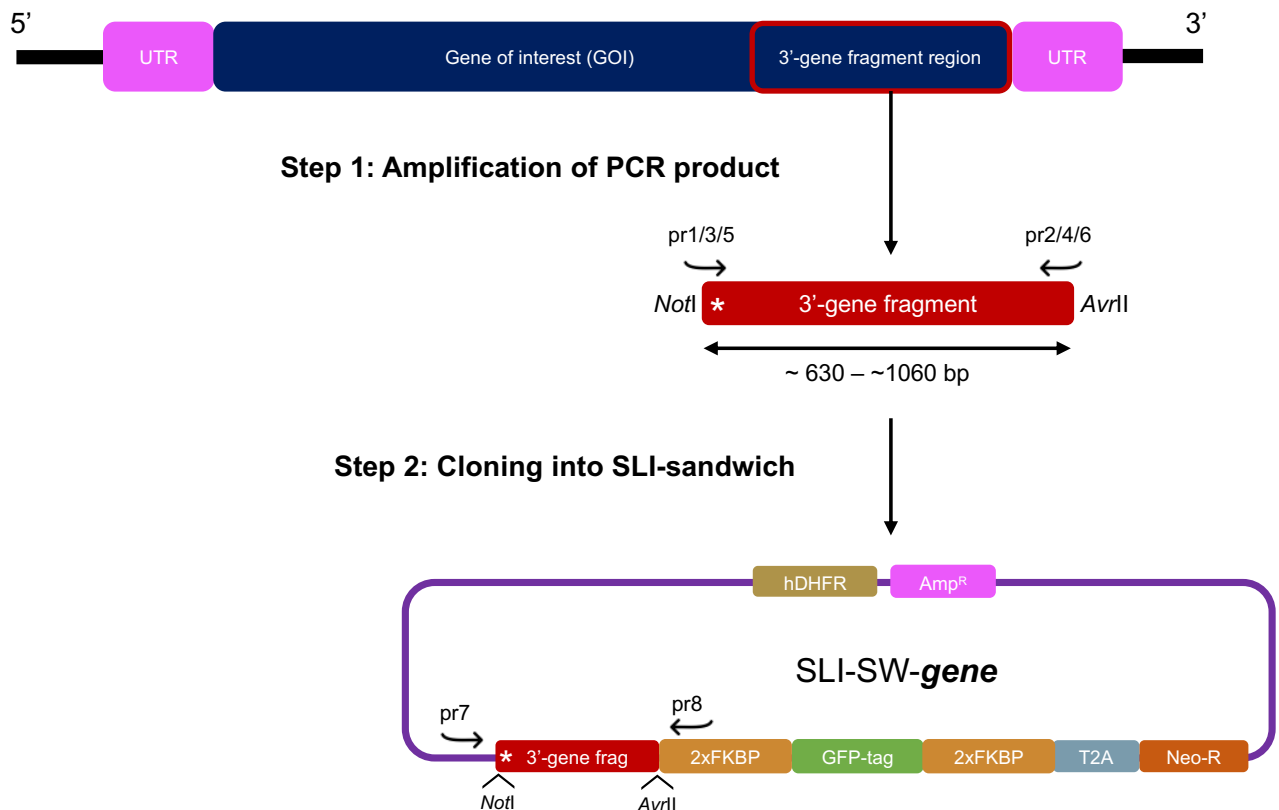
Figure 2–1: Cloning strategy to produce recombinant SLI-sandwich plasmid for transfection. Step 1: The selected 3'-gene fragment regions of the putative kinase genes were amplified using the specified primer pairs listed in Table 1. Step 2: the amplified 3'-gene fragments were cloned into SLI-sandwich plasmids. SLI-sandwich plasmid backbone primers flanking the insert region are indicated by the specific primer code. **Asterisk (*):** TAA stop codon. **GFP-tag:** green fluorescent protein tag. **Amp^R:** ampicillin resistance selection marker. **hDHFR** human dihydrofolate reductase resistance selection marker. **Neo-R:** neomycin resistance selection marker. **T2A:** skip peptide. **FKBP:** FK506 binding protein.

2.4.2. Amplification of 3'-gene fragments of selected putative kinase genes for cloning into SLI-sandwich plasmid

Primers were designed using Benchling (www.benchling.com) and SnapGene (version 5.3.2.) to allow amplification of a 3'-fragment region for each gene of interest, with the different characteristics of each primer provided in Table 1. Specific RE cut sites required for downstream cloning were added to each primer designed for 3'-gene fragment amplification. The RE cut site *Not*I (5'-GCGGCCGC-3') was added to the forward primers and an *Avr*II (5'-CCTAGG-3') was added to the reverse primers. A stop codon (TAA) was also added to each forward primer to prevent expression of the fragment before genomic integration. Due to the AT-rich genome of *P. falciparum* parasites, obtaining a sufficient GC % for each primer is challenging. Therefore, to increase the GC content, overhang sequences were added to each primer.

Each PCR amplification reaction was performed using an Applied Biosystems 2720 Thermal Cycler (Applied Biosystems, USA) and each reaction contained 1x KAPA Ready mix [KAPA Taq DNA polymerase (0.5 U/25 µL), KAPA Taq buffer, dNTPs (0.2 mM), MgCl$_2$ (1.5 mM)], 5 pmol of the designated SLI-sandwich primer sets for each specific putative kinase gene (Table 1) and 20–40 ng of

gDNA isolated as described in section 2.4.1. PCR conditions included an initial denaturation step of 95 °C for 5 min, followed by 30 cycles of denaturation at 95 °C for 30 s, annealing at 60 °C for 30 s and extension at 68 °C for 1 min, with a final extension step of 4 min at 68 °C. The amplified fragments were examined on a 2 % (w/v) agarose/Tris-Acetate-EDTA (TAE) gel, poststained in ethidium bromide (0.5 µg/mL in 1x TAE) for ~10 min and visualised with a Gel Doc EZ Imaging system (Bio-Rad, USA). A 1 kb DNA ladder (Promega, USA) was used to determine DNA fragment sizes. Gel images were analysed using Image Lab version 3.0 (Bio- Rad, USA).

Table 1: SLI-sandwich primer sequences for selected putative kinase gene PCR products. The sequence of each primer used is indicated from 5' end to 3' end with the respective RE cut sites indicated in bold text and the stop codon added to each forward primer indicated in red text. The overhang nucleotides added to each primer are indicated in lower case text. Each primer was also assigned a primer code, which will be used to refer to the primer hereafter.

PlasmoDB gene ID	Primer ID	Orientation	Primer code	Primer sequence (5'–3')	PCR product length (bp)
pf3d7_0105800	GS_0105800_Fw	Forward	pr1	gcat**GCGGCCGC**TAAGGGGAATTAAATTTTATAGACGAGTTG	1051
	SW_0105800_Rv	Reverse	pr2	gcat**CCTAGG**ATTATTTTTAGGTCGTCTAAAAAATAGGAC	
pf3d7_1112100	GS_1112100_Fw	Forward	pr3	gcat**GCGGCCGC**TAAGATATAATATTGTCAACAAATAAAAATATCCCAACAAAACATCCC	634
	SW_1112100_Rv	Reverse	pr4	gcat**CCTAGG**AAAAAAAGTGGAGGCGTTATAAAGTTCGTTTAACAAGATTGTTTG	
pf3d7_1364400	GS_1364400_Fw	Forward	pr5	gcat**GCGGCCGC**TAATTAAATTATTTTAAAAGCTATTTTCCG	940
	SW_1364400_Rv	Reverse	pr6	gcat**CCTAGG**AGTTTTTATTTGCCTTGTTACTTCTCAACATCCTTTG	

Successfully amplified gene fragments were excised from the agarose gel and mixed with a binding buffer (30–45 % guanidinium thiocyanate, composition proprietary) and heated to dissolve the agarose. In the presence of the guanidinium thiocyanate chaotropic salt, DNA was bound to the silica membrane of a NucleoSpin Gel and PCR Clean-up Column (Machery-Nagel, Germany) and contaminants were removed through two wash steps with an ethanolic wash buffer. The pure DNA was eluted under low salt conditions with a slightly alkaline elution buffer (5 mM Tris/HCl, pH 8.5), as per the manufacturer's instructions.

DNA concentration of each sample was determined with a NanoDrop One^C spectrophotometer (Thermo Fischer Scientific, USA) by measuring nucleic acid absorbance at 260 nm (for the carbon-nitrogen π-bonds of nucleotides) as well as the A_{260}/A_{280} and A_{260}/A_{230} ratios to determine the purity of each sample. In an aqueous solution, the maximal absorbance of double-stranded DNA is close to 260 nm; however, many other components within the aqueous environment can interfere with quantification including, organic compounds such as guanidine salts, which have a maximal absorbance at 230 nm, proteins, and aromatic compounds like tryptophan and tyrosine that have a maximal absorbance at 280 nm. An A_{260}/A_{280} absorbance value of 1.8–2.0 was indicated a sufficient purity for downstream cloning experiments. The purified gene fragment DNA was stored at -20 °C until required.

2.4.3. Cloning of amplified 3'-gene fragments into SLI-sandwich plasmids

Before the amplied 3'-gene fragments could be directionally cloned into the SLI-sandwich plasmid, plasmid DNA was isolated and verified through RE mapping. SLI-sandwich plasmid was isolated from saturated *Escherichia coli* DH5α cell cultures, which were incubated overnight (O/N) at 37 °C (at ~180 rpm) in Luria-Bertani (LB) liquid medium (1 % (w/v) tryptone, 0.5 % (w/v) yeast extract and 1 % (w/v) NaCl, pH 7.5) containing 50 µg/mL ampicillin, using a NucleoSpin plasmid isolation kit (Machery-Nagel, Germany) following manufacturer's instructions. The plasmid DNA concentration and purity was measured as described in section 2.4.2 and stored at -20 °C until use. The identity of the isolated plasmid was verified by digesting ~1 µg of the isolated DNA with 3 U *Not*I-HF (high fidelity, New England Biolabs, UK) and 3 U *Avr*II (New England Biolabs, UK) in 1x CutSmart buffer (New England Biolabs, UK) for 3 h at 37 °C. After digestion, the products were analysed on a 1 % agarose gel as described in section 2.4.2.

To prepare the 3'-gene fragments and SLI-sandwich for downstream ligation experiments, the gene fragments and verified SLI-sandwich plasmid were digested with the respective RE to produce 5'- and 3'-overhangs required for sticky-end ligation (outlined in Figure 2-1). The digested plasmid products were separated on an agarose gel, and the plasmid backbone was excised from the gel. The 3'-gene fragments and plasmid backbone were purified using a NucleoSpin Gel and PCR Clean-up kit (Macherey-Nagel GmbH & Co.KG, Germany) following the manufacturer's instructions and stored at -20 °C until used. All ligation reactions were performed using a 1:3 plasmid to insert ratio and 400 U of the T4 DNA ligase (New England Biolabs, USA) in 1x ligase buffer (NEB, USA). The reactions were incubated O/N at 4 °C, after which they were incubated at room temperature for an additional ~8 h and used to transform competent *E. coli* DH5α cells.

Competent *E. coli* DH5α cells were prepared from saturated *E. coli* DH5α cell cultures that were incubated O/N at 37 °C (at ~180 rpm) in LB medium . The saturated culture was diluted in a 1/50 in LB and incubated at 37 °C with shaking. The optical density (OD_{600}) was measured every 30 min using a NanoDrop One^C spectrophotometer (Thermo Fischer Scientific Inc.) until an OD_{600} value of 0.4 was achieved, indicating log-phase growth. The cells were placed on ice for 15 min, then centrifuged at 1865 *xg* for 30 min at 4 °C. The cells were then resuspended in ice-cold 0.1 M $CaCl_2$ and centrifuged as described earlier. The cells were then resuspended in ice-cold 0.1 M $CaCl_2$ and 100 % (v/v) glycerol and incubated on ice for 45 min–1 h before aliquoting into 100 µL volumes and stored at -80 °C until use.

The ligation reaction mixture was added to 100 µL of the prepared competent cells and incubated on ice for ~30 min. Thereafter, the competent cell cultures were heat shocked at 42 °C for 90 s and immediately transferred to ice for 2 min. The entire competent cell mixture was transferred to 900 µL of pre-warmed LB-glucose (LB medium supplemented with 20 mM glucose) and incubated for 1 h at 37 °C

with shaking. Of this culture, 100 μL was transferred onto 1 % LB-agar-amp plates (1 % (w/v) agar in LB containing 100 μg/mL ampicillin). The plates were incubated at 37 °C O/N.

2.4.4. Screening and confirmation of recombinant SLI-sandwich plasmids

Single positive colonies were selected from the LB-agar-amp plates at random and used to inoculate 100 μL of LB-amp medium (LB medium supplemented with 50 μg/mL ampicillin) and grown at 37 °C for 3 h in a shaking incubator at ~180 rpm. Colony PCR was performed to confirm positive clones using the primers listed in Table 2. Each of the PCR reaction conditions stated in section 2.4.2, with 2 μL of bacterial culture added instead of DNA, and an added initial denaturation step of 95 °C for 5 min to lyse the bacterial cells. The reactions were analysed on 1.5 % (w/v) agarose gel and positive clones were identified based on the presence of amplified bands corresponding to the expected sizes of the DNA inserts for each gene. After confirmation of positive transformants, the respective bacterial cultures were transferred to 10 mL LB-amp medium and grown O/N at 37 °C with shaking at ~180 rpm. Plasmid DNA was isolated and purified from the saturated bacterial cultures and subjected to RE mapping using *Not*I-HF and *Avr*II to successfully verify ligation of each respective gene fragment of interest into the plasmid. The digested products were separated on a 1.5 % (w/v) agarose gel, poststained in ethidium bromide (0.5 μg/mL in 1x TAE) for ~10 min and visualised with a Gel Doc EZ Imaging system (Bio-Rad, USA). Image was analysed using Image Lab Software version 3.0 (Bio-Rad, USA).

Table 2: Primer sequences used for colony PCR and sequencing. The primer sequences flank the insert region within the SLI-sandwich plasmid. Primer Lz116 is located upstream of the insert region and primer Lz115 is located downstream of the insert region.

Plasmid ID	Primer ID	Orientation	Primer code	Primer sequence (5' - 3')
SLI-sandwich	Lz_116	Forward	pr7	AGCGGATAACAATTTCACACAGGA
	Lz_115	Reverse	pr8	TCTCTGCAGAGCAGCTCTAGCA

To confirm the identity and orientation of the insert and absence of unwanted mutations, Sanger sequencing was performed where fluorescently-labelled dideoxynucleotides (ddNTPs) along with deoxynucleotides are incorporated at random during replication. Incorporation of a ddNTP causes a chain termination during DNA replication. These ddNTPs (A, T, G, or C) are each labelled with a different fluorophore colour, allowing identification of sequential nucleotides based on fluorescent colour. Each sequencing reaction was completed using the BigDye 3.1 sequencing kit (Applied Biosystems, Foster City, USA) and the reaction mixtures consisted of ~300–400 ng plasmid DNA, 2x BigDye buffer (proprietary composition, Applied Biosystems, USA), 1x BigDye reaction mix (proprietary composition, Applied Biosystems, USA) and 5 pmol of either the forward (Lz116) or reverse (Lz115) backbone primer indicated in Table 2. The reactions were performed in an Applied Biosystems 2720 Thermal Cycler (Applied biosystems, USA) with the following parameters: an initial denaturation

temperature of 96 °C for 1 min, 25 cycles of denaturation at 96 °C for 10 s, primer annealing at 50 °C for 5 s, and extension at 60 °C for 4 min.

The sequencing reaction mixtures were purified by EtOH precipitation before being submitted for analysis. A solution of ice-cold 3 M NaOAc (pH 5.2) (1/10th of the reaction volume) and 100 % EtOH (3x the reaction volume) was added to each sequencing sample and incubated on ice for 15 min, then centrifuged at 11 000 *xg* for 30 min at 4 °C. The pellet was then washed with 250 µL of ice-cold 70 % (v/v) EtOH and centrifuged as before. The pellet was retained and any remaining EtOH was removed by evaporation in a heating block at 50 °C. Sequencing was performed at the University of Pretoria's FABI AGCT Sequencing facility. The ABI PRISM Genetic Analyzer (Applied Biosystems, USA) was used to determine the sequence, and the sequences were analysed with the SnapGene software (version 5.3.2.). The successfully generated recombinant SLI-sandwich plasmids will be referred to as SLI-SW-*0105800,* SLI-SW-*1112100* and SLI-SW-*1364400* henceforth.

2.5. Cloning strategy for generation of recombinant SLI-*glmS*/*glmS*-mut plasmids

In addition to the knock sideways system, a knockdown system was used to functionally analyse the selected putative kinase proteins throughout the different parasite developmental stages by altering the mRNA levels of the target gene. A 3'-gene fragment of ~600–1100 bp was selected and directionally cloned into both the SLI-*glmS* and SLI-*glmS*-mut plasmid (Figure 2-2). In addition to the SLI-*glmS* plasmid is the SLI-*glmS*-mut plasmid (M9) which possesses a mutation in the *glmS* encoding region rendering the ribozyme inactive and will act as a control during knockdown studies (see introduction section 1.8). All the primers designed were as in section 2.4.2. The purpose for each primer set and the different characteristics of the primers are presented in Table 3.

Table 3: SLI-*glmS* and SLI-*glmS*-mut primer sequences for selected putative kinase gene PCR products. The sequence of each primer used is indicated from 5' end to 3' end with the respective RE cut sites indicated in bold text and the stop codon added to each forward primer indicated in red text. The four overhang nucleotides added to each primer are indicated in lower case. Each primer was also assigned a primer code which will used to refer to the primer hereafter.

PlasmoDB ID	Primer ID	Orientation	Primer code	Primer sequence (5' - 3')	PCR product length (bp)
pf3d7_0105800	GS_0105800_Fw	Forward	pr1	gcat**GCGGCCGC**TAAGGGGAATTAAATTTTATAGACGAGTTG	1051
	GS_0105800_Rv	Reverse	pr9	gcat**ACGCGT**ATTATTTTTAGGTCGTCTAAAAAATAGGAC	
pf3d7_1112100	GS_1112100_Fw	Forward	pr3	gcat**GCGGCCGC**TAAGATATAATATTGTCAACAAATAAAAATATCCCAACAAAACATCCC	634
	GS_1112100_Rv	Reverse	pr10	gcat**ACGCGT**AAAAAAAGTGGAGGCGTTATAAAGTTCGTTTAACAAGATTGTTTG	
pf3d7_1364400	GS_1364400_Fw	Forward	pr5	gcat**GCGGCCGC**TAATTAAATTATTTTAAAAGCTATTTTCCG	940
	GS_1364400_Rv	Reverse	pr11	gcat**ACGCGT**AGTTTTATTTGCCTTGTTACTTCTCAACATCCTTTG	

Specific REs required for downstream cloning were added to each primer designed for 3'-gene fragment amplification. The forward primers used in amplifying the 3'-gene fragments intended to be cloned into SLI-*glmS* and SLI-*glmS*-mut plasmids are the same primers used in section 2.4. However, the reverse

primers used are different, given that these primers contain an *Mlu*I (5'-ACGCGT-3') cut site instead of the *Avr*II cut site (Table 3).

The PCR amplification reaction elements and thermal cycler settings were the same as described in section 2.4.2 for each of the corresponding 3'-gene fragments, with each PCR amplification reaction containing 5 pmol of forward and reverse primer listed in Table 3.
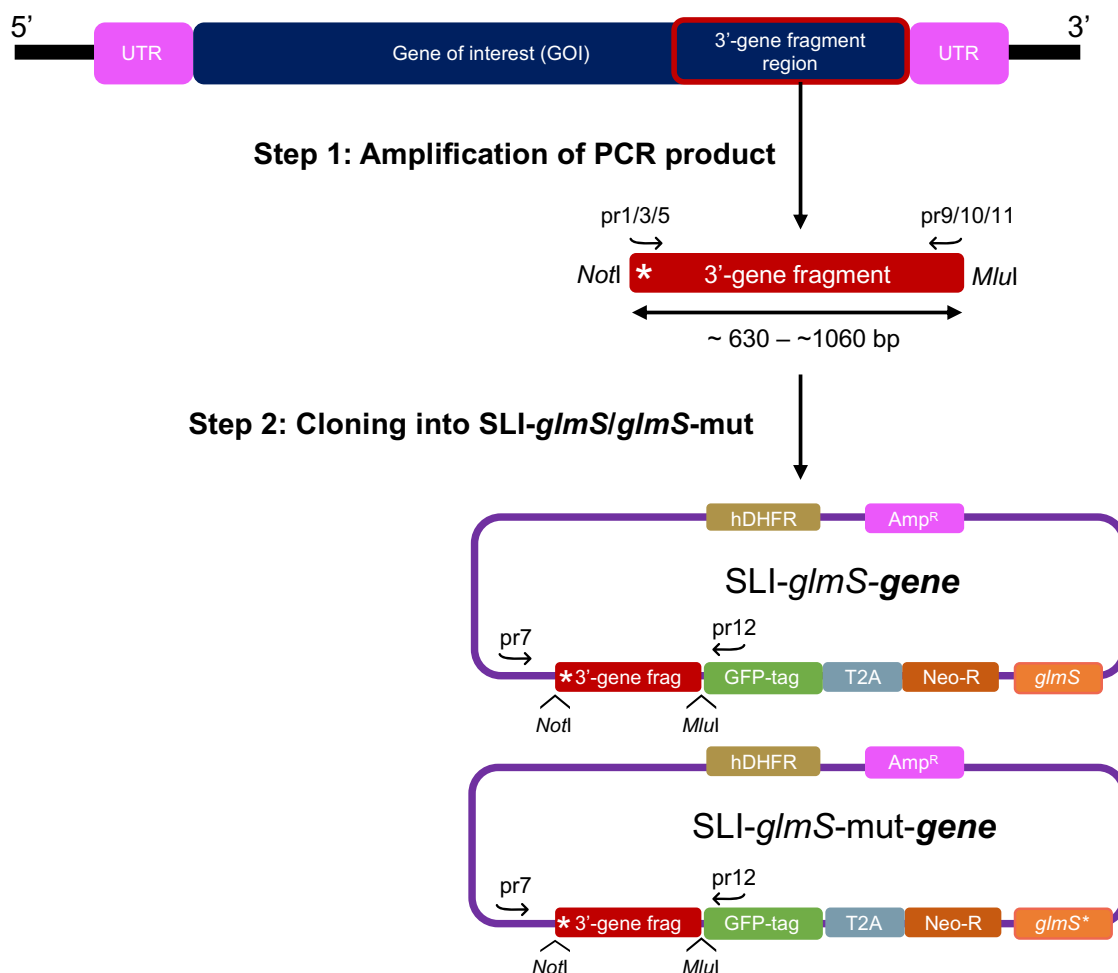
Figure 2–2: Cloning strategy to produce recombinant SLI-*glmS* and SLI-*glmS*-mut plasmids for transfection. Step 1: The selected 3'-gene fragment regions of the putative kinase genes were amplified using the specified primer pairs listed in Table 1. Step 2: the amplified 3'-gene fragments were cloned into SLI-*glmS*/*glmS*-mut plasmids. SLI-*glmS*/*glmS*-mut plasmid backbone primers flanking the insert region are indicated by the specific primer code. **Asterisk (*)**: TAA stop codon. **GFP-tag**: green fluorescent protein tag. **Amp^R**: ampicillin resistance selection marker. **hDHFR:** human dihydrofolate reductase resistance selection marker. **Neo-R**: neomycin resistance selection marker. **T2A**: skip peptide. ***glmS***: functional glucosamine-6-phosphate riboswitch ribozyme. ***glmS****: non-functional glucosamine-6-phosphate riboswitch ribozyme.

Successfully amplified gene fragments were excised from the agarose gel and purified using a NucleoSpin Gel and PCR clean-up kit, following the manufacturer's instructions. The DNA concentration of each sample was determined as described in section 2.4.2 and stored at -20 °C until use.

2.5.1. Cloning of amplified 3'-gene fragments into SLI-*glmS* and SLI-*glmS*-mut plasmids

The amplified 3'-gene fragments were directionally cloned into the SLI-*glmS* and SLI-*glmS*-mut plasmids and plasmid DNA was isolated and verified through RE mapping described in section 2.4.3. However, instead of using the RE 3 U *Avr*II, 3 U *Mlu*I-HF was used. To prepare the 3'-gene fragments and SLI-*glmS*/*glmS*-mut plasmids for downstream ligation experiments, the gene fragments and verified SLI-*glmS*/*glmS*-mut were digested with the respective restriction enzymes to produce 5'- and 3'-overhangs required for sticky-end ligation (outlined in Figure 2-2). The digested plasmid products were separated on an agarose gel, and the plasmid backbone was excised from the gel. The 3'-gene fragments and plasmid backbone were purified using a NucleoSpin Gel and PCR Clean-up kit following the manufacturer's instructions and stored at -20 °C until use. The ligation reactions performed as described in section 2.4.3.

2.5.2. Screening and confirmation of recombinant SLI-*glmS* and SLI-*glmS*-mut plasmids

The colony screening PCR procedure was as described in section 2.4.4, where bacterial cultures of suspected positive clones were screened by PCR and RE mapping, using 5 pmol of Lz116 forward primer. However, a different reverse primer, Lz114, was used for these screening PCRs, as listed in Table 4.

Table 4: Primer sequences used for colony PCR and sequencing. The primer sequences flank the 3'insert region within the SLI-*glmS* and SLI-*glmS*-mut plasmid. Primer Lz116 is located upstream of the insert region and primer Lz114 is located downstream of the insert region.

Plasmid ID	Primer ID	Orientation	Primer code	Primer sequence (5' - 3')
SLI-*glmS*/*glmS*-mut	Lz_116	Forward	pr7	AGCGGATAACAATTTCACACAGGA
	Lz_114	Reverse	pr12	ACAAGAATTGGGACAACTCCAGTGA

Plasmid DNA was isolated and purified from the saturated bacterial cultures and subjected to RE mapping using *Not*I-HF and *Mlu*I-HF to verify if each respective gene fragment of interest was successfully ligated into the plasmid. To further validate the identity of the insert, Sanger sequencing was performed using the BigDye 3.1 sequencing kit and 5 pmol of either the forward (Lz116) or reverse (Lz114) primers, as described in section 2.4.4. The successfully generated recombinant SLI-*glmS* plasmids will be referred to as SLI-*glmS*-*0105800,* SLI-*glmS*-*1112100* and SLI-*glmS*-*1364400* and for the recombinant SLI-*glmS*-mut plasmids SLI-*glmS*-mut-*0105800,* SLI-*glmS*-mut-*1112100* and SLI-*glmS*-mut-*1364400* hereafter.

2.6. Recombinant plasmid preparation and transfection of asexual *P. falciparum* parasites

The recombinant SLI-TGD plasmids (SLI-TGD-*0105800,* SLI-TGD-*1112100* and SLI-TGD-*1364400*) were generated in a previous study (H Langeveld, BSc Hons, University of Pretoria, 2019) and were prepared here for transfection of *P. falciparum* parasites, described below. In all cases, ~440–830 bp of the 5'-end of the coding strand of the gene was displaced to generate N-terminal truncated versions of the proteins, which should be non-functional, leading to targeted gene deletion.

2.6.1. Large scale plasmid isolation

Of the successfully generated recombinant SLI-plasmids, 100 ng of plasmid DNA was used to transform 100 µL of competent DH5α *E. coli* cells as described in section 2.4.3. The transformed bacterial cultures were then transferred to 5 mL of fresh LB-amp medium (50 µg/mL ampicillin) and grown at 37 °C O/N in a shaking incubator at ~180 rpm. After this, 3 mL of the saturated bacterial culture was used to inoculate 200 mL of LB-amp medium (50 µg/mL ampicillin) and grown at 37 °C O/N in a shaking incubator at ~180 rpm in order obtain greater quantities of the plasmid DNA. Plasmid DNA was isolated from saturated bacterial cultures using a NucleoBond® Xtra Midi / Maxi purification kit (Macherey-Nagel GmbH & Co.KG, Germany) according to manufacturer's specification. After plasmid DNA isolation, ~1–2 µg of plasmid DNA was subjected to RE mapping to verify the identity of the recombinant plasmid DNA using the respective RE enzymes combinations: *Not*I-HF and *Mlu*I-HF for SLI-TGD and SLI-*glmS*/*glmS*-mut, and *Not*I-HF and *Avr*II for SLI-sandwich.

After validation of the recombinant plasmid DNA identity, the eluted plasmid DNA was concentrated by adding 3.5 mL of ice-cold isopropanol to the eluted plasmid DNA, vortexed for ~6–10 s and centrifuged at 15000 *xg* for 30 min at 4 °C. Thereafter, 1 mL of 70 % (v/v) ethanol was added to the DNA pellet and centrifuged as described above for 15 min, after which the ethanol was removed, and the pelleted DNA was allowed to dry at 50 °C in a heating block. Once dried, the pellet was resuspended in 250 µL dddH$_2$O and stored at -20 °C until further use. One to two days before transfection, 100–250 µg of the respective recombinant plasmid DNA was pelleted with EtOH precipitation (as described in section 2.4.4) to allow resuspension of the DNA pellets into 250 µL cytomix (120 mM KCl, 0.15 mM CaCl$_2$, 2 mM EGTA, 5 mM MgCl$_2$, 10 mM K$_2$PO$_4$, 25 mM HEPES, pH 7.6) for downstream transfection experiments. These DNA samples were stored at -20 °C.

2.6.2. Transfection of asexual *P. falciparum* parasites

P. falciparum (NF54) parasite cultures consisting of >5 % ring-stage parasites (5 % haematocrit) was used for each transfection procedure. The parasitaemia of the parasite cultures was determined 3 h before transfection. The cultures were centrifuged (3500 *xg* for 3 min) to remove spent medium and washed once with cytomix (1:1), then centrifuged again as previously stated. The parasite-infected

erythrocyte pellets (200 μL) were resuspended in 250 μL of cytomix containing a total of 70–250 μg of recombinant SLI-plasmid DNA to yield a final volume of 450 μL. The mixtures were transferred to pre-chilled 2 mm electroporation cuvettes and electroporated using a Gene Pulser Xcell Electroporation System (BioRad, USA) at a high capacitance of 950 μF and a low voltage of 310 V, ensuring optimal time constants of 10–20 ms.

Electroporated, infected erythrocytes were mixed with 2 mL pre-warmed culture medium and transferred to a culture flask containing 3 mL pre-warmed culture medium, and parasites were allowed to recover at 37 °C for 2–3 h. The recovered parasite culture was centrifuged at 3500 xg for 3 min and lysed erythrocyte debris was aspirated. Transfected cells were resuspended in 5 mL pre-warmed culture medium supplemented with 100 μL fresh erythrocytes (50 % haematocrit) to compensate for lysed cells during electroporation and transferred back to the stationary incubator at 37 °C in a 90 % N_2, 5 % O_2 and 5 % CO_2 atmosphere. This was regarded as day 0 of transfection.

2.7.   Selection and validation of transgenic parasite lines

To successfully obtain transgenic parasite lines for downstream evaluation, transfected parasites were selected for episomal uptake and integration of the recombinant SLI plasmids into *P. falciparum* asexual parasites (Figure 2-3), with various checkpoints throughout the selection process to confirm success.
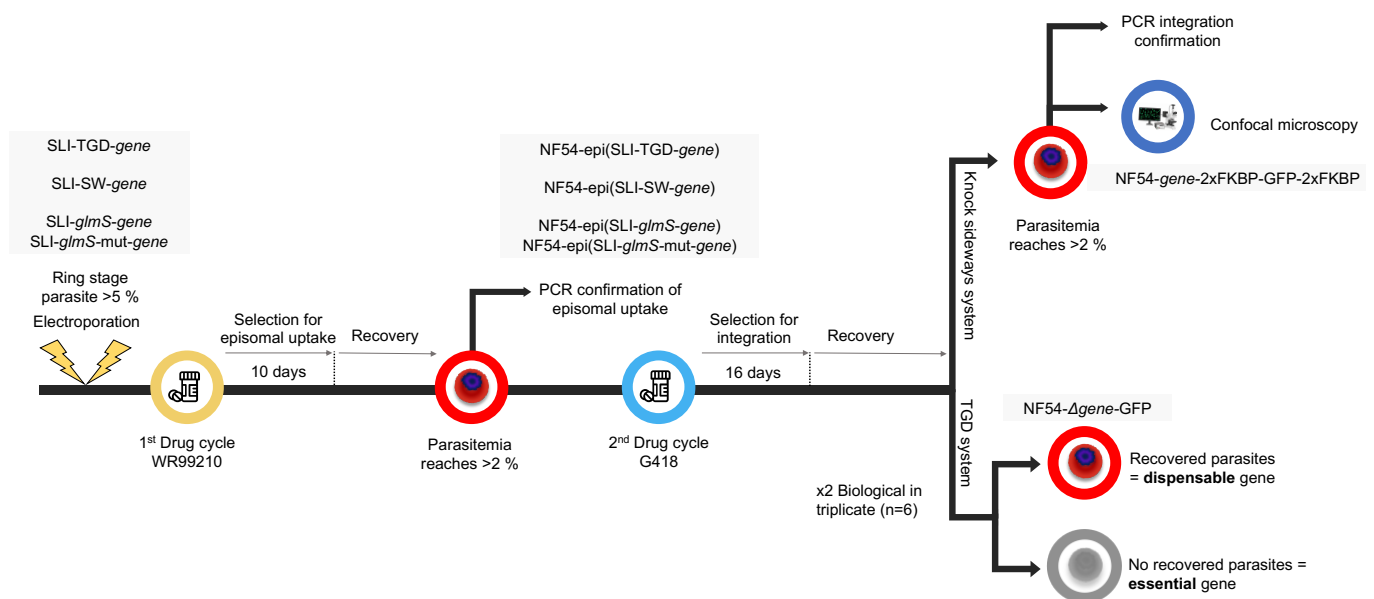
Figure 2–3: Drug selection and screening of transgenic parasites to confirm episomal uptake and integration of recombinant SLI-plasmids. NF54 parasite cultures of >5 % ring-staged were transfected with recombinant SLI-TGD-*gene,* SLI-SW-*gene*, SLI-*glmS* and SLI-*glmS*-mut plasmids through electroporation. The transfected parasites were selected for episomal uptake of the recombinant plasmids with WR99210 for 10 consecutive days and episomal uptake was confirmed via PCR on recovered parasites. NF54-epi(SLI-TGD-*gene*) and NF54-epi(SLI-SW-*gene*) parasites were placed under G418 drug selection for 10 consecutive days and every thereafter for a total of 16 days. Each biological replicate of NF54-epi(SLI-TGD-*gene*) cultures was split in triplicate before G418 selection. Essentiality was determined after 4 weeks in recovery. Integration of recombinant SLI-SW-*gene* plasmid was confirmed via PCR and knock sideways studies were completed using fluorescent confocal microscopy.

2.7.1. Selection for and confirmation of recombinant SLI-TGD, SLI-sandwich and SLI-*glmS*/*glmS*-mut episomal uptake

The day after transfection (day 1), transfected *P. falciparum* parasite cultures were maintained under selective single-drug pressure for 10 consecutive days to mediate episomal uptake of the plasmids through the addition of 4 nM of WR99210 (Jacobus Pharmaceuticals, USA) [106]. WR99210, an antifolate drug, is a potent inhibitor of *P. falciparum* DHFR, preventing nucleic acid synthesis and killing parasites [109]. However, parasites where episomal uptake took place will have the resistance marker, human hDHFR, present on the SLI-plasmid backbone, and only parasites that have taken up and maintained the SLI-plasmids episomally are able to survive [106, 109]. Culture medium containing WR99210 was changed every day throughout a 10-day selection period (Figure 2-3). After this, drug pressure was removed, and complete medium was changed twice weekly until parasite recovery was established. Fresh erythrocytes were added every 7 days to replace lysed erythrocytes and to maintain a 5 % haematocrit. After three weeks in drug-free medium, parasites recovered, and once the parasitaemia reached >4 %, samples were collected, and genomic DNA was isolated from majority trophozoite stage cultures using the Quick gDNA Mini-Prep kit (Zymo, USA) as per manufactures specifications as described in section 2.4.1.

To determine the episomal presence of the recombinant SLI-plasmids, amplification of the gene fragment insert region was completed using the respective SLI-plasmid backbone primers listed in Table 2 for SLI-sandwich and Table 4 for SLI-TGD and SLI-*glmS*/*glmS*-mut (Figure 2-4). Each PCR amplification reaction consisted of 5 pmol of plasmid backbone primer (Table 2 and 4) with ~20–40 ng of template DNA and 1x KAPA-Taq polymerase, while the negative control contained no template DNA. Thermocycler settings consisted of an initial denaturation step at 95 °C for 5 min, followed by denaturation at 95 °C for 30 s, 58 °C for 30 s for annealing of primers and 68 C for 90 s extension for 30 cycles. PCR products were analysed using gel electrophoresis as described in section 2.4.2.
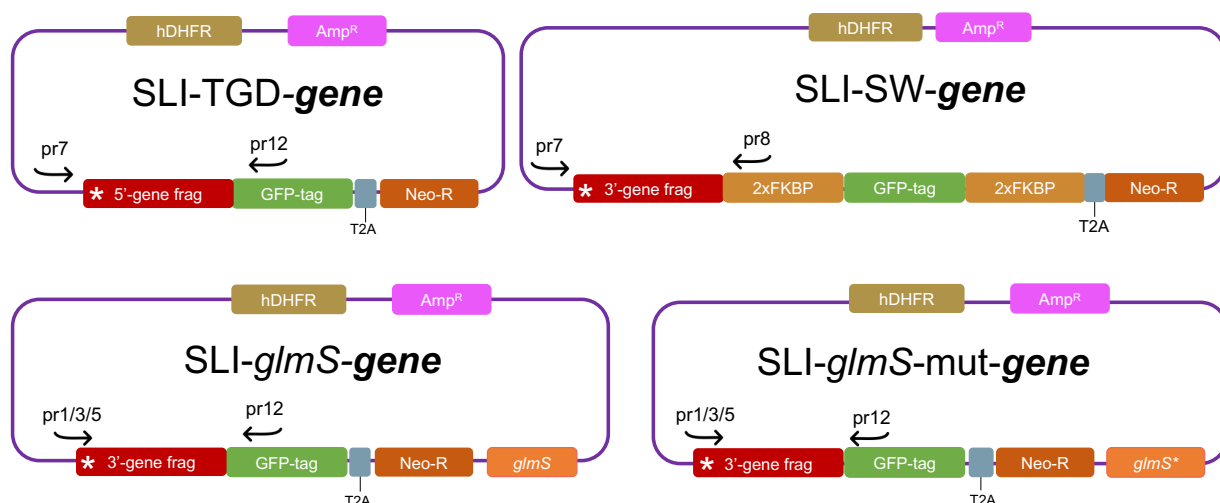
Figure 2–4: Schematic representation of primer combinations used to determine successful episomal uptake of recombinant SLI-TGD, SLI-sandwich and SLI-*glmS*/*glmS*-mut plasmids. The different primers used to screen for episomal uptake are indicated on the respective recombinant plasmids. The primers used are situated upstream and downstream of the insert region within the plasmids. The primers used for SLI-SW-*gene* episomal uptake are listed in Table 2 while primers used in SLI-TGD-*gene* and SLI-*glmS*/*glmS*-mut episomal screening are listed in Table 4.

31

Following confirmation of episomal uptake by PCR amplification, parasite culture volumes were increase to 20 mL by adding culture medium and fresh erythrocytes, maintaining a 5 % haematocrit. Once the parasitaemia of the 20 mL cultures reached >5 % ring-stage parasites, 10 mL of the culture was split off and centrifuged for 5 min at 3500 *xg*. The supernatant was aspirated and the 500 µL of packed erythrocyte pelleted was subsequently resuspended in freezing medium (28 % (v/v) glycerol, 3 % (w/v) D-sorbitol, 0.65 % (w/v) NaCl) in a 1:1 ratio and stored in liquid nitrogen. New culture medium and fresh erythrocytes were added to the remaining 10 mL cultures, maintaining a 5 % haematocrit. This process was repeated 3-4 times on sequential cycles to ensure adequate parasite stocks for future work. The recombinant parasites lines were referred to as NF54-epi(SLI-SW-*gene*) for SLI-sandwich, NF54-epi(SLI-TGD-*gene*) for SLI-TGD and NF54-epi(SLI-*glmS*/-mut-*gene*) for SLI-*glmS*/*glmS*-mut.

2.7.2. Selection for genomic integration of SLI-TGD and SLI-sandwich

Recombinant parasite lines (NF54-epi(SLI-TGD-*0105800*), NF54-epi(SLI-TGD-*1112100*) and NF54-epi(SLI-TGD-*1364400*)) were cultivated to a ~2–4 % parasitaemia and were split into three 5 mL (5 % haematocrit) cultures and subjected to a second drug selection cycle with 400 µg/mL G418 (Thermo Fisher Scientific). G418 (geneticin – an analogue of neomycin sulphate and used for selection of eukaryotic cells displaying neomycin resistance markers), blocks polypeptide synthesis and ensures that only parasites with genomic integration will survive, as the neomycin resistance marker is expressed under the endogenous promoter of the selected gene [108].

NF54-epi(SLI-TGD-*0105800*), NF54-epi(SLI-TGD-*1112100*) and NF54-epi(SLI-TGD-*1364400*) cultures were additionally synchronised and subsequently placed under G418 selection to further delineate the contribution of these putative protein kinases to a particular phase of the cell cycle and associated asexual replication cycle. Cultures of ~2–3 % parasitaemia (>50 % ring stage parasites) were synchronised once with 5 % (w/v) D-sorbitol as described in section 2.3. Synchronised cultures were then placed under G418 (400 µg/mL) drug pressure for six days, until no parasites were observed on a thin blood smear. Parasite distributions for each culture were evaluated by counting ~500–1000 erythrocytes on Rapi-Diff-stained thin blood smears at 1000x magnification every 24 h.

For the knock sideways lines, NF54-epi(SLI-SW-*0105800*), NF54-epi(SLI-SW-*1112100*) and NF54-epi(SLI-SW-*1364400*) cultures of ~2–4 % parasitaemia were maintained in single culture flasks each and subjected to 400 µg/mL G418 drug pressure. Complete culture medium containing G418 was changed every day for the first 10 days and thereafter every second day for a total of 16 days for all of the above parasite lines [106] (Figure 2-3). Following selection, drug pressure was removed, and cultures were cultured twice weekly in drug-free culture medium until parasitaemia recovered (Figure 2-3). Fresh erythrocytes were added once a week to maintain a 5 % haematocrit.

Parasites reappeared during the recovery period for each of the lines undergoing selection for SLI-SW-*gene* plasmid integration. PCR screening could therefore be performed once the parasitaemia reached >4 %. Figure 2-5 provides a schematic overview of the locations of the primers used to evaluate if successful integration occurred. The PCR reactions contained 5 pmol of the forward and reverse primers listed in Table 5 alongside 1x KAPA-Taq polymerase and genomic DNA isolated from recovered parasites. A two-step PCR was used with an initial denaturation at 95 °C for 5 min, then 30 cycles of denaturation at 95 °C for 30 s with a merged annealing and extension step for 3 min at 60 °C.
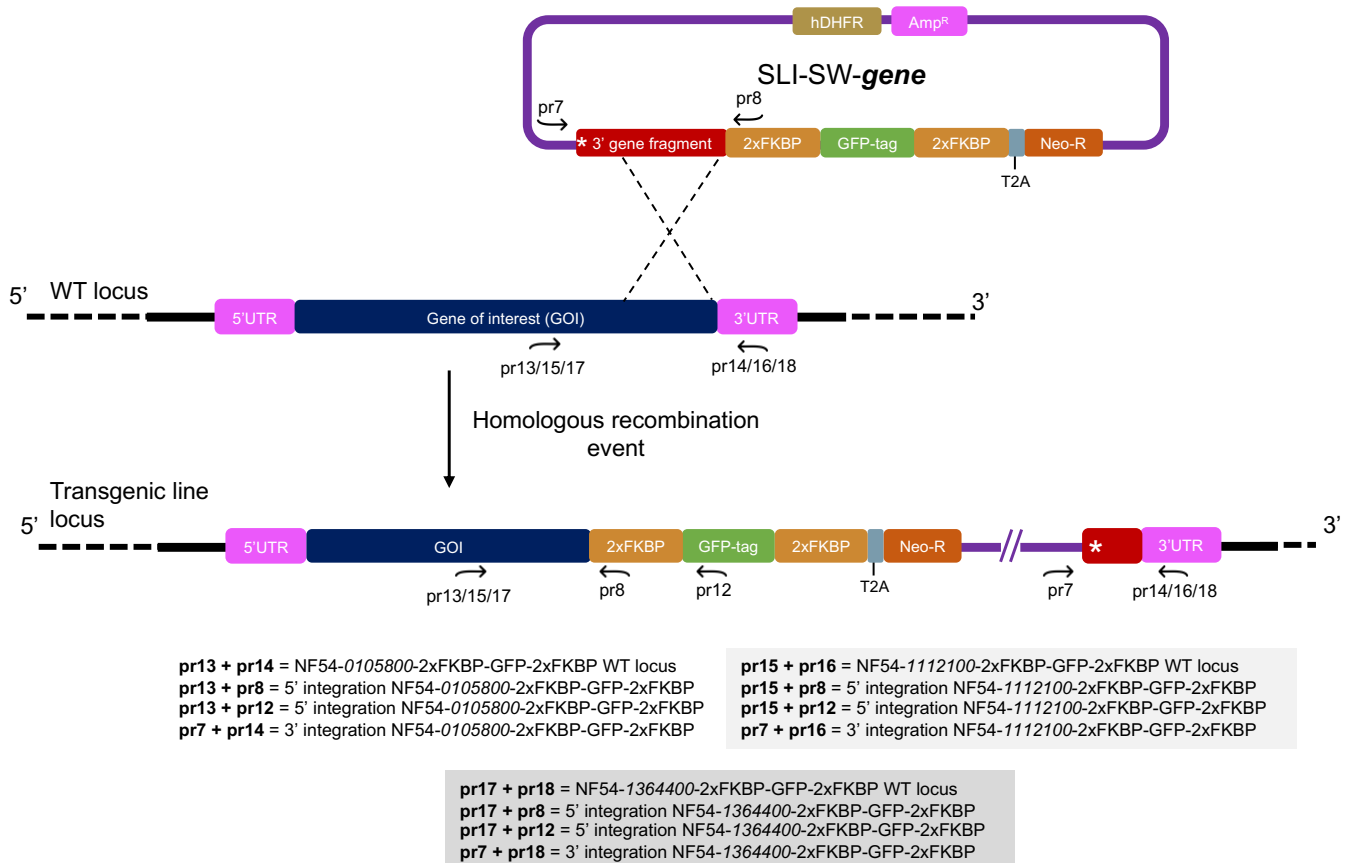
Figure 2–5: Schematic representation of determination of successful integration of recombinant SLI-sandwich plasmid into parasite genome. Schematic of the recombinant SLI-SW-*gene* plasmid undergoing a single homologous recombinant event into the wild-type (WT) of the target gene. Primers used in determining successful integration are indicated by the respective primer codes (pr) and arrows (indicting direction of the respective primer) along with the different primer combinations used listed in Table 5.

PCR products were analysed using gel electrophoresis RE mapping as described in section 2.4.3. Where amplification of the wild-type (WT) locus indicated continued presence of WT parasites within the recovered parasite cultures, these were placed under an additional round of 800 µg/mL G418 drug selection to eliminate remaining WT parasites. Once integration had been confirmed and no WT parasites remained, parasite cultures were stored in liquid nitrogen as described in section 2.7.1. Recombinant parasite lines are referred to as NF54-*0105800*-2xFKBP-GFP-2xFKBP, NF54-*1112100*-2xFKBP-GFP-2xFKBP and NF54-*1364400*-2xFKBP-GFP-2xFKBP.

Table 5: PCR primers used to confirm 5', 3' integration and wild-type loci in recombinant parasite lines NF54-*0105800*-2xFKBP-GFP-2xFKBP, NF54-*1112100*-2xFKBP-GFP-2xFKBP and NF54-*1364400*-2xFKBP-GFP-2xFKBP.

Parasite line	Primer ID	Orientation	Primer code	Primer sequence (5' - 3')	PCR product length (bp)
NF54-*0105800*-2xFKBP-GFP-2xFKBP	5' integration	Forward	pr13	GCGGAAGATTTTGAGAACAACGATA	1517
		Reverse	pr8	TCTCTGCAGAGCAGCTCTAGCA	
		Reverse	pr12	ACAAGAATTGGGACAACTCCAGTGA	2271
	3' integration	Forward	pr7	AGCGGATAACAATTTCACACAGGA	1643
		Reverse	pr14	GGAGGGTACACCATAACAAAAGAGC	
	WT locus	Forward	pr13	GCGGAAGATTTTGAGAACAACGATA	1966
		Reverse	pr14	GGAGGGTACACCATAACAAAAGAGC	
NF54-*1112100*-2xFKBP-GFP-2xFKBP	5' integration	Forward	pr15	GCTCCTCCAGTTTATATGATGAAAATCATG	1265
		Reverse	pr8	TCTCTGCAGAGCAGCTCTAGCA	
		Reverse	pr12	ACAAGAATTGGGACAACTCCAGTGA	2020
	3' integration	Forward	pr7	AGCGGATAACAATTTCACACAGGA	930
		Reverse	pr16	GGAAAAAACACATGAAAAATGAGAATTATATGATAAC	
	WT locus	Forward	pr15	GCTCCTCCAGTTTATATGATGAAAATCATG	1420
		Reverse	pr16	GGAAAAAACACATGAAAAATGAGAATTATATGATAAC	
NF54-*1364400*-2xFKBP-GFP-2xFKBP	5' integration	Forward	pr17	TATACAAACATCAACGGTATCAATGAATTGTC	1440
		Reverse	pr8	TCTCTGCAGAGCAGCTCTAGCA	
		Reverse	pr12	ACAAGAATTGGGACAACTCCAGTGA	2200
	3' integration	Forward	pr7	AGCGGATAACAATTTCACACAGGA	1210
		Reverse	pr18	GAACAGTACACACAAAATAAATTCGTATGG	
	WT locus	Forward	pr17	TATACAAACATCAACGGTATCAATGAATTGTC	1545
		Reverse	pr18	GAACAGTACACACAAAATAAATTCGTATGG	

2.8. Growth rate and morphological analysis of NF54-*0105800*-2xFKBP-GFP-2xFKBP and NF54-*1112100*-2xFKBP-GFP-2xFKBP transgenic lines

To evaluate if the genetic alterations had any undesirable effects on parasite morphology and proliferation, the transgenic NF54-*0105800*-2xFKBP-GFP-2xFKBP and NF54-*1112100*-2xFKBP-GFP-2xFKBP lines were assessed by quantifying the different asexual stages compared to WT NF54 *P. falciparum* parasites. For evaluation of proliferation, both transgenic lines and WT NF54 cultures were synchronised twice as described in section 2.3. After the second round of synchronisation, parasitaemia of the various cultures was determined by counting ~1000–1500 erythrocytes on Rapi-Diff-stained thin blood smears at 1000x magnification and parasitaemia was adjusted to ~0.5 %. Parasite proliferation was evaluated every 24 h for a period of 120 h (2.5 life cycles) with Rapi-Diff-stained blood smears with parasitaemia determined as described earlier and compared to WT NF54.

2.9. Fluorescent evaluation of transgenic *P. falciparum* parasites lines using confocal microscopy

The 1 mm coverslips (Menzel-Gläser, Germany) were cleaned in 1 M HCl and left at 4 °C for 24 h, after which they were rinsed with dddH$_2$O three times to remove remaining HCl. To remove any chemical residue, coverslips were rinsed three times with 100 % EtOH. Parasite adherence to the coverslip surface was ensured through application of a cationic surface charge by incubating coverslips in 0.01 % (w/v) poly-L-lysine (PPL) (Sigma Aldrich, USA) for 5–10 min, allowing ionic attraction to negative charges in cell membranes. The coverslips were stored at 4 °C until use.

Samples of 2–3 mL intraerythrocytic *P. falciparum* parasites (5 % haematocrit, 2–5 % parasitaemia) were aliquoted and centrifuged at 3000 *xg* for 3 min. To minimise background fluorescence, culture medium was removed from each sample and samples were washed three times in 2 mL 1x PBS (0.137 M NaCl, 3 mM KCl, 1.9 mM NaH$_2$PO$_4$, 8.1 mM Na$_2$HPO$_4$) at room temperature and centrifuged at 3000 *xg* for 3 min between wash steps. The haematocrit was adjusted to ~2–3 % in 1x PBS. Parasite nuclei were stained by incubation in 30 mM Hoechst 33342 at room temperature for 30 min. The samples were washed three times in 1x PBS and centrifuged at 3000 *xg* to remove any residual Hoechst.

P. falciparum parasites were transferred to the poly-L-lysine-coated coverslips and centrifuged for 3 min at 300 *xg,* and non-adherent cells were carefully removed with 1x iso-PBS (1–2 mL). Preservation of parasite sub-cellular molecular arrangements at a given time is required for accurate parasite morphology assessment. The parasites were therefore fixed by adding 2 mL of a 4 % (w/v) formaldehyde and 0.025 % (v/v) glutaraldehyde fixative in 1x PBS to the coverslips and incubating for 45–60 min at room temperature to create cross-linkages between amine groups on proteins and nucleic acids. The fixative was removed by aspirating, and remaining fixative was gently removed by washing the coverslips twice with PBS-T (1x Iso-PBS with 0.1 % (v/v) Tween-20). Fluoroshield (Sigma Aldrich, USA) was added to the coverslip to minimise the quenching of the fluorescent dyes. The coverslip was affixed to a slide and sealed and stored at 4 °C in the dark until use.

For parasite kinase protein localisation and mislocalisation experiments, imaging was performed on a Zeiss LSM 880 Inverted Confocal Laser Scanning Microscope (LSM) with an Airyscan detector (Zeiss, Germany) for super-resolution imaging with appropriate channels, based on fluorophore emission and excitation wavelengths. GFP has an excitation wavelength of 488 nm and emission at 500 nm, which could be detected through the green channel. Hoechst has an excitation wavelength of 350 nm and emission at 460–490 nm and could therefore be detected on the blue channel. A 100x oil immersion objective with 1.4 numerical aperture was used for imaging parasites. Zeiss ZEN lite blue edition software (Zeiss, Germany) was used for digital image processing.

2.10. Knock sideways of NF54-*0105800*-2xFKBP-GFP-2xFKBP and NF54-*1112100*-2xFKBP-GFP-2xFKBP

2.10.1. Transfection and selection of pLyn-FRB-*mcherry*-nmd3-BSD and p1xNLS-FRB-*mcherry*-hsp86-BSD into transgenic line

Before the knock-sideways system could be performed to remove the selected target protein from its predicted site of action, an additional plasmid (pLyn-FRB-mcherry-nmd3-BSD and p1xNLS-FRB-mcherry-hsp86-BSD) encoding a mislocaliser sequence for an episomally-expressed FRB protein was transfected into the existing recombinant NF54-*0105800*-2xFKBP-GFP-2xFKBP, NF54-*1112100*-2xFKBP-GFP-2xFKBP and NF54-*1364400*-2xFKBP-GFP-2xFKBP lines. The FRB protein is important for protein-protein dimerisation with the FKBP proteins attached to the target kinase protein, thereby achieving mislocalisation after introduction to the NF54-*gene*-2xFKBP-GFP-2xFKBP transgenic line. The pLyn-FRB-mcherry-nmd3-BSD plasmid contains a plasma membrane mislocaliser, Lyn (lyn proto-oncogene fragment) sequence, while p1xNLS-FRB-mcherry-hsp86-BSD contains a nuclear mislocaliser, SV40 Large T-antigen nuclear localisation signal (NLS) derived peptide sequence. In both mislocalising plasmids, an mCherry tag is included attached to the FRB to trace cellular localisation through red fluorescence.

To isolate large quantities of pure pLyn-FRB-mcherry-nmd3-BSD and p1xNLS-FRB-mcherry-hsp86-BSD plasmid DNA, the same large-scale plasmid isolation procedure described in section 2.6.1 was used. Before proceeding to further purification, 1–2 µg of DNA was subjected to RE mapping using 3 U each of *Mlu*I-HF + *Xma*I and 3 U each of *Xma*I + *Xho*I to verify the identities of the plasmid DNA as pLyn-FRB-mcherry-nmd3-BSD and p1xNLS-FRB-mcherry-hsp86-BSD (Figure 2-6). The plasmid DNA was then subjected to further isopropanol and EtOH purification steps as described in section 2.6.1 to prepare for downstream transfection.

Separate transfection of pLyn-FRB-mcherry-nmd3-BSD and p1xNLS-FRB-mcherry-hsp86-BSD was performed using NF54-*0105800*-2xFKBP-GFP-2xFKBP and NF54-*1112100*-2xFKBP-GFP-2xFKBP transgenic parasites as generated in section 2.6.2. Episomal selection was, however, completed under blasticidin selection for presence of the BSD selection marker. The transfected parasite cultures were subjected to 2 µg/mL blasticidin drug pressure (Thermo Fisher Scientific, USA) for 8 consecutive days and allowed to recover. Recovered culture volumes were increased to 20 mL and DNA was extracted as described in section 2.7.1. Figure 2-6 indicates the primer combinations used for confirmation of episomal uptake of pLyn-FRB-mcherry-nmd3-BSD and p1xNLS-FRB-mcherry-hsp86-BSD through PCR amplification.

To isolate large quantities of pure p1xNLS-FRB-mcherry-hsp86-BSD and pLyn-FRB-mcherry-nmd3-BSD plasmid DNA, the same large scale plasmid isolation procedure described in section 2.6.1 was used. Before proceeding to further purification, 1–2 µg of DNA was subjected to RE mapping using

3 U *Mlu*I-HF and 3 U *Xma*I in one reaction and 3 U *Xma*I and 3 U *Xho*I in another to verify the identity of the plasmid DNA as pLyn-FRB-mcherry-nmd3-BSD and p1xNLS-FRB-mcherry-hsp86-BSD (Figure 2-6). The plasmid DNA was then subjected to further isopropanol and EtOH purification steps as described in section 2.6.1 to prepare for downstream transfection.
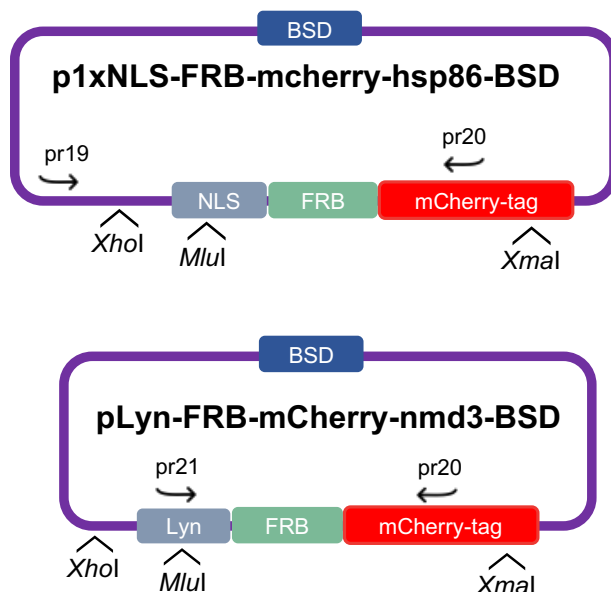
Figure 2–6: Schematic representation of pLyn-FRB-mcherry-nmd3-BSD and p1xNLS-FRB-mcherry-hsp86-BSD plasmid and episomal uptake confirmation primer combinations. The plasmids include mislocaliser sequences, Lyn (lyn proto-oncogene fragment) for plasma membrane mislocalisation and NLS (SV40 Large T-antigen nuclear localisation signal derived peptide) for nuclear mislocalisation, FRB (FKBP12-rapamycin binding domain) and a mcherry cassette. The primer combinations used in PCR amplification reactions used to confirm episomal uptake are indicated by arrows as well as primer codes corresponding to primers listed in Table 6.

Once parasitaemia of the recovered transfected parasite culture reached >4 %, samples were collected, and genomic DNA was isolated using the Quick gDNA Mini-Prep kit as before. To determine if the pLyn-FRB-mcherry-nmd3-BSD and p1xNLS-FRB-mcherry-hsp86-BSD plasmids were present episomally, PCR screening was performed with ~20–40 ng template DNA using 1x KAPA-Taq polymerase and 5 pmol of forward and revers primers listed in Table 6.

Table 6: Primer sequences used for episomal uptake confirmation of pLyn-FRB-mcherry-nmd3-BSD and p1xNLS-FRB-mcherry-hsp86-BSD

Plasmid ID	Primer ID	Orientation	Primer code	Primer sequence (5' - 3')	PCR product length (bp)
p1xNLS-FRB-mcherry-hsp86-BSD	pHSP86_F	Forward	pr19	GAAAGGGGCCATTGGATATATATTTAGT	1488
	mcherry_Rv	Reverse	pr20	CCTTGGTCACCTTCAGCTTGG	
pLyn-FRB-mcherry-nmd3-BSD	mcherry_Fw	Forward	pr21	CGAGATGGGATGTATAAAATCAAAAGGGA	647
	mcherry_Rv	Reverse	pr20	CCTTGGTCACCTTCAGCTTGG	

The thermocycler cycler settings used for the screening reactions included an initial denaturation step at 95 °C for 5 min followed by a denaturation at 95 °C for 30 s, 52 °C for 30 s for annealing of primers

and 68 °C for 90 s for extension. Amplified fragments were analysed using gel electrophoresis as described in section 2.4.2.

2.10.2. Functional analysis of NF54-*0105800*-2xFKBP-GFP-2xFKBP and NF54-*1112100*-2xFKBP-GFP-2xFKBP nuclear and plasma membrane mislocalisation

NF54-*0105800*-2xFKBP-GFP-2xFKBP and NF54-*1112100*-2xFKBP-GFP-2xFKBP parasite cultures that episomally maintained the p1xNLS-FRB-mcherry-hsp86-BSD and pLyn-FRB-mcherry-nmd3-BSD were subjected to two synchronisation steps, as described in section 2.3, to obtain a tightly synchronised 10 mL culture at ~2–5 % parasitaemia (>95 % ring-stage parasites). This was split into two 5 mL cultures, of which one was used to assess mislocalisation using confocal microscopy, described in section 2.9, whilst the other culture was used to determine the effect of nuclear mislocalisation on asexual parasite proliferation.

For the fluorescent assessment, parasites were allowed to progress into late trophozoite/schizont-stage parasites, whereupon 250 nM of rapalog (25 µM in culture medium, AP21967, Clontech, Takara Bio, Japan) was added and incubated at 37 °C for 1 h. The addition of rapalog induces FKBP/FRB dimerisation, thereby inducing mislocalisation of the target protein. After this, parasite samples were taken and prepared for fluorescence confocal microscopy as described in section 2.9. The mCherry protein has an excitation wavelength of 587 nm and an emission of 610 nm which is detectable through the red channel. A 5 mL synchronised culture (>95 % ring-stage parasites) was split into two 2 mL cultures and the parasitaemia was adjusted to ~0.5 %. One culture was used as a vehicle control (- Rap) while to the other 250 nM of rapalog (25 µM in culture medium, AP21967, Clontech, Takara Bio, Japan) was added every 24 h (+ Rap) for a period of 96 h (2 life cycles). Parasite proliferation was evaluated every 24 h with Rapi-Diff-stained blood smears and parasitaemia was determined by counting ~1000–1500 erythrocytes at 1000x magnification.

Chapter 3: Results

3.1. *In silico* analysis of selected putative kinase proteins

3.1.1. Protein domain predictions of the selected kinase proteins

To obtain a clearer indication of the potential of the three proteins under investigation as potential kinase protein family members, *in silico* analyses were performed. Protein domain and family predictions were done using InterPro and SMART to evaluate the identity and functionality of each PF3D7_0105800, PF3D7_1112100 and PF3D7_1364400.

PF3D7_0105800 encodes a 99 kDa protein that contained a signature that defines cyclin-dependent regulatory subunit (CKS) family members (InterPro: IPR000789), as well as a cyclin-dependent regulatory subunit superfamily signature (IPR036858); both are located at the C-terminus of the protein (residues 736–831) (Figure 3-1A). These signatures were confirmed using SMART (Figure 3-1B). This indicates the possibility that PF3D7_0105800 could have CDK-related function. CKS proteins from mammalians are typically associated in a hexamer, with symmetrical interlocking repeats of three small (~16 kDa) homodimers (PMID: 8211159). The larger size of the proposed CKS member in *P. falciparum* encoded by PF3D7_0105800 is attributed to an extended N-terminus containing low-complexity regions, typical of proteins from this parasite [110], and a single coiled-coil domain (Figure 3-1B).
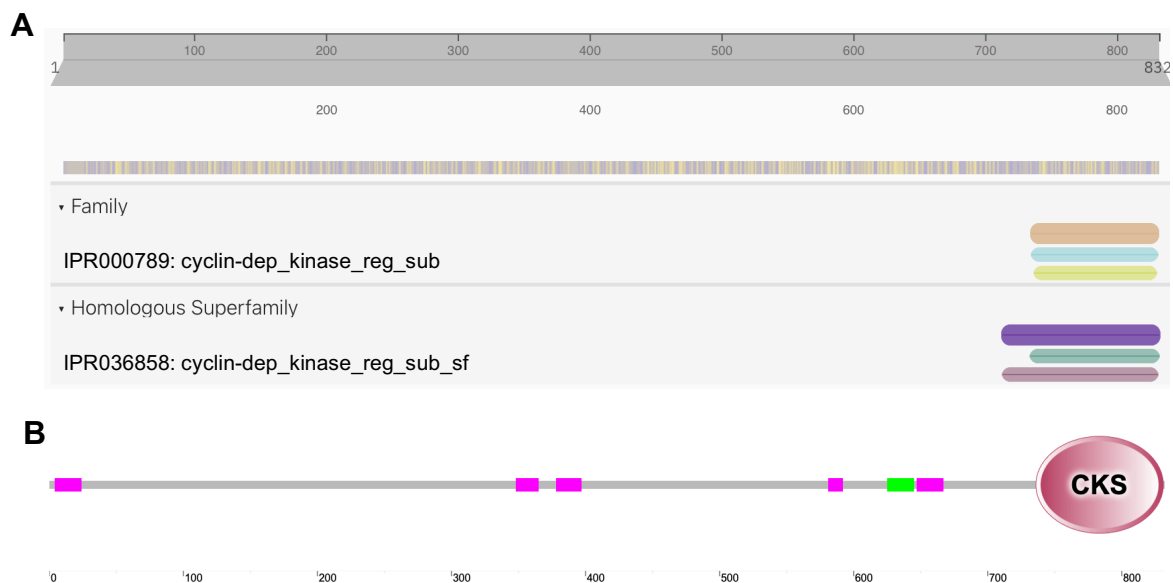
Figure 3–1: Schematic representation of PF3D7_0105800 architecture. (A) A cyclin-dependent regulatory subunit family (CKS) (IPR000789) shown in orange in addition to a cyclin-dependent regulatory subunit superfamily (IPR036858) shown in purple. Information obtained from InterPro (https://www.ebi.ac.uk/interpro). **(B)** A CKS region is predicated at the C-terminus of the protein along with low complexity regions indicated in pink throughout the protein. A coiled-coil region, as predicted by SMART, is shown in bright green (http://smart.embl- heidelberg).

PF3D7_1112100 encodes a large protein of 296 kDa and is predicted to belong to the Bub1/Mad3 family (InterPro: IPR015661) in addition to containing a serine/threonine protein kinase-like superfamily domain (InterPro: IPR011009) at residues 1636–1720 (Figure 3-2A). The protein also contains a protein

kinase domain (InterPro: IPR000719) at residues 1518–1967 (Figure 3-2A). Interestingly, this indicates the possibility that PF3D7_1112100 could potentially have a role during cell cycle progression from metaphase to anaphase as proteins belonging to the Bub1/Mad3 family are usually implicated in and important to spindle damage detection [49, 111].

Figure 3–2: Schematic representation of PF3D7_1112100 architecture. (A) A mitotic spindle checkpoint protein Bub1/Mad3 family (IPR015661) as predicted along indicated in blue/purple with a Ser/Thr kinase-like superfamily signature (IPR011009) indicated in green. Additionally, a protein kinase domain (IPR000719) is indicated in brown. Information obtained from InterPro (https://www.ebi.ac.uk/interpro). (B) Low complexity regions are predicted throughout the protein indicated in pink along with three transmembrane domains indicated in blue in addition to three coiled-coil regions shown in green as predicted by from SMART (http://smart.embl- heidelberg).

Lastly, PF3D7_1364400 encodes a very large protein of 386 kDa predicted to belong to a cyclin-like superfamily as predicted by a 3022–3111 region at the C-terminus (InterPro: IPR036915) (Figure 3-3A). The cyclin-like domain superfamily does not only contain cyclins, but also transcription factors like transcription factor IIB which in other eukaryotes are involved in the formation of the RNA polymerase II preinitiation complex [112]. Additionally, the cyclin-like domain superfamily contains Rb tumour suppressor proteins, which are involved in regulating cell growth and cell cycle progression [113]. However, SMART analysis predicted a broad distribution of multiple low-complexity regions throughout the protein with one coiled-coiled region, questioning whether structural plasticity may influence the activity associated with the annotated kinase domains (Figure 3-3B).

A

▾ Homologous Superfamily

IPR036915: Cyclin-like_sf

B
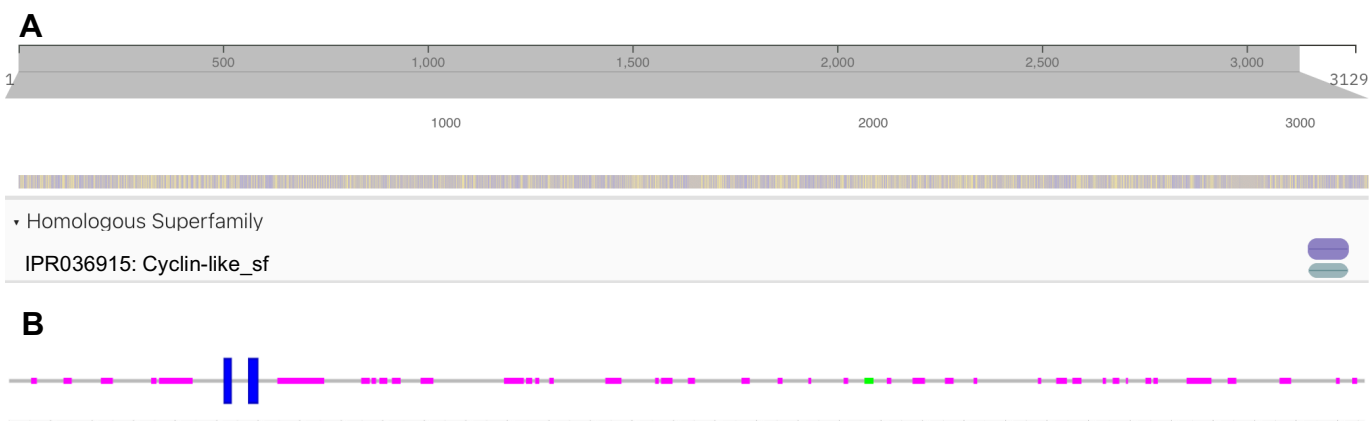
Figure 3–3: Schematic representation of PF3D7_1364400 architecture. (A) Only a cyclin-like superfamily (IPR036915) signature is predicted at the end of the C-terminus indicated in purple. Information obtained from InterPro (https://www.ebi.ac.uk/interpro). **(B)** Low complexity regions are shown in pink; transmembrane domains are indicated in blue while coiled-coil regions are shown in green as predicted by from SMART (http://smart.embl- heidelberg).

These *in silico* predictions of protein domains and homologous protein families indicate that PF3D7_0105800, PF3D7_1112100 and PF3D7_1364400 proteins are not only potential kinase proteins but may particularly be involved in cell cycle regulation.

3.1.2. Predicted protein-protein interactions of the selected kinase proteins

Since kinases are known members of large protein interaction networks, and in some instances are indeed the main controlling hubs in such networks, STRING protein-protein networks (https://string-db.org/) based on *P. falciparum* protein interactions were generated to obtain further indication of the functional importance of the proposed kinases under investigation. The STRING network was based on qualitative information obtained from neighbourhood, experiments, databases, co-occurrence in literature and co-expression for each kinase protein, individually.

The predicted STRING interactions for PF3D7_0105800 indicated direct interaction with a conserved protein with unknown function, PF3D7_0606600, from two-hybrid screening data (Figure 3-4). Co-occurrence in literature also connected PF3D7_0105800 to PF3D7_0109000 (PHIL1), which has been indicated to be important for the parasite inner membrane complex [114, 115]. Co-expression data indicated that PF3D7_0105800 was connected to PF3D7_1227500 (SOC2), a cyclin-related protein, and PF3D7_0919900 (RCC-PIP), a regulator of chromosome condensation-PP1-interacting protein, and PF3D7_1364100, a membrane anchor protein [116-118] (Figure 3-4). This interconnection with multiple different proteins which perform different functions could indicate that PF3D7_0105800 is part of a signalling cascade during the early stages of the G_1 phase, as this protein was described as an early responder in cell cycle re-entry in *P. falciparum* [8].

Figure 3–4: Schematic model of the protein–protein interaction complex of PF3D7_0105800 and its predicted partners. This interaction network was generated by using the STRING software (https://string-db.org). The putative kinase protein PF3D7_0105800 is indicated by the red sphere. Solid black lines indicate co-expression between the connected proteins (spheres), a light green line indicates connection between the proteins through co-occurrence in literature while a pink line indicates interaction through experimental determination.

The STRING interactions for PF3D7_1112100 indicated its connection to three proteins via co-occurrence in literature - PF3D7_0704300 (conserved *Plasmodium* protein), PF3D7_1467900 (Rab GTPase activator) and PF3D7_0613800 (ApiAP2) (Figure 3-5). The latter was also identified by co-expression in addition to PF3D7_0604100 (SIP2). Both of these proteins are annotated to contain AP2 transcription factor domains, indicating their involvement in DNA-binding and gene regulation [119]. PF3D7_1112100 is also co-expressed with PF3D7_1209300, a telomere repeat-binding zinc finger protein, and PF3D7_1227600 (SPC24), a kinetochore protein, which supports its predicted membership in the Bub1/Mad3 family and its predicted function in spindle attachment (Figure 3-5).
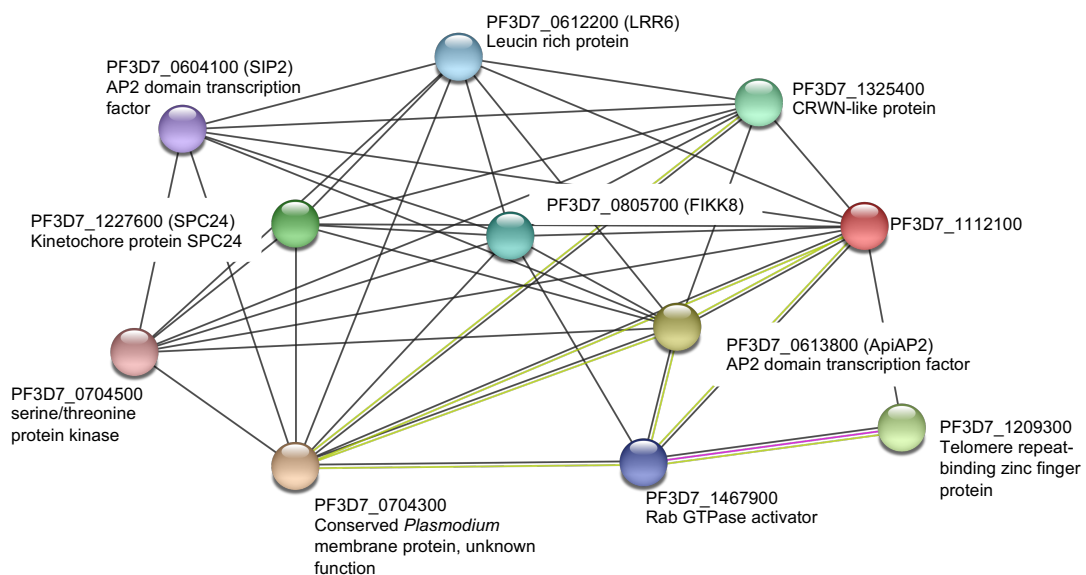
Figure 3–5: Schematic model of the protein–protein interaction complex of PF3D7_1112100 and its predicted partners. This interaction network was generated by using the STRING software (https://string-db.org). The putative kinase protein PF3D7_1112100 is indicated by the red sphere. Solid black lines indicate co-expression between the connected proteins (spheres), a light green line indicates connection between the proteins through co-occurrence in literature while a pink line indicates interaction through experimental determination.

The predicted STRING interactions for PF3D7_1364400 indicated connections with only four other proteins – PF3D7_0401800, PF3D7_1133100, PF3D7_1307100 and PF3D7_1323400 (Figure 3-6). PF3D7_1307100 is annotated as a putative U3 small nucleolar RNA-associated protein 6, which is commonly associated with pre-rRNA cleavage and 18S rRNA formation [120]. Similarly, PF3D7_1323400 is annotated as 60S ribosomal protein L23. Interestingly, in eukaryotes ribosomal protein L23 associates with E3 ubiquitin-protein ligase Mdm2, which ultimately leads to activation of p53 in addition to regulation of cell growth [121] (Figure 3-6). These findings support predictions that PF3D7_1364400 could possibly have similar functions to Rb tumour suppressor proteins play within mammalian cells. Furthermore, the increase in expression during asexual *P. falciparum* cell cycle arrest indicate that PF3D7_1364400 could possibly be part of early cell growth regulation during the G_1 phase of asexual *P. falciparum* parasites.
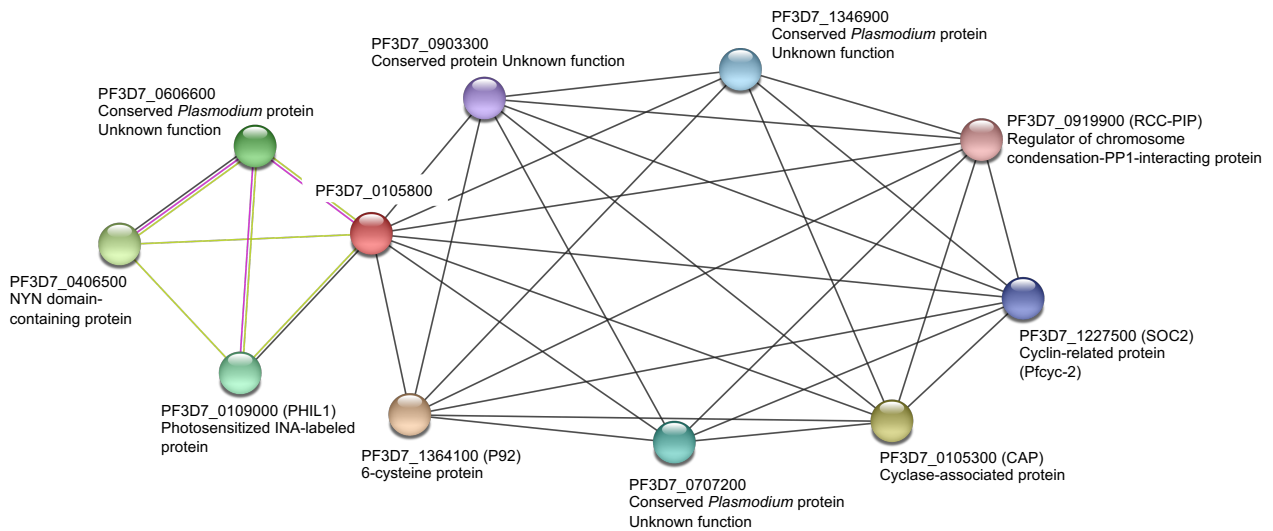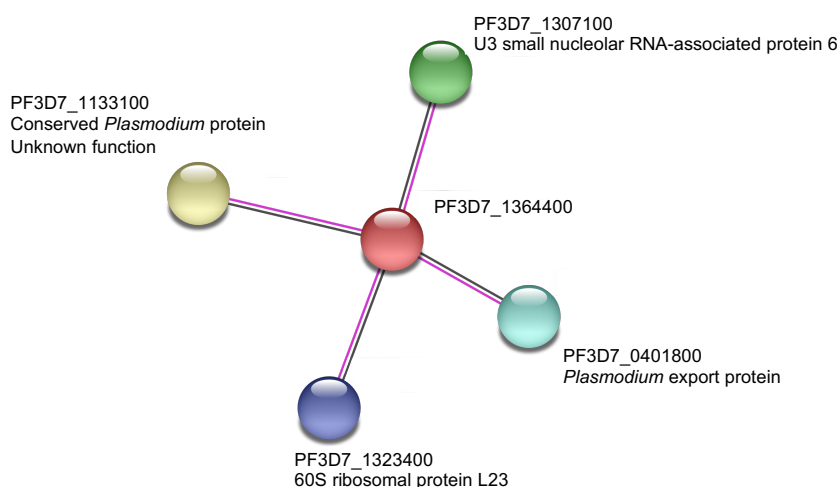

Figure 3–6: Schematic model of the protein–protein interaction complex of PF3D7_1364400 and its predicted partners. This interaction network was generated by using the STRING software (https://string-db.org). The selected putative kinase protein PF3D7_1364400 is indicated by the red sphere. Solid black lines indicate co-expression between the connected proteins (spheres), while a pink line indicates interaction through experimental determination.

3.2. Determining essentiality of the selected kinase proteins during asexual proliferation

3.2.1. Large scale recombinant SLI-TGD-*gene* plasmid isolation

Recombinant constructs for *pf3d7_0105800*, *pf3d7_1112100* and *pf3d7_1364400* cloned into SLI-TGD plasmids were generated previously (H Langeveld, BSc Hons, University of Pretoria, 2019) and used here from the validation steps onwards (Figure 3-7A). The 5'-gene fragments corresponding to the coding strand of each selected putative kinase gene, *pf3d7_0105800* (~540 bp), *pf3d7_1112100* (~440 bp) and *pf3d7_1364400* (~820 bp), were previously successfully amplified (Figure 3-7B) and cloned into SLI-TGD plasmids. Positive constructs were confirmed here based on the presence of the correct size inserts after RE mapping using *Not*I-HF and *Mlu*I-HF (Figure 3-7C). Therefore, recombinant SLI-TGD plasmids named SLI-TGD-*0105800,* SLI-TGD-*1112100* and SLI-TGD-*1364400,* were validated and ready to be used in downstream transfection experiments.
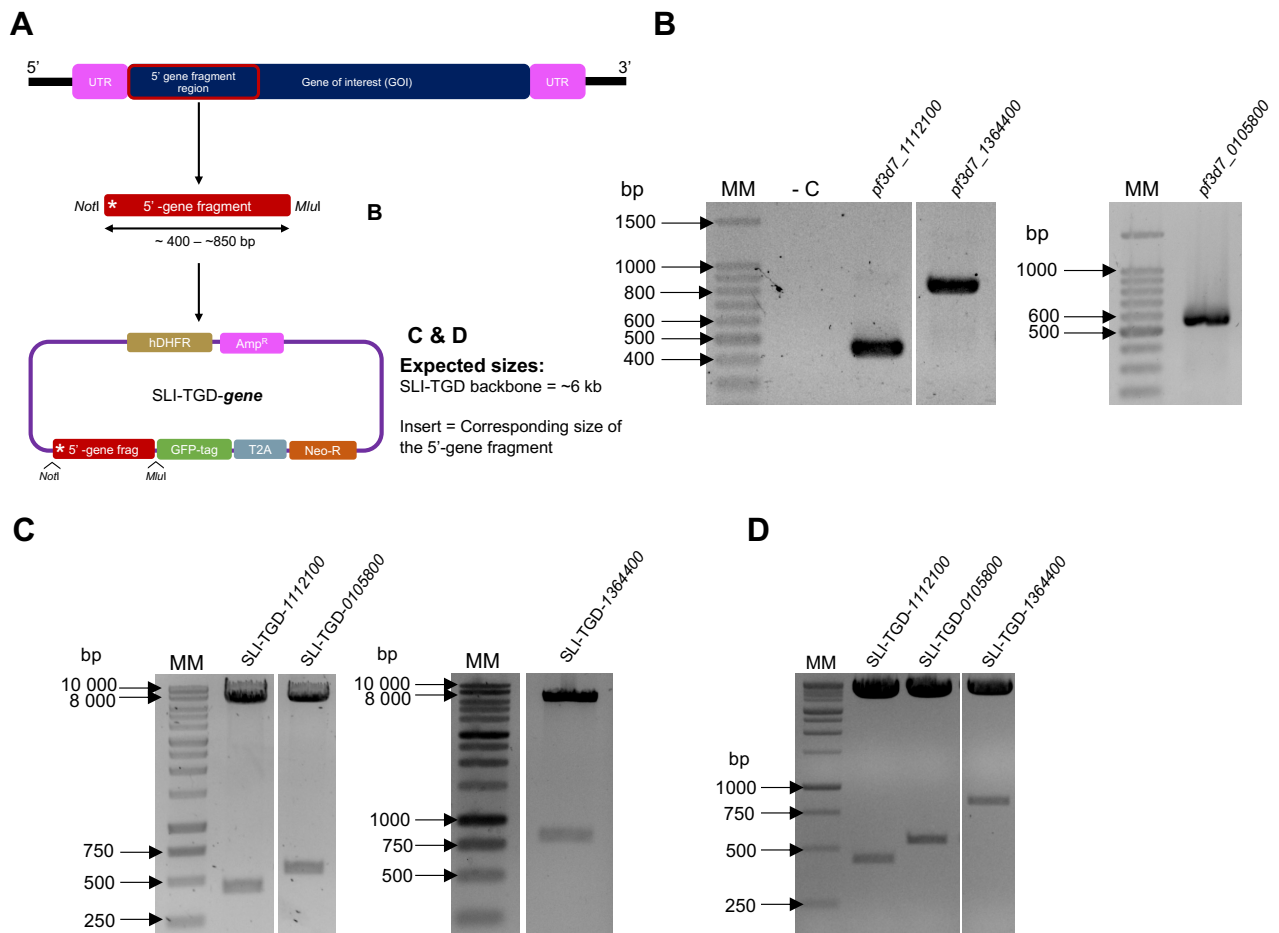
Figure 3–7: Cloning and validation of recombinant SLI-TGD-*0105800*, SLI-TGD-*1112100* and SLI-TGD-*1364400*. (A) Schematic representation of the cloning process and validation of recombinant SLI-TGD plasmids. **(B)** Negative control (-C) PCR containing no template DNA. PCR amplification of 5'-gene fragments of the selected putative kinase genes. Amplified products were analysed on 1.2 % (w/v) agarose gel post stained with EtBr (0.4 mg/mL). Molecular marker (MM): 100 bp ladder (Promega, USA). The expected amplified band sizes were obtained for each 5'-gene fragment of ~440 bp (*pf3d7_1112100*), ~540 bp (*pf3d7_0105800*) and ~820 bp (*pf3d7_1364400*). **(C)** RE mapping of recombinant SLI-TGD-*0105800*, SLI-TGD-*1112100* and SLI-TGD-*1364400* was completed by digesting 1 µg of plasmid DNA for 3 h at 37 °C and analysed on a 1.2 % (w/v) agarose gel post stained with EtBr (0.4 mg/mL). Molecular marker (MM): 1 kb ladder (Promega, USA). **(D)** Additional validation step was done by digesting 2 µg of newly isolated recombinant SLI-TGD-*0105800*, SLI-TGD-*1112100* and SLI-TGD-*1364400* plasmid DNA for 3 h at 37 °C and analysing on a 1.5 % (w/v) agarose gel post stained with EtBr (0.4 mg/mL). Molecular marker (MM): 1 kb ladder (Promega, USA). For both C and D, the expected sized insert bands for recombinant SLI-TGD-*0105800* (~540 bp), SLI-TGD-*1112100* (~440 bp) and SLI-TGD-*1364400* (~820 bp) were obtained.

To transfect the recombinant plasmids into asexual parasites, a large quantity (~50–100 µg) of pure plasmid is required [106]. Enough pure DNA was isolated for each recombinant SLI-TGD plasmid with total DNA yields ranging from 510–760 µg with $A_{260}/_{280}$ and $A_{260}/_{230}$ ratios ranging between 1.7–1.9 and 2.0–2.4, respectively, indicating good quality, pure DNA. The isolated plasmid was confirmed to be recombinant SLI-TGD-*0105800*, SLI-TGD-*1112100* and SLI-TGD-*1364400* plasmids through RE mapping (Figure 3-7D). The RE digest yielded two bands for each of the recombinant SLI-TGD plasmids, with the larger band of ~6 kb corresponding to the expected size of the SLI-TGD backbone while the smaller bands of ~540 bp, ~440 bp and ~820 bp in size corresponded to the expected *pf3d7_0105800*, *pf3d7_1112100* and *pf3d7_1364400* 5'-gene fragments, respectively (Figure 3-7D).

This confirmed that the recombinant SLI-TGD-*0105800,* SLI-TGD-*1112100* and SLI-TGD-*1364400* plasmids were each successfully isolated and could be used in downstream transfection experiments.

3.2.2. Asexual parasite transfection and episomal uptake

Asexual NF54 strain *P. falciparum* parasites were transfected with SLI-TGD-*0105800,* SLI-TGD-*1112100* and SLI-TGD-*1364400* plasmids and subjected to 10 days of WR22910 treatment to select for parasites that had successfully taken up and episomally maintained the recombinant plasmids, and therefore expressed the hDHFR gene that confers WR99210 resistance (Figure 3-8).
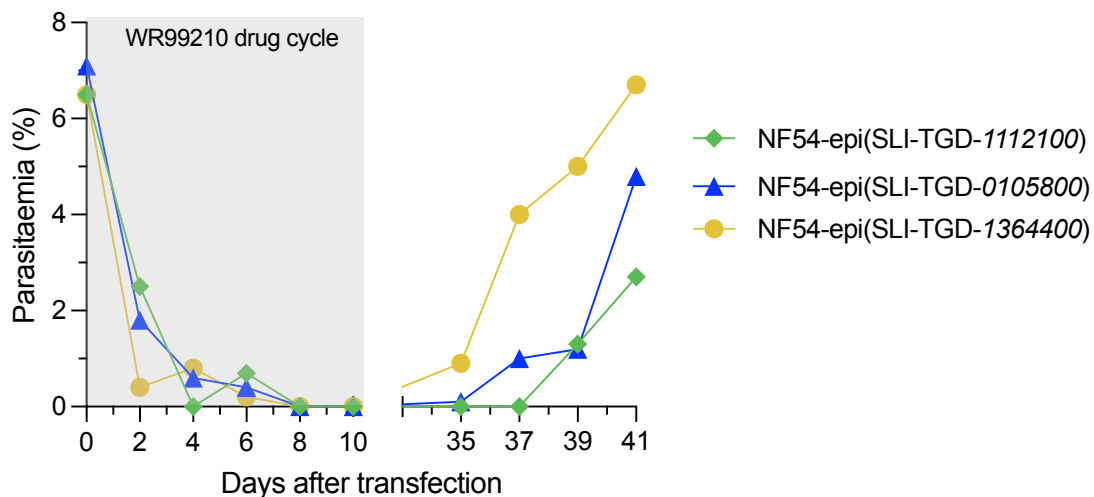
Figure 3–8: Selection and recovery of *P. falciparum* parasites that had episomally taken up and episomally maintained the recombinant plasmids after transfection. Parasitaemia of *P. falciparum* NF54 parasites were determined before transfection (day 0) and every second day post-transfection up to 41 days by Rapi-diff-stained thin blood smears. As of day, 1 post-transfection, parasitaemia decreased due to WR99210 drug selection to unobservable levels by day 8. WR99210 selection pressure was applied for 10 days post-transfection after which parasites were cultured in drug-free medium. Figure was generated using GraphPad Prism version 9.2.0.

Electroporation during the transfection process resulted in a rapid drop in parasitaemia (from ~7 % to ~1–3 %) within the first two days following transfection, likely due to erythrocyte lysis. The WR99210 drug selection caused a further decrease in parasitaemia after 6 days of selection from ~2–3 % until no parasites were visible on a thin blood smear. WR22910 selection pressure was removed, and parasites were allowed to recover in drug-free medium. After 25 days in drug free medium (~35 days post transfection), parasites started to reappear (Figure 3-8).

To assess whether the recovered parasites did contain the respective recombinant SLI-TGD-*0105800,* SLI-TGD-*1112100* and SLI-TGD-*1364400* plasmids episomally, DNA isolated from the recovered parasites were used in PCR screening. The presence of episomally-maintained recombinant plasmids in the parasite lines could be confirmed using primers specific to the SLI-TGD backbone and spanning the gene of interest (Figure 3-9A). In two independent biological replicates, episomal presence was confirmed for NF54-epi(SLI-TGD-*0105800*)*,* NF54-epi(SLI-TGD-*1112100*) and NF54-epi(SLI-TGD-*1364400*) with single bands of 740 bp, ~640 bp and ~1020 bp in size obtained, corresponding to the

expected amplified region containing the 5'-gene fragments of *pf3d7_0105800*, *pf3d7_1112100* and *pf3d7_1364400* respectively (Figure 3-9B, C).
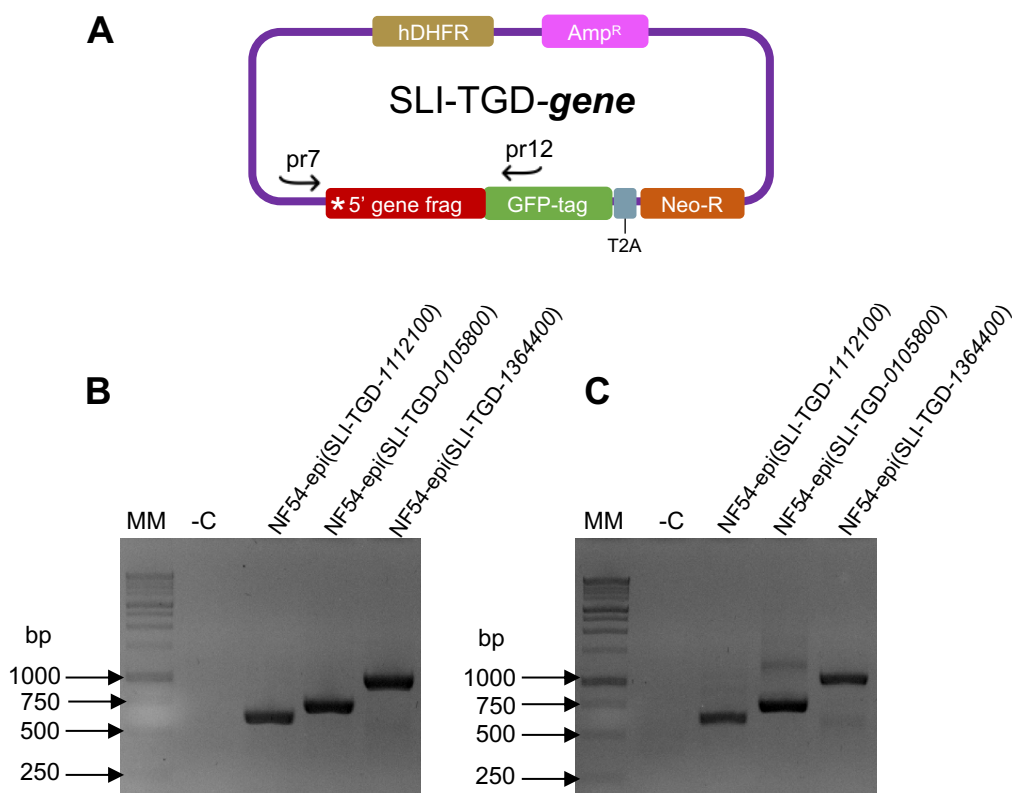
Figure 3–9: Confirmation of episomal uptake of recombinant SLI-TGD plasmids by transfected parasites. **(A)** Schematic representation showing the primer pair (pr7 and pr12) used during the screening PCR, listed in Table 4. The primers (pr7 and pr12) bind upstream and downstream respectively on the SLI-TGD backbone flanking the insert region. **(B)** Screening PCR of the first biological repeat indicating episomal uptake confirmation. **(C)** Negative control (-C) PCR containing no template DNA. Screening PCR of the second biological repeat indicating episomal uptake confirmation. Amplified PCR products were analysed on a 1.5 % (w/v) agarose gel post stained with EtBr (0.4 mg/mL). Molecular marker (MM): 1 kb ladder (Promega, USA).

To ensure that the recombinant plasmids that were being maintained episomally in the three lines did not cause any unwanted growth phenotypes, parasite morphology of the asexual *P. falciparum* populations were assessed microscopically (Figure 3-10). Ring-stage parasites, characterised by their flat, circular shape, were observed in each line, and all of these developed into trophozoites, associated with increased cell size and formation of haemozoin crystals. Schizogony in all three lines was comparable to that of the wild-type NF54 parasites, with multiple nuclei present (Figure 3-10). Thus, compared to WT NF54 parasites, no morphological abnormalities were observed in any of the asexual parasite stages in NF54-epi(SLI-TGD-*0105800*), NF54-epi(SLI-TGD-*1112100*) and NF54-epi(SLI-TGD-*1364400*).
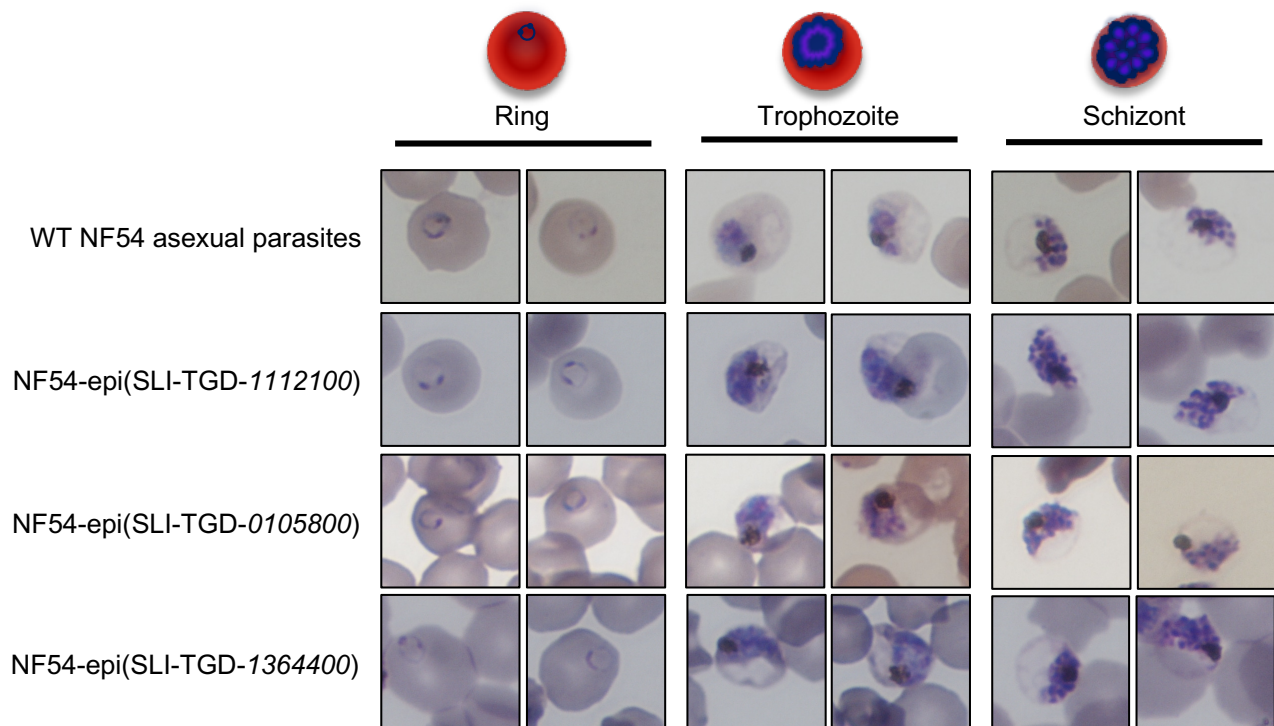
Figure 3–10: Morphological evaluation NF54-epi(SLI-TGD-*0105800*), NF54-epi(SLI-TGD-*1112100*) and NF54-epi(SLI-TGD-*1364400*) parasite lines. Intra-erythrocytic development of asexual-stage parasites of the four different transfected parasite cultures containing the respective recombinant SLI-TGD plasmids episomally were evaluated by visualising Rapi-Diff-stained thin blood smears under a light microscope at 1000x magnification.

3.2.3. Integration selection of SLI-TGD-*gene* plasmids

After confirming the episomal uptake of the recombinant plasmids, without any proliferation defects in each of the NF54-epi(SLI-TGD-*0105800*), NF54-epi(SLI-TGD-*1112100*) and NF54-epi(SLI-TGD-*1364400*) lines, parasite cultures were subjected to a second round of drug selection with G418 to select for genomic integration, with resistance conferred by the consequent presence of Neo-R in the parasite genome. Drug selection was maintained for 16 days, whereafter drug pressure was removed and parasitaemia was monitored for 4 weeks (31 days) (Figure 3-11). If integration of the recombinant SLI-TGD plasmids occurred successfully and no parasites recovered within 4 weeks, it could indicate an essential nature of the gene of interest to asexual parasite development and proliferation. By contrast, if parasites do recover after successful gene disruption, the gene is likely not essential.

The parasitaemia for each of the parasite lines ((NF54-epi(SLI-TGD-*0105800*), NF54-epi(SLI-TGD-*1112100*) and NF54-epi(SLI-TGD-*1364400*)) undergoing integration selection decreased to undetectable levels after 8 days of G418 drug pressure. After 4 weeks of recovery in drug-free medium, no parasites were observed microscopically (Figure 3-11). This phenotype was confirmed for two independent biological repeats, each in technical triplicates. This indicated that targeted gene disruption of all three of the putative kinases under investigation resulted in *P. falciparum* parasites that were unable to recover and supports the hypothesis that each of these three kinases are essential to asexual proliferation of *P. falciparum* parasites. This essential nature was compared to the ability of parasites

47

transfected with a control gene (*sap18*) [122], in which case the parasites were fully able to recover and proliferate after targeted gene deletion of sap18 as a non-essential gene (results from MSc study, T Rabie, University of Pretoria, 2021). This indicates that the SLI-TGD system is an effective indicator of essentiality of the proteins of interest.
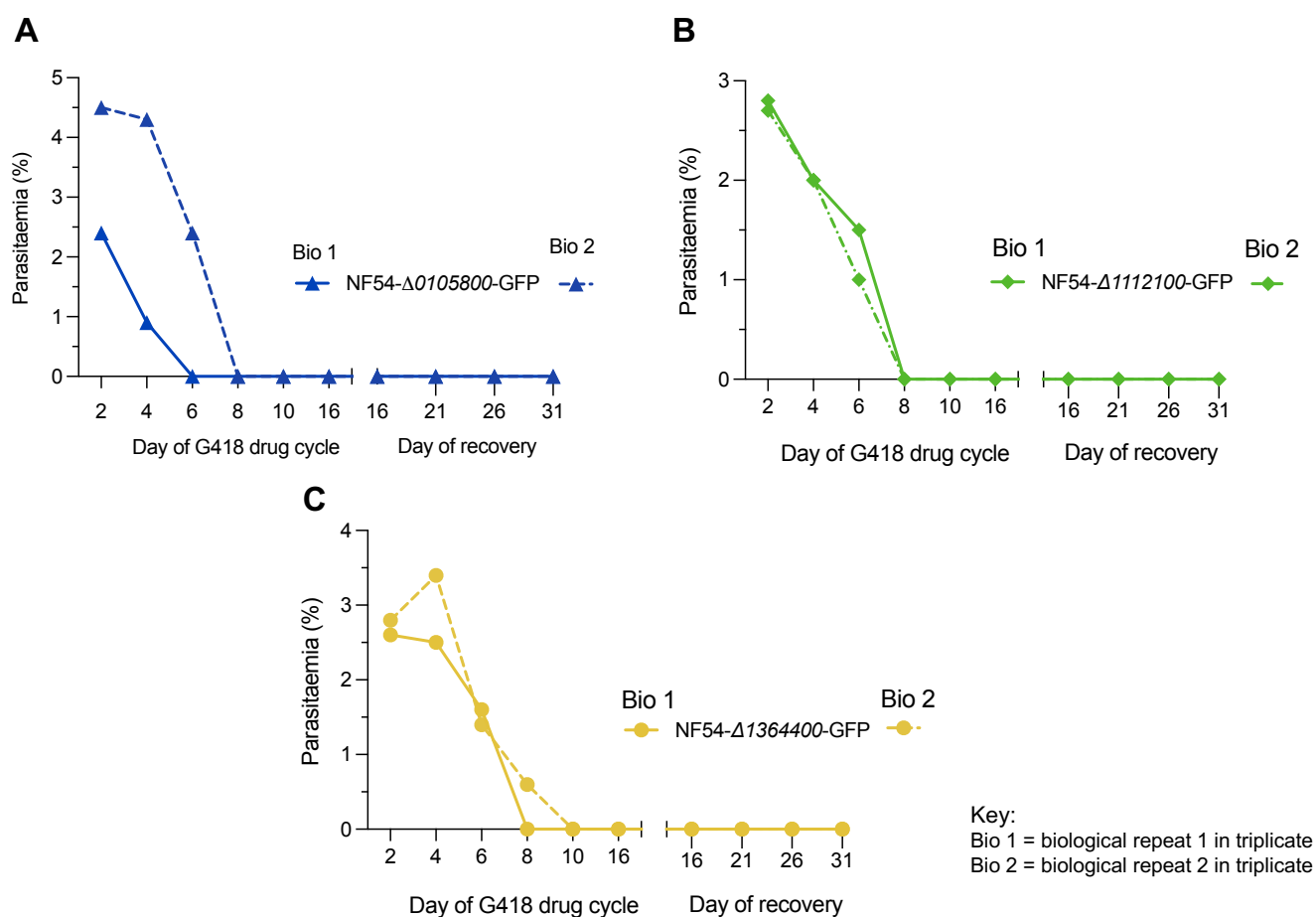
Figure 3–11: Determining essentiality of the selected kinase genes through selection of recombinant *P. falciparum* parasites. Each biological repeat (Bio1 & 2) was divided into triplicates. Thus, a total of six cultures per parasite line was subjected to integration selection. NF54-epi(SLI-TGD-*0105800*), NF54-epi(SLI-TGD-*1112100*) and NF54-epi(SLI-TGD-*1364400*) parasite lines were subjected to a 16-day G418 drug cycle and allowed to recover for 4 weeks. Parasitaemia was evaluated every second day by Rapi-Diff-stained thin blood smears during the drug cycle and twice a week during the recovery period. Figures were generated using GraphPad Prism version 9.2.0. **(A)** Parasitaemia during and after genomic integration selection of NF54-Δ*0105800*-GFP. **(B)** Parasitaemia during and after genomic integration selection of NF54-Δ*1112100*-GFP. **(C)** Parasitaemia during and after genomic integration selection of NF54-Δ*1364400*-GFP. Parasitaemia in all cases decreased to undetectable levels between day 6 and 10 of the G418 drug cycle and no parasites were observed after 4 weeks (day 31) in recovery.

To obtain a more detailed analysis of the effect of targeted gene deletion of the three putative kinases on a particular stage of asexual proliferation of *P. falciparum* parasites, as an indication of association to a particular cell cycle phase, parasite stage distribution was investigated for NF54-Δ*0105800*-GFP, NF54-Δ*1112100*-GFP and NF54-Δ*1364400*-GFP during the selection for integration (Figure 3-12). Differential phenotypes were seen for NF54-Δ*0105800*-GFP and NF54-Δ*1364400*-GFP, which both displayed a delay in asexual parasite stage progression (Figure 3-12). These parasites showed a halt in progression at the ring-/early-trophozoite stage within the first replication cycle after integration of the shortened gene fragments, compared to wild type parasites. However, NF54-Δ*1112100*-GFP did not

compromise parasite progression during the first cycle of proliferation but in the second cycle only, where these parasites could not progress past the ring stage. (Figure 3-12B). Hence, both PF3D7_0105800 and PF3D7_1364400 may in fact have an important role during cell-cycle progression at the G_1/S transition stage and PF3D7_1112100 during the final stages of schizogony.
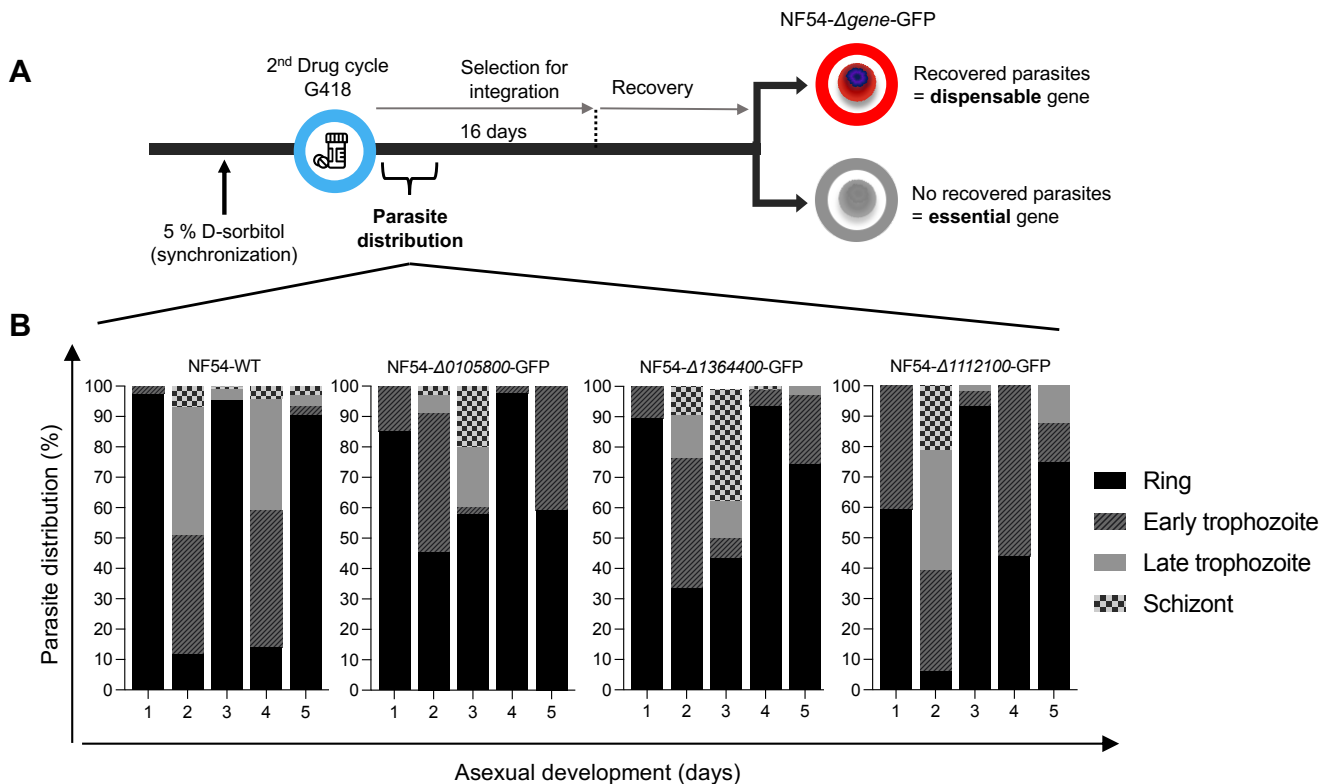
Figure 3–12: Parasite distribution of NF54-Δ*0105800*-GFP, NF54-Δ*1112100*-GFP and NF54-Δ*1364400*-GFP during integration selection. **(A)** Schematic overview of the stage of the integration selection process at which parasite distribution was determined. NF54-epi(SLI-TGD-*0105800*), NF54-epi(SLI-TGD-*1112100*) and NF54-epi(SLI-TGD-*1364400*) parasites were synchronised once before G418 integration selection stated. **(B)** Parasite distribution of NF54-Δ*0105800*-GFP, NF54-Δ*1112100*-GFP, NF54-Δ*1364400*-GFP and WT NF54 (control) during the first five days of G418 drug selection. Differential parasite distributions were observed for NF54-Δ*0105800*-GFP and NF54-Δ*1364400*-GFP during the first proliferation cycle while only during the second proliferation cycle was there a deviation in parasite distribution of NF54-Δ*1112100*-GFP compared to WT NF54 parasites

Since the three kinases were seemingly essential to parasite proliferation, expansion of the parasite population could not be performed and therefore gDNA could not be isolated to confirm integration of the plasmids into the parasite genomes through PCR amplification, as is typically experienced for essential genes. Additionally, the importance of these kinases in any other life cycle stage like gametocytes cannot be determined with the TGD system. Therefore, to obtain parasite lines that could allow investigation of the function of these kinases beyond essentiality, inducible gene manipulation tools like knock sideways or knockdown were used for subsequent investigation.

3.3. Cloning of a 3'-gene fragment from each selected kinase encoding gene into the SLI-sandwich system

To enable cloning into the SLI-sandwich system for knock sideways for subsequent mislocalisation of the kinases under investigation, gene-specific 3'-gene fragments of each of the selected kinase genes were successfully amplified from gDNA, with PCR amplicons corresponding to the expected fragment sizes of ~1050 bp, ~640 bp and ~940 bp (Figure 3-12).
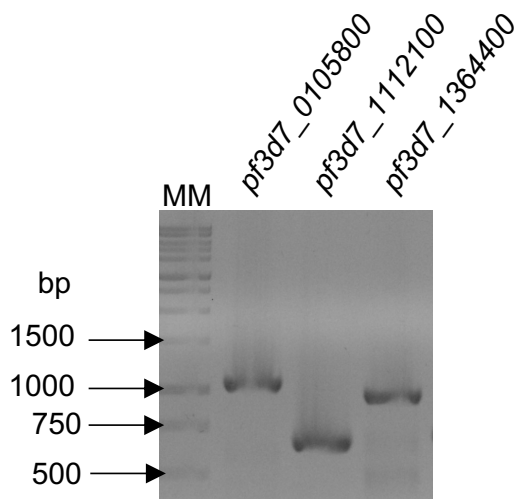
Figure 3–13: PCR amplification of gene-specific 3'-gene fragments to be cloned into the SLI-sandwich plasmid. Amplified PCR products were analysed on a 2 % (w/v) agarose gel, post stained with EtBr (0.4 mg/mL). Molecular marker (MM): 1 kb ladder (Promega, USA). The expected amplicon band sizes were obtained: ~1050 bp (*pf3d7_0105800* 3'-gene fragment), ~640 bp (*pf3d7_1112100* 3'-gene fragment), ~940 bp (*pf3d7_1364400* 3'-gene fragment).

PCR optimization for the different amplification reactions included slight changes to the annealing temperature, with an optimal annealing temperature of 60 °C which, was used for each of the gene fragment amplification reactions. However, faint non-specific bands were observed for the 3'-gene fragment of *pf3d7_1364400,* and changes to annealing temperature and time could not eliminate this non-specific amplification. Therefore, all the PCR products of the correct sizes were extracted from the gel and purified, resulting in DNA yields ranging from 360–1290 ng, with $A_{260}/_{280}$ ratios ranging from 1.7–1.9 for each PCR product isolated.

SLI-sandwich plasmid DNA was isolated and digested with *Not*I-HF and *Avr*II to verify the plasmid identity (Figure 3-14A). This yielded two bands, a larger band of ~8 kb which corresponds to the expected size of the plasmid backbone and a smaller band of ~600 bp which corresponds to the expected size of the original insert (*pf3d7_0209700*), which was removed (Figure 3-14B). The plasmid backbone was excised from the gel and purified, resulting in a total DNA yield of 1.4 µg, with an $A_{260}/_{280}$ ratio of 1.7. Even though, a low $A_{260}/_{230}$ ratio of 0.9 was obtained, outside the optimal range (2.0–2.2) indicating chaotropic salt contamination, the plasmid backbone was considered sufficiently pure to be used in ligation reactions.
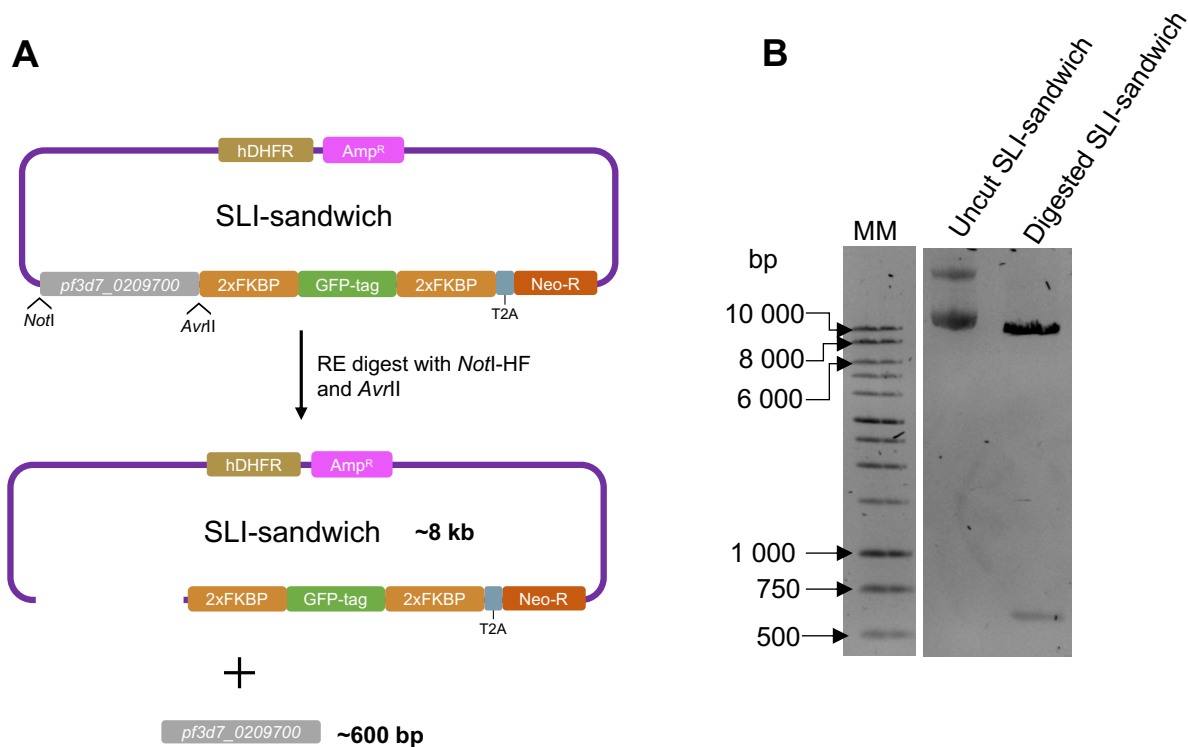
Figure 3–14: Restriction enzyme digest of original SLI-sandwich plasmids. (A) Schematic representation of RE mapping of the original SLI-sandwich plasmid with the expected sized plasmid backbone and insert indicated. **(B)** Plasmid DNA (550 ng) was analysed on 1 % (w/v) agarose gel post stained with EtBr (0.4 mg/mL) after RE digestion for 3 h at 37 °C. Molecular marker (MM): 1 kb ladder (Promega, USA). Complete digestion of the original SLI-Sandwich plasmid with *Not*I-HF and *Avr*II yielded two bands with the larger band corresponding to the expected size of the plasmid backbone and the smaller to the original insert.

The 3'-gene fragments amplified and isolated in section 3.3 were prepared for ligation by digesting each PCR product with *Not*I-HF and *Avr*II to allow for sticky-end cloning. The digested gene fragments were purified and ligated into digested SLI-sandwich backbone. The ligation reactions were used to transform competent DH5α *E. coli* cells, and colony PCR screening was performed to confirm the presence of recombinant clones. Recombinant SLI-SW-*0105800*, SLI-SW-*1112100* and SLI-SW-*1364400* clones were obtained and were confirmed to contain the expected sized 3'-gene fragments, with PCR products of ~1200 bp, ~770 bp and ~1100 bp obtained (Figure 3-15B, Supplementary Figure S1).

Plasmid DNA was isolated from positive colonies and subjected to RE mapping with *Not*I and *Avr*II, which resulted in a larger band of the expected size for the SLI-sandwich backbone and smaller bands correlating to the expected sizes of the respective 3'-gene fragments of interest (Figure 3-15C). Thus, the RE mapping indicates that each 3'-gene fragment was successfully cloned into its respective SLI-sandwich plasmid. For full RE mapping gels see supplementary Figure S2.
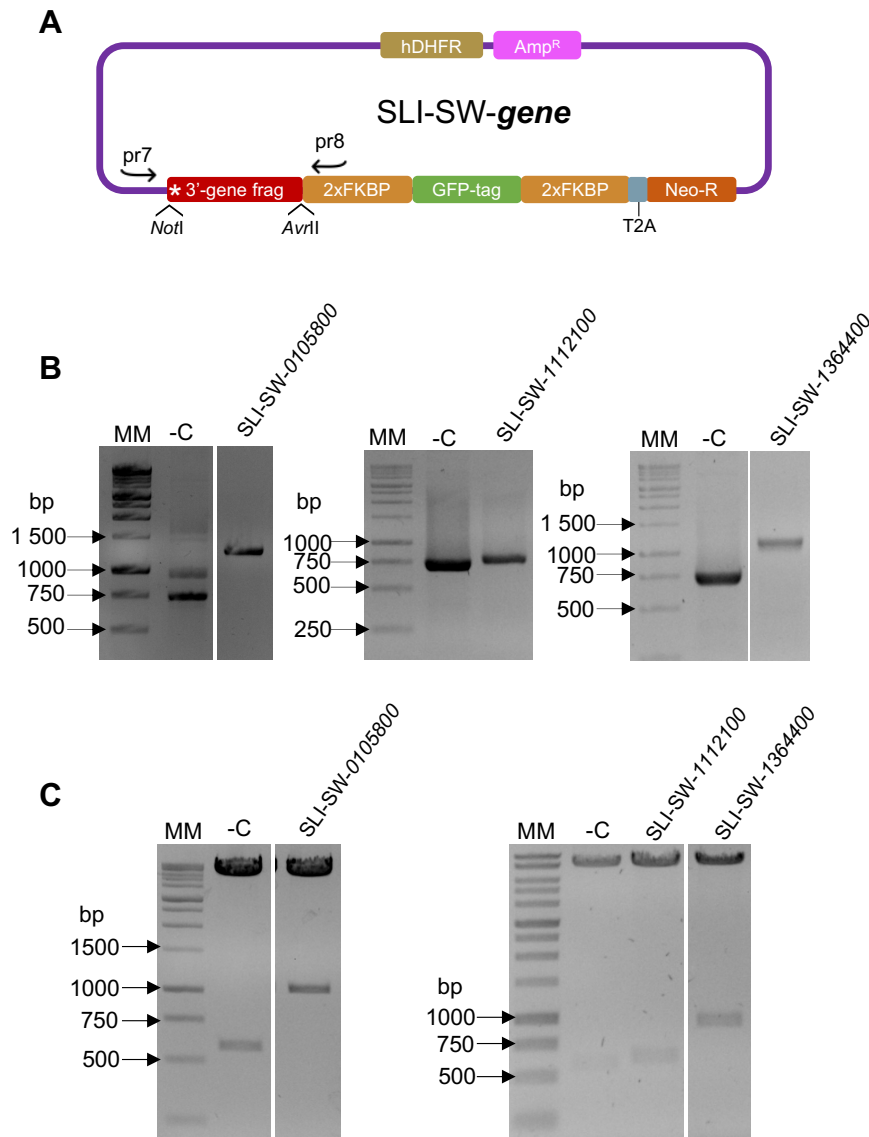
Figure 3–15: Validation of SLI-SW-*0105800*, SLI-SW-*1112100* and SLI-SW-*1364400* recombinant plasmids. DNA samples were analysed on 1.5 % (w/v) agarose gel post stained with EtBr (0.4 mg/mL). Molecular marker (MM): 1 kb ladder (Promega, USA). **(A)** Schematic representation showing the primer pair (pr7 and pr8) used during the screening PCR which is listed in Table 2. The primers (pr7 and pr8) bind upstream and downstream respectively on the SLI-sandwich backbone flanking the insert region. **(B)** Negative control (-C) is the amplification of the original insert region of the SLI-sandwich plasmid, which is the undesired outcome and the negative control indication for generation of positive construct. Colony screening PCR of the *pf3d7_0105800, pf3d7_1112100* and *pf3d7_1364400* 3'fragments cloned into the SLI-sandwich plasmid. The expected regions were amplified for all of the 3'-gene fragments with PCR products of ~1200 bp (SLI-SW-*0105800*), ~770 bp (SLI-SW-*1112100*) and ~1100 bp (SLI-SW-*1364400*). **(C)** Negative control (-C) is the complete digestion of the original SLI-sandwich plasmid. Restriction enzyme mapping of isolated plasmid DNA from SLI-SW-*0105800,* SLI-SW-*1112100* and SLI-SW-*1364400* positive clones using *Not*I-HF and *Avr*II. The expected sizes insert regions were excised from the isolated plasmid DNA, with bands of ~1050 bp (SLI-SW-*0105800*), ~640 bp (SLI-SW-*1112100*) and ~940 bp (SLI-SW-*1364400*) obtained.

As a final verification step, Sanger sequencing of the constructs confirmed the identity and orientation of the gene fragments and the absence of unwanted mutations (Figure 3-16). The sequencing alignment revealed that the gene fragments were cloned in the correct orientation, with no missense or nonsense mutations present. The identity of each 3'-gene fragment of interest was confirmed, indicating that these were successfully cloned into their SLI-sandwich plasmids and were suitable for downstream transfection experiments.
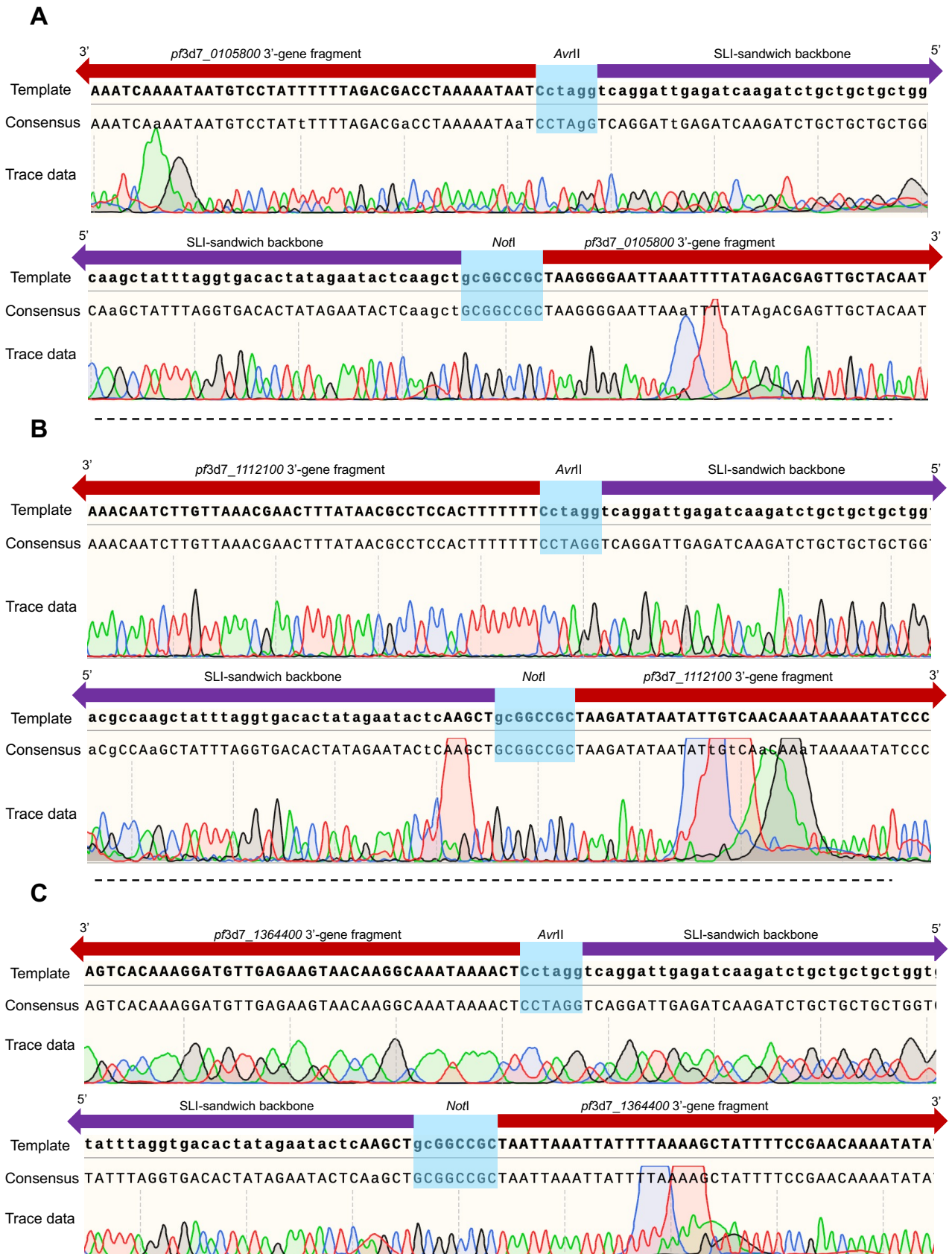
Figure 3–16: Sanger sequencing alignment of SLI-SW-*0105800*, SLI-SW-*1112100* and SLI-SW-*1364400* 3'-gene fragments. The chromatogram surrounding the cloning sites is indicated, including a section of aligned plasmid backbone (purple), 3'-gene fragment (red), and the restriction enzyme cleavage sites (light blue). DNA fragments in schematics not drawn to scale. A representative forward or reverse chromatogram (trace data) is shown below the consensus sequence. **(A)** Sequence alignment confirming the identity of the *pf3d7_0105800* 3'-gene fragment. **(B)** Sequence alignment confirming the identity of the *pf3d7_1112100* 3'-gene fragment. **(C)** Sequence alignment confirming the identity of the *pf3d7_1364400* 3'-gene fragment. Chromatograms generated using SnapGene alignment. Images were designed using SnapGene V 5.3.2.

3.4. Generation of transgenic knock sideways *P. falciparum* lines using SLI-SW-*0105800*, SLI-SW-*1112100* and SLI-SW-*1364400*

As described in section 3.2.1, a large quantity of pure recombinant plasmid DNA is required for successful transfection of asexual parasites. As such, total DNA yields ranging from 0.9–1.3 mg of the SLI-SW-*0105800*, SLI-SW-*1112100* and SLI-SW-*1364400* plasmid were obtained and validated by RE mapping with *Not*I-HF and *Avr*II, yielding the expected band sizes (Figure 3-17), and confirming that each recombinant plasmid was successfully isolated for transfection.
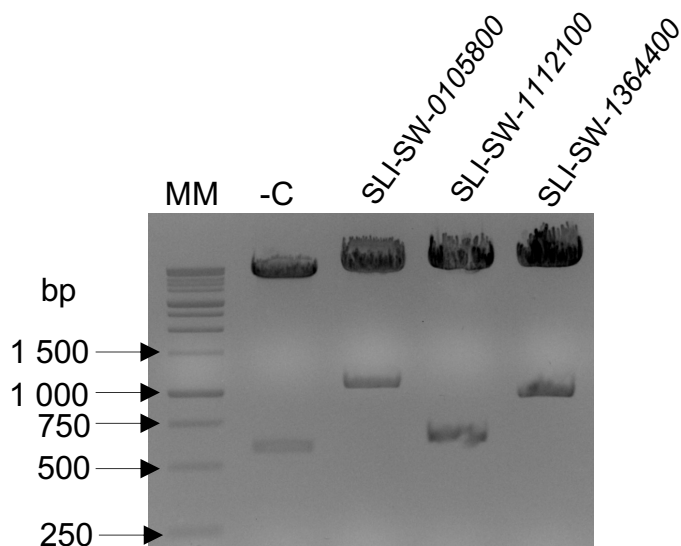
Figure 3–17: Restriction enzyme mapping of recombinant SLI-SW-*0105800*, SLI-SW-*1112100* and SLI-SW-*1364400* plasmids. Plasmid DNA (2 µg) was digested for 3 h at 37 °C. Digested DNA samples were analysed on 1.5 % (w/v) agarose gel post stained with EtBr (0.4 mg/mL). Molecular marker (MM): 1 kb ladder (Promega, USA). Negative control (-C) is the complete digestion of the original SLI-sandwich plasmid. Complete digestion of SLI-SW-*0105800*, SLI-SW-*1112100* and SLI-SW-*1364400* by using the *Not*I-HF and *Avr*II restriction enzymes. Each digested yielded two bands with the smaller bands corresponding to the expected 3'-gene fragment sizes, ~1050 bp (SLI-SW-*0105800*), ~640 bp (SLI-SW-*1112100*) and ~940 bp (SLI-SW-*1364400*).

Following transfection of asexual NF54 *P. falciparum* parasites with recombinant SLI-SW-*0105800*, SLI-SW-*1112100* and SLI-SW-*1364400* plasmid DNA, the parasites cultures were subjected to 10 days of WR22910 drug selection for episomal uptake as before. Electroporation again resulted in a rapid drop in parasitaemia (from ~9 % to ~2–4 %) within the first two days following transfection, with further decreases observed thereafter, until no detectable parasites were present after 6–10 days. After removal of WR22910 pressure, transfected parasites recovered after 6 days in drug-free medium (Figure 3-18).
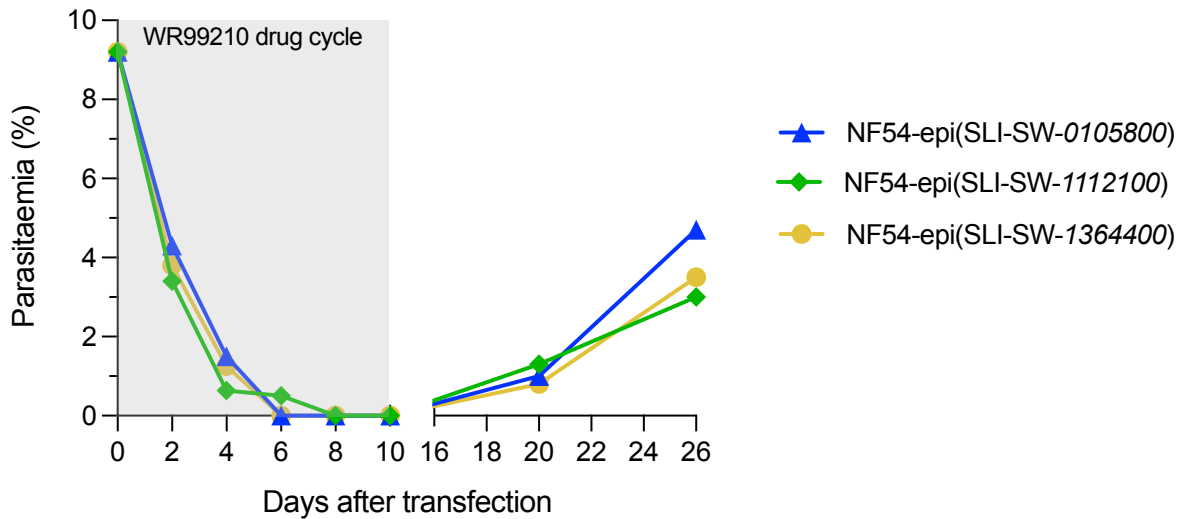
Figure 3–18: Selection and recovery of *P. falciparum* parasites transfected with recombinant SLI-SW-*0105800*, SLI-SW-*1112100* and SLI-SW-*1364400* plasmids. The graph displays WT NF54 *P. falciparum* parasites transfected with SLI-SW-*0105800*, SLI-SW-*1112100* and SLI-SW-*1364400* and selected with WR22910 drug for episomal uptake. The parasitaemia was determined before transfection (day 0) and every second day post-transfection by Rapi-Diff-stained thin blood smears at 1000x magnification. Figure was generated using GraphPad Prism version 9.2.0.

To confirm if the plasmids were maintained episomally in the recovered NF54-epi(SLI-SW-*0105800*), NF54-epi(SLI-SW-*1112100*) and NF54-epi(SLI-SW-*1364400*) parasites, DNA was isolated from the recovered parasites and used in screening PCRs using SLI-sandwich backbone primers (pr7 and pr8 listed in Table 2) flanking the inserts on the SLI-sandwich plasmid (Figure 3-19B). All three lines contained the expected plasmids as evident from ~1200 bp (SLI-SW-*0105800*), ~770 bp (SLI-SW-*1112100*) and ~1100 bp (SLI-SW-*1364400*) bands obtained.
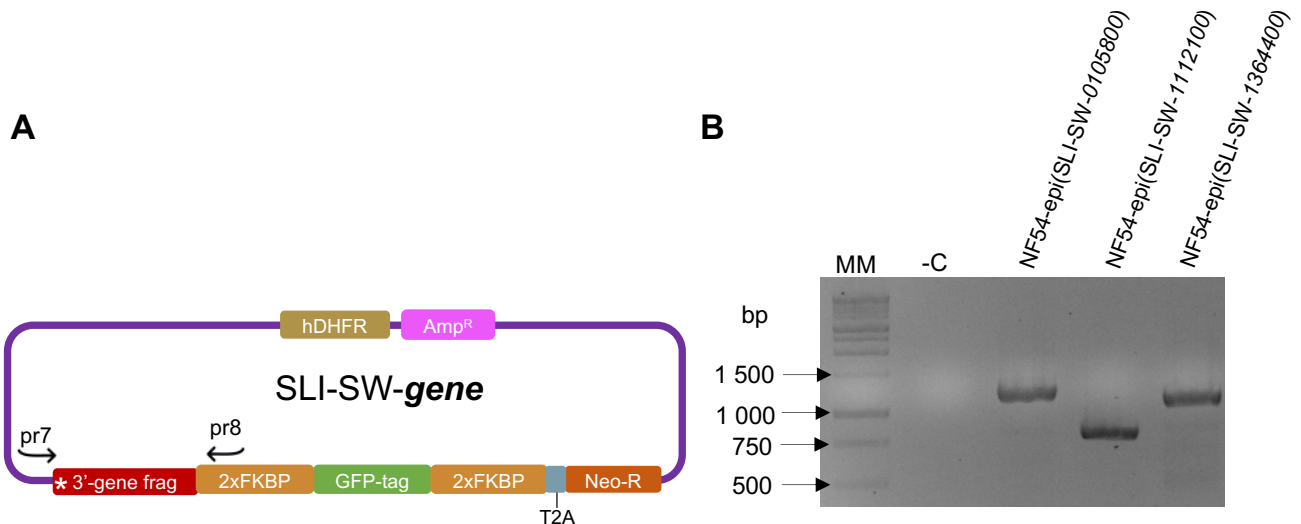
Figure 3–19: Validation of *P. falciparum* parasites that have episomally taken up and maintained recombinant SLI-SW-*0105800*, SLI-SW-*1112100* and SLI-SW-*1364400* plasmids. (A) Schematic representation showing the primer pair (pr7 and pr8) used during the screening PCR, listed in Table 2. The primers (pr7 and pr8) bind upstream and downstream respectively on the SLI-sandwich backbone flanking the insert region. **(B)** Episomal confirmation screening PCR results were analysed on 1.5 % (w/v) agarose gel post stained with EtBr (0.4 mg/mL). Molecular marker (MM): 1 kb ladder (Promega, USA). Negative control (-C) containing no template DNA. Amplification using the specific SLI-sandwich backbone primers pr7 and pr8. The expected insert regions were amplified for all of the 3'-gene fragments with PCR products of ~1200 bp (SLI-SW-*0105800*), ~770 bp (SLI-SW-*1112100*), and ~1100 bp (SLI-SW-*1364400*) observed.

A second round of drug pressure with G418 was performed to select for parasites where integration of the recombinant plasmids had occurred, and neomycin resistance was now present. In all three cases, parasitaemia decreased 4 days after integration selection, with the parasitaemia of NF54-epi(SLI-SW-*1364400*) recovering at day 10, indicating successful integration and neomycin resistance (Figure 3-20). However, for both NF54-epi(SLI-SW-*0105800*) and NF54-epi(SLI-SW-*1112100*), parasites only recovered after drug pressure was removed.
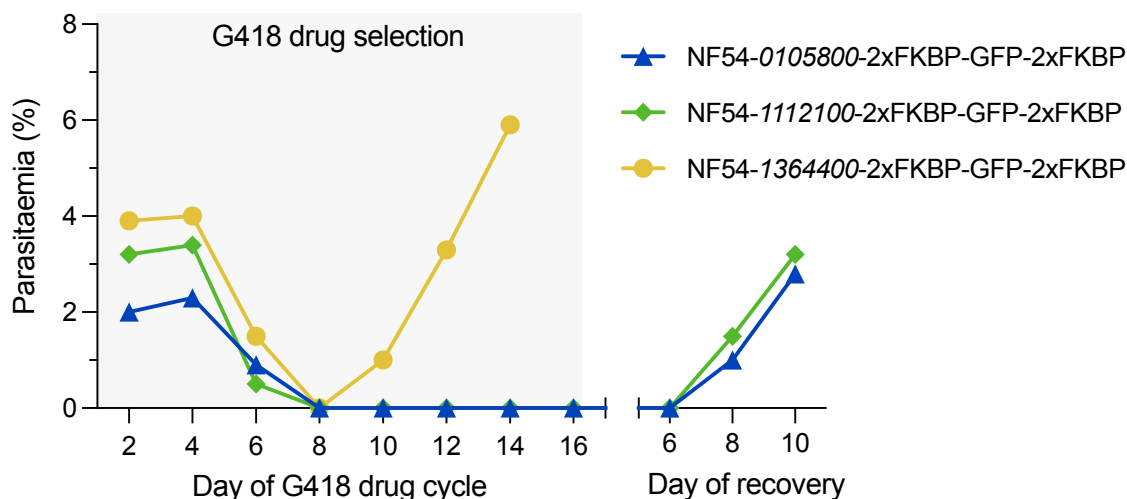
Figure 3–20: Selection for genomic integration and recovery of SLI-SW-*0105800*, SLI-SW-*1112100* and SLI-SW-*1364400 P. falciparum* parasite lines. *P. falciparum* NF54-epi(SLI-SW-*0105800*), NF54-epi(SLI-SW-*1112100*) and NF54-epi(SLI-SW-*1364400*) parasite lines were subjected to G418 drug selection to select for genomic integration. The parasitaemia was determined every second day during the drug cycle by Rapi-Diff-stained thin blood smears at 1000x magnification. Figure was generated using GraphPad Prism version 9.2.0.

Genomic integration was assessed via PCR using primers at the 5' and 3' regions flanking the inserts. A transgenic line is achieved if the WT locus, amplified by the 5' and 3' integration primers, is absent in the integrated line.

Successful integration of the recombinant SLI-SW-*0105800* plasmid into the *pf3d7_0105800* locus was indicated by the amplification of a single DNA band of ~1517 bp, indicating 5' integration, and a single DNA band of ~1643 bp, indicating 3' integration (Figure 3-21B). However, the integration was not homogeneous and WT parasites were still present as indicated by the amplification of the *pf3d7_0105800* locus seen as a single ~1966 bp band (Figure 3-21B). Therefore, the parasite culture was subjected to a second round of integration selection for 16 days where the concentration of G418 was increased to 800 μg/mL to ensure that all parasites that did not contain the Neo-R were eliminated. This resulted in full integration with no amplification of the *pf3d7_0105800* locus (Figure 3-21C).

Figure 3–21: PCR screening of SLI-SW-*0105800* integration into the *pf3d7_0105800* locus of *P. falciparum* parasites. PCR products were analysed on 1.5 % (w/v) agarose gel post stained with EtBr (0.4 mg/mL). Molecular marker (MM): 1 kb ladder (Promega, USA). **(A)** Schematic representation of the different primer pairs used, listed in Table 5, as well as the expected sizes for 5', 3' and loci integration checks. **(B)** Negative control (-C) containing no template DNA. NF54-*0105800*-2xFKBP-GFP-2xFKBP parasites were PCR screened for the presence of 5' and 3' integration. The presence of 5' and 3' integration bands indicate integration did occur. However, the presence of the original locus (WT LC) indicates that wild type parasites were present (1966 bp) within the parasite population. **(C)** NF54-*0105800*-2xFKBP-GFP-2xFKBP parasites which were subjected to a second round of G418 selection (800 µg/mL) were screened for the presence of 5' and 3' integration. The presence of 5' and 3' integration bands indicate successful integration, with no WT parasites present within the population as confirmed by the absence of the WT locus. INT=integrated parasite line, WT= NF54 wild type control, LC= original locus.

NF54-*1112100*-2xFKBP-GFP-2xFKBP was successfully integrated, as evidenced by amplification at the 5' (~1265 bp) and 3' (~930 bp) ends (Figure 3-22B). However, WT parasites were also present, necessitating a second round of integration selection, after which full integration was evident (Figure 3-22C).

Figure 3–22: PCR screening of SLI-SW-*1112100* integration into the *pf3d7_1112100* locus of *P. falciparum* parasites. PCR products were analysed on 1.5 % (w/v) agarose gel post stained with EtBr (0.4 mg/mL). Molecular marker (MM): 1 kb ladder (Promega, USA). **(A)** Schematic representation of the different primer pairs used, listed in Table 5, as well as the expected sizes for 5', 3' and loci integration checks. **(B)** Negative control (-C) containing no template DNA. NF54-*1112100*-2xFKBP-GFP-2xFKBP parasites were PCR screened for 5' and 3' integration. The presence of 5' and 3' integration bands confirmed integration. However, the presence of the original locus (WT LC) indicated presence of wild type parasites (1420 bp) within the parasite population. **(C)** NF54-*1112100*-2xFKBP-GFP-2xFKBP parasites which were subjected to a second round of G418 selection (800 µg/mL) and screened for 5' and 3' integration. The presence of 5' and 3' integration bands indicated that successful integration did occur and that no WT parasites were present within the population, due to the absence of the WT locus. INT=integrated parasite line, WT= NF54 wild type control, LC= original locus.

For NF54-*1364400*-2xFKBP-GFP-2xFKBP, successful integration of the recombinant SLI-SW-*1364400* plasmid occurred at the 5' end and 3' end with the amplification of a single DNA band of ~1440 bp and ~1210 bp respectively (Figure 3-23B). Again, additional G418 selection was required to force full integration. However, amplification of the *pf3d7_1364400* locus (~1560 bp) still occurred indicating a heterogeneous parasite population, which could not be improved with extended G418 drug selection (Figure 3-23C). Therefore, this line was not taken forward in subsequent analyses.
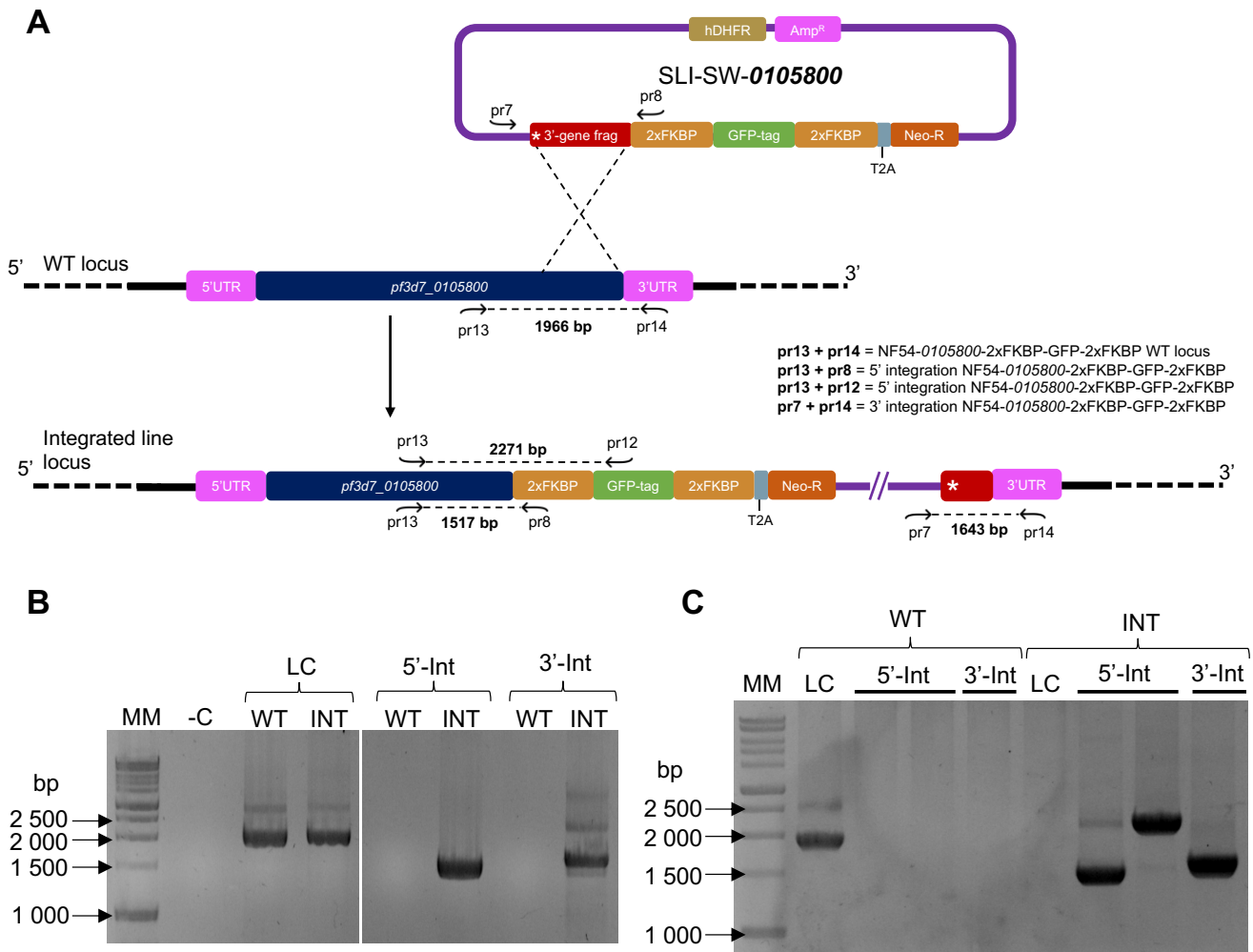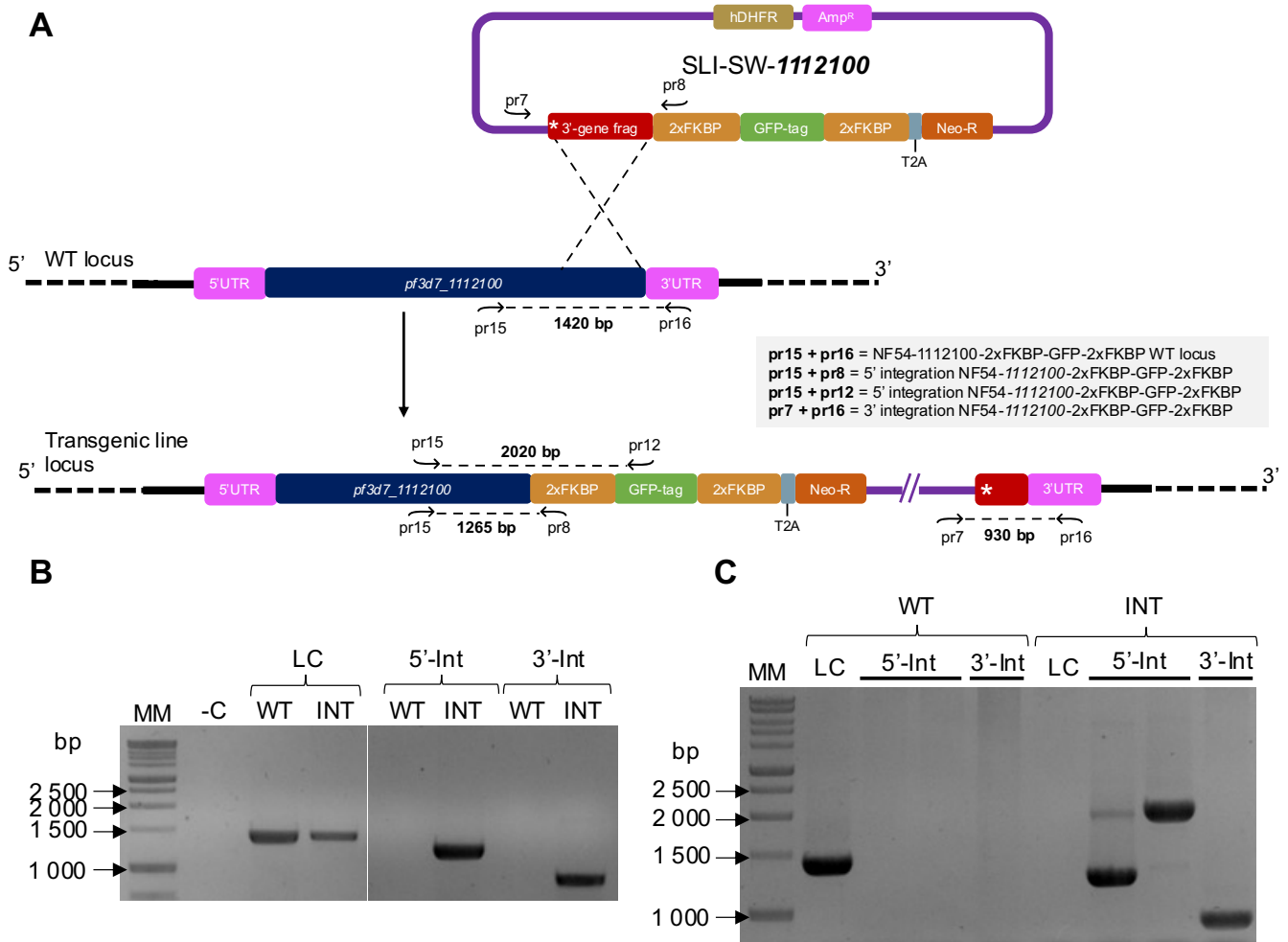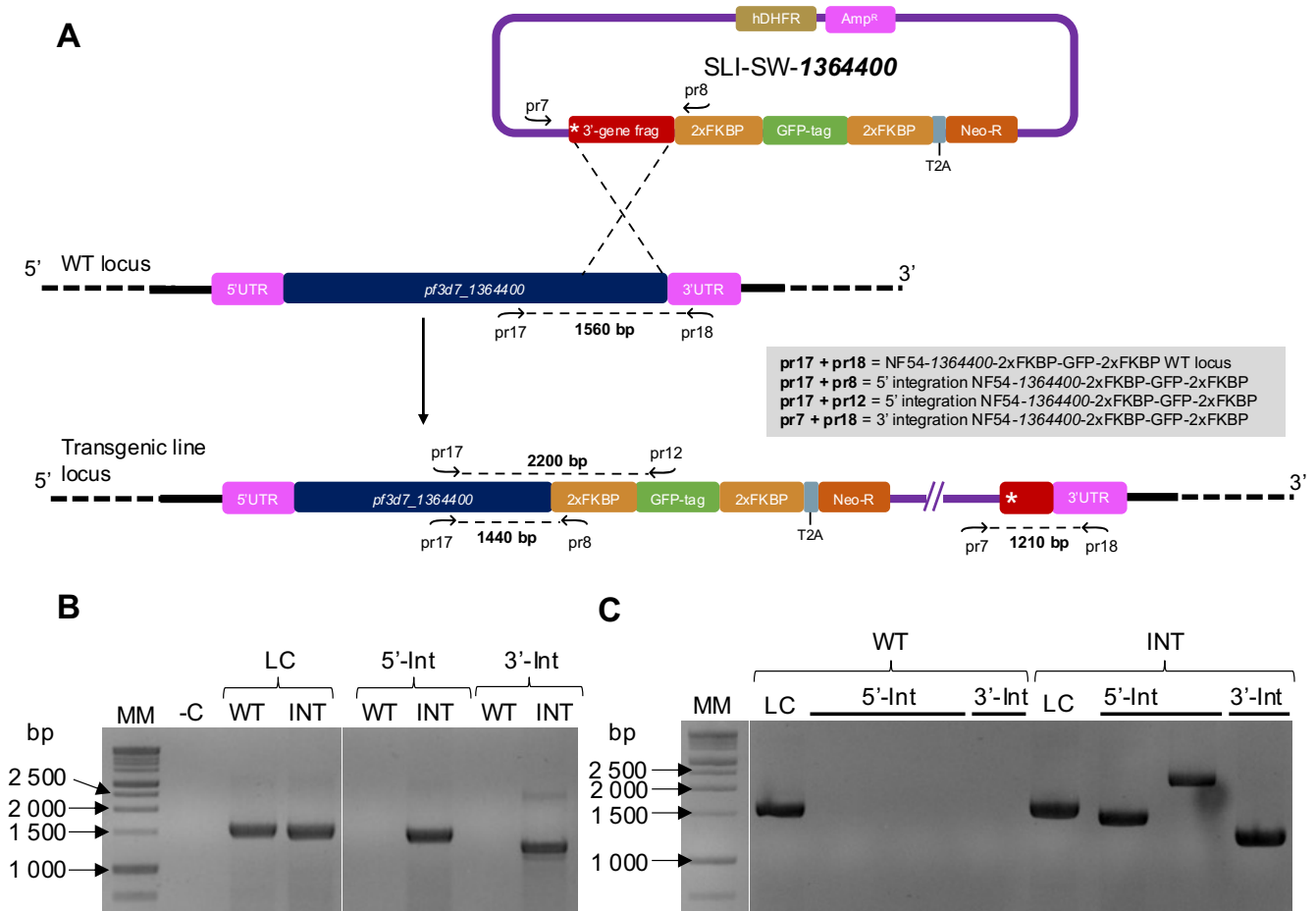
Figure 3–23: PCR screening of SLI-SW-*1364400* integration into the *pf3d7_1364400* locus of *P. falciparum* parasites. PCR products were analysed on 1.5 % (w/v) agarose gel post stained with EtBr (0.4 mg/mL). Molecular marker (MM): 1 kb ladder (Promega, USA). **(A)** Schematic representation of the different primer pairs used, listed in Table 5, as well as the expected sizes for 5', 3' and loci integration checks. **(B)** Negative control (-C) containing no template DNA. NF54-*1364400*-2xFKBP-GFP-2xFKBP parasites were PCR screened for the presence of 5' and 3' integration. The presence of 5' and 3' integration bands confirmed integration did occur. However, the presence of the original locus (WT LC) indicates wild type parasites were present (1560 bp) within the parasite population. **(C)** NF54-*1364400*-2xFKBP-GFP-2xFKBP parasites which were subjected to a second round of G418 selection (800 µg/mL) and screened for the presence of 5' and 3' integration. The presence of 5' and 3' integration bands indicate integration did occur, but that WT parasites were still present within the population due to the presence of the WT locus (1560 bp). INT=integrated parasite line, WT= NF54 wild type control, LC= original locus.

3.5. Validation of NF54-*0105800*-2xFKBP-GFP-2xFKBP and NF54-*1112100*-2xFKBP-GFP-2xFKBP transgenic parasite lines

3.5.1. Growth rate and morphological evaluation of knock sideways transgenic parasite lines

Transgenic NF54-*0105800*-2xFKBP-GFP-2xFKBP and NF54-*1112100*-2xFKBP-GFP-2xFKBP parasite lines were evaluated for changes in asexual proliferation and parasite morphology to ensure that no unwanted abnormalities resulting from integration had arisen. Tightly synchronised parasites from these two lines were monitored over 2.5 IDCs and compared to that of a WT *P. falciparum* NF54 parasite line (Figure 3-24). The proliferation results showed similar increases in parasitaemia between the WT *P. falciparum* NF54 parasite line and NF54-*0105800*-2xFKBP-GFP-2xFKBP and NF54-*1112100*-2xFKBP-GFP-2xFKBP transgenic parasites.

Figure 3–24: Proliferation analysis of NF54-*0105800*-2xFKBP-GFP-2xFKBP and NF54-*1112100*-2xFKBP-GFP-2xFKBP transgenic parasite lines. Intra-erythrocytic asexual proliferation rate evaluation. Tightly synchronised parasites were allowed to proliferate for 120 h. Parasitaemia was determined every 24 h. Figure was generated using GraphPad Prism version 9.2.0. The increase in parasitaemia of the NF54-*0105800*-2xFKBP-GFP-2xFKBP and NF54-*1112100*-2xFKBP-GFP-2xFKBP parasite lines was similar to that of WT *P. falciparum* NF54 parasites.

Furthermore, no morphological abnormalities where present in the asexual parasite stages of either of the transgenic parasite lines (Figure 3-25). Thus, it could be confirmed that integration of the GFP-FKBP tagged versions of *pf3d7_0105800* and *pf3d7_1112100* into their respective loci caused no unwanted effects on asexual proliferation rates, with no phenotypic abnormalities observed, and both lines could be further evaluated for localisation (through GFP imaging) and mislocalisation (through FKBP-FRB dimerisation) of the protein products.
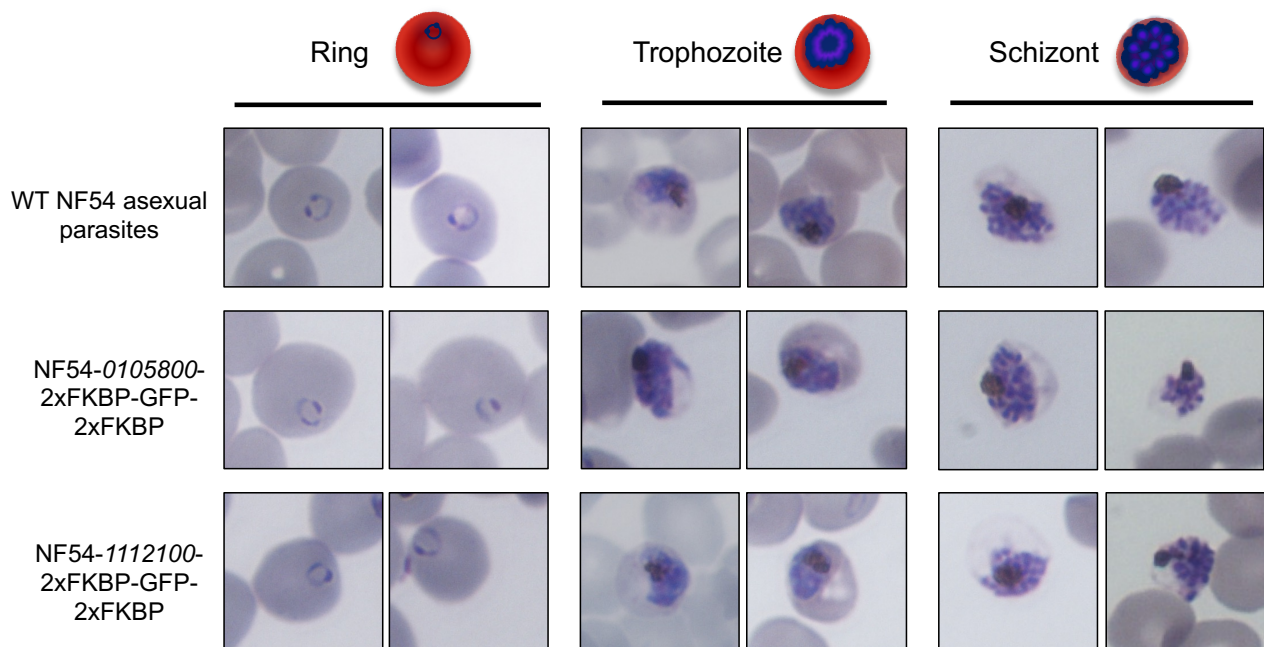
Figure 3–25: Intra-erythrocytic IDC phenotype analysis of NF54-*0105800*-2xFKBP-GFP-2xFKBP and NF54-*1112100*-2xFKBP-GFP-2xFKBP transgenic parasite lines. The different intra-erythrocytic asexual stage phenotypes of NF54-*0105800*-2xFKBP-GFP-2xFKBP and NF54-*1112100*-2xFKBP-GFP-2xFKBP parasites were morphologically evaluated by visualising Rapi-Diff-stained thin blood smears under a light microscope at 1000x magnification. The different intra-erythrocytic asexual parasite stages compared to WT *P. falciparum* NF54 parasites to ensure that no morphological abnormalities were present. NF54-*0105800*-2xFKBP-GFP-2xFKBP and NF54-*1112100*-2xFKBP-GFP-2xFKBP parasites had similar morphology to that of the WT *P. falciparum* NF54 parasites when comparing ring, trophozoite and schizont stages of development.

3.5.2. PF3D7_0105800 and PF3D7_1112100 localise to the cytoplasm of asexual *P. falciparum* parasites

Localisation of both PF3D7_0105800 and PF3D7_1112100 was possible, as these are tagged with GFP in the SLI-SW-*0105800* and SLI-SW-*1112100* constructs. Early- to late-stage schizonts (~40–44 hpi) indicated localisation of both PF3D7_0105800 and PF3D7_1112100 to the cytoplasm with no distinct co-localisation with the nuclear stain Hoechst as DNA marker, due to the absence of yellow overlap signal (Figure 3-26). However, detecting overlapping signals is complicated in multinucleated schizonts, where the nuclei signal is surrounded by cytoplasmic signal and would require Z-stacking to distinguish plane of localisation. Both *pf3d7_0105800* and *pf3d7_1112100* have an increased transcript abundance during late trophozoites (27-35 hpi), which peaks during late schizont-stage parasites [123].
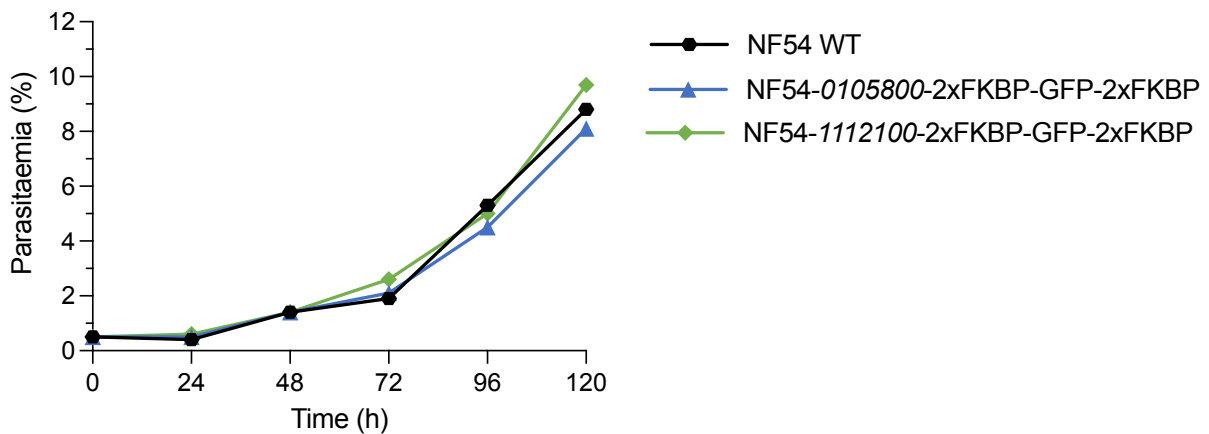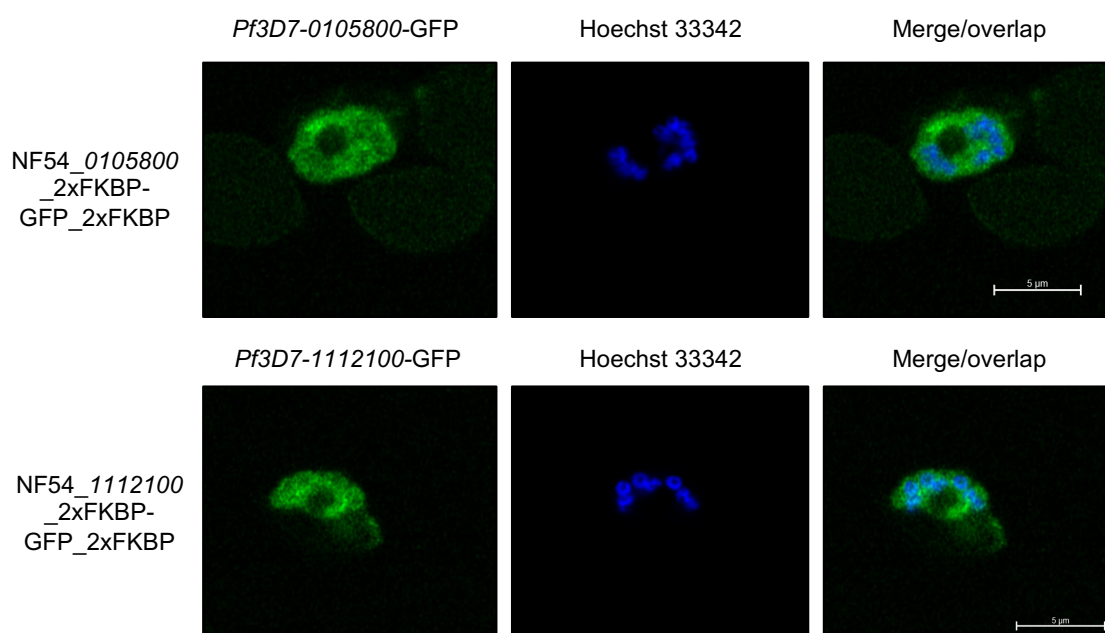

Figure 3–26: Localisation of NF54-*0105800*-2xFKBP-GFP-2xFKBP and NF54-*1112100*-2xFKBP-GFP-2xFKBP transgenic parasite lines. Hoechst 33342, indicated in blue, stains the DNA of the parasite. The GFP-target fusion protein is indicated in green. Scale bars represent 5 μm distance. This image is representative of similar phenotypes observed in >10 parasite images.

3.6. Functional analysis of PF3D7_0105800 and PF3D7_1112100 using knock sideways

To interrogate the functionality of PF3D7_0105800 and PF3D7_1112100 during asexual proliferation of *P. falciparum*, mislocalisation through knock sideways was performed. Given that each protein kinase was observed to localise to the cytosol (Figure 3-27), both were subjected to nuclear mislocalisation using the p1xNLS-FRB-mcherry-hsp86-BSD plasmid [106].

3.6.1. Transfection and episomal uptake confirmation of p1xNLS-FRB-mcherry-hsp86-BSD

To induce the knock sideways, an additional plasmid (p1xNLS-FRB-mcherry-hsp86-BSD), was introduced to the transgenic lines through transfection. This plasmid contains mCherry as a fluorophore,

expressed as a fusion protein with a nuclear localisation signal (NLS). The FKBP-tagged proteins of interest would associate with FRB in the FRB-mCherry fusion protein transcribed on this additional plasmid and is induced by the addition of rapalog.

The identity of the p1xNLS-FRB-mcherry-hsp86-BSD was confirmed with *Xma*I and *Mlu*I-HF as well as *Xma*I and *Xho*I RE mapping (Figure 3-27B) and successful episomal uptake was achieved after transfection and blasticidin drug pressure (~1499 bp band amplified, Figure 3-27C).
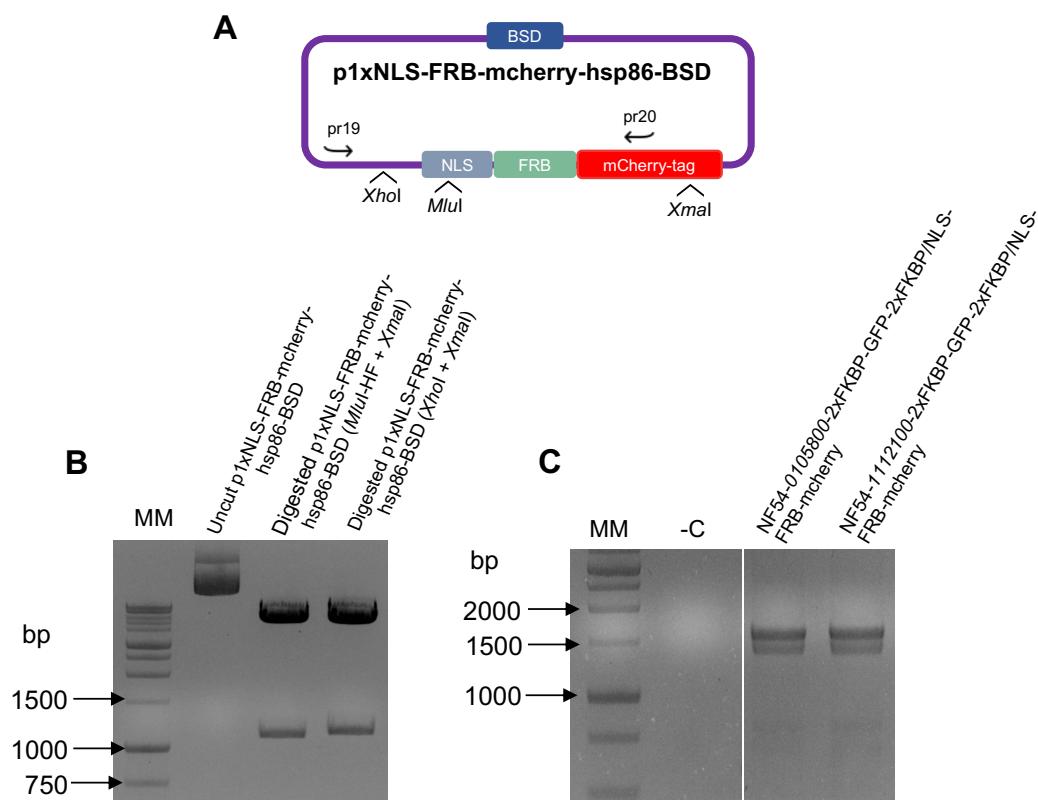
Figure 3–27: Verification of identity and episomal uptake of p1xNLS-FRB-mcherry-hsp86-BSD plasmid. DNA samples were analysed on 1.5 % (w/v) agarose gel post stained with EtBr (0.4 mg/mL). Molecular marker (MM): 1 kb ladder (Promega, USA). **(A)** Schematic representing the p1xNLS-FRB-mcherry-hsp86-BSD plasmid showing the restriction enzymes used during RE mapping and the primers used to confirm episomal uptake. **(B)** p1xNLS-FRB-mcherry-hsp86-BSD plasmid DNA (2 µg) was digested for 3 h at 37 °C with *Mlu*I-HF and *Xma*I as well as *Xho*I and *Xma*I which yielded bands of expected sizes, ~1130 bp and ~1190 bp respectively. **(C)** Negative control (-C) containing no template DNA. PCR amplification of the p1xNLS-FRB-mcherry-hsp86-BSD plasmid (~1488 bp) showing episomal presence in both NF54-*0105800*-2xFKBP-GFP-2xFKBP and NF54-*1112100*-2xFKBP-GFP-2xFKBP parasites.

3.6.2. Nuclear mislocalisation of PF3D7_0105800 and PF3D7_1112100 using the knock sideways system

Mislocalisation (knock sideways) was induced in the above parasite lines with rapalog (rapamycin). The asexual proliferation rate of rapalog-treated and untreated parasites was monitored every 24 h for 96 h, (Figure 3-28). There was no difference in the asexual proliferation rate between untreated- and rapalog-treated parasites in either the NF54-*0105800*-2xFKBP-GFP-2xFKBP/NLS-FRB-mcherry or the NF54-*1112100*-2xFKBP-GFP-2xFKBP/NLS-FRB-mcherry parasites as the parasitaemia increased

consistently 48 h, indicating that mislocalisation of the target protein kinase from the cytosol to the nucleus did not result in any abnormal growth rates (Figure 3-28).
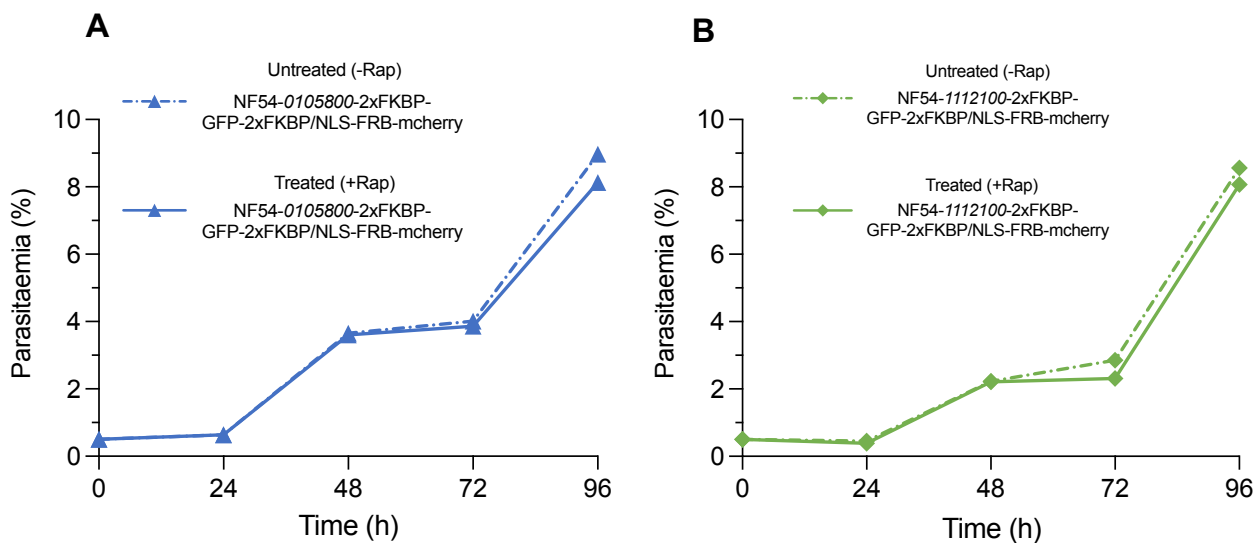
Figure 3–28: Growth rate of untreated and rapalog-treated NF54-*0105800*-2xFKBP-GFP-2xFKBP/NLS-FRB-mcherry and NF54-*1112100*-2xFKBP-GFP-2xFKBP/NLS-FRB-mcherry parasite lines. Proliferation of synchronised NF54-*0105800*-2xFKBP-GFP-2xFKBP/NLS-FRB-mcherry and NF54-*1112100*-2xFKBP-GFP-2xFKBP/NLS-FRB-mcherry parasites was determined for 96 h. Parasites were treated with rapalog every 24 h. Parasitaemia was calculated every day by counting >1000 erythrocytes for each sample. Figures were generated using GraphPad Prism version 9.2.0.

However, this lack of phenotypic effect on parasite proliferation could be due to inefficient mislocalisation of the target proteins, with a portion of protein sufficient for execution of essential functions remaining in the predicted site of action. Therefore, to evaluate if mislocalisation of the target proteins from the cytosol to the nucleus did occur, NF54-*0105800*-2xFKBP-GFP-2xFKBP/NLS-FRB-mcherry and NF54-*1112100*-2xFKBP-GFP-2xFKBP/NLS-FRB-mcherry parasites were treated with rapamycin for 1 h to induce mislocalisation and then evaluated using a Zeiss LSM 880 Confocal Laser Scanning Microscope (LSM) (Figure 3-29).

Both untreated NF54-*0105800*-2xFKBP-GFP-2xFKBP/NLS-FRB-mcherry and NF54-*1112100*-2xFKBP-GFP-2xFKBP/NLS-FRB-mcherry parasites showed localisation of the target proteins associated with GFP (indicated in green) to the cytosol and not to the nucleus as expected. However, unexpectedly the nuclear mislocaliser mCherry-signal (indicated in red) did not colocalise to the nucleus of the parasites as expected (Figure 3-29). A similar phenomenon was observed for NF54-*0105800*-2xFKBP-GFP-2xFKBP/NLS-FRB-mcherry and NF54-*1112100*-2xFKBP-GFP-2xFKBP/NLS-FRB-mcherry parasites treated with rapalog, where the mCherry- and GFP-signals colocalised to the cytosol instead of to the nucleus of the parasites, indicating that nuclear mislocalisation did not occur (Figure 3-29).

This explains the results observed for asexual proliferation of NF54-*0105800*-2xFKBP-GFP-2xFKBP/NLS-FRB-mcherry and NF54-*1112100*-2xFKBP-GFP-2xFKBP/NLS-FRB-mcherry parasites, as the target proteins were not being displaced from their predicted sites of action and could therefore continue to perform their biological functions. As nuclear mislocalisation of the putative kinase proteins did not work as expected based on prior data [106], the efficiency of the knock sideways system was interrogated by testing plasma membrane mislocalisation for PF3D7_0105800 only.

Figure 3–29: Fluorescent evaluation of plasma membrane knock sideways of NF54-*0105800*-2xFKBP-GFP-2xFKBP/NLS-FRB-mcherry and NF54-*1112100*-2xFKBP-GFP-2xFKBP/NLS-FRB-mcherry parasite lines via confocal microscopy. Synchronised untreated (control) and 1 h rapalog-treated (+Rap) NF54-*0105800*-2xFKBP-GFP-2xFKBP/NLS-FRB-mcherry and NF54-*1112100*-2xFKBP-GFP-2xFKBP/NLS-FRB-mcherry parasites were examined using a Zeiss LSM 880 Confocal Laser Scanning Microscope (LSM). DIC: differential interference contrast. Target protein kinase associated with GFP-tag (green); Hoechst 33342: parasite nuclear stain (blue); MislocaliserN: Nuclear localisation signal with the mCherry-tag shown in red. Scale bars represent a5 µm distance.

3.6.3. Transfection and episomal uptake confirmation of pLyn-FRB-mcherry-nmd3-BSD

pLyn-FRB-mcherry-nmd3-BSD containing a membrane localisation signal was successfully isolated and verified with RE mapping (Figure 3-30B). The confirmed pLyn-FRB-mcherry-nmd3-BSD plasmid was subsequently used to transfect NF54-*0105800*-2xFKBP-GFP-2xFKBP parasites, and blasticidin drug pressure was used to select for episomal uptake. Episomal presence was confirmed on recovered NF54-*0105800*-2xFKBP-GFP-2xFKBP/Lyn-FRB-mcherry parasites (amplification of a ~650 bp band, Figure 3-30C).
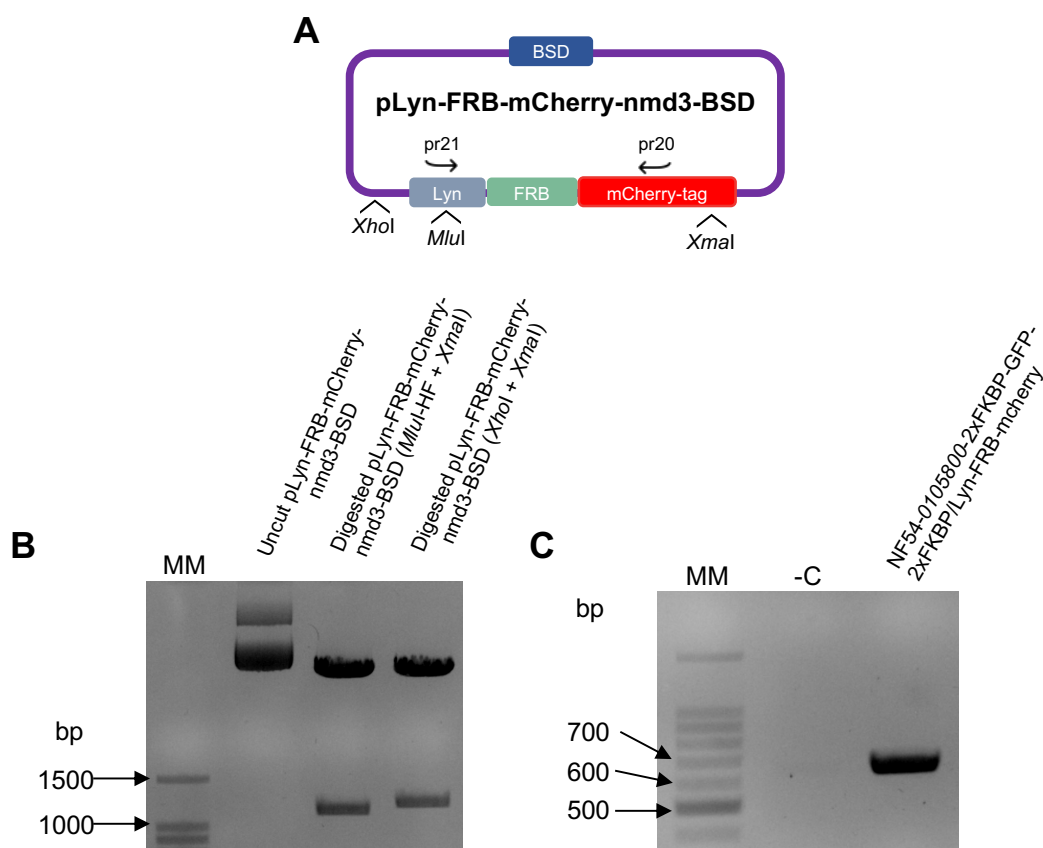
Figure 3–30: Verification of identity and episomal uptake of pLyn-FRB-mcherry-nmd3-BSD plasmid. Plasmid DNA. DNA samples were analysed on 1.5 % (w/v) agarose gel post stained with EtBr (0.4 mg/mL). Molecular marker (MM): 1 kb ladder (Promega, USA). **(A)** Schematic representing the pLyn-FRB-mcherry-nmd3-BSD plasmid showing the restriction enzymes used during RE mapping and the primers used to confirm episomal uptake. **(B)** pLyn-FRB-mcherry-nmd3-BSD plasmid DNA (2 μg) was digested for 3 h at 37 °C with *Mlu*I-HF and *Xma*I as well as *Xho*I and *Xma*I which yielded bands of expected sizes, ~1130 bp and ~1190 bp respectively. **(C)** Negative control (-C) containing no template DNA. PCR amplification of the pLyn-FRB-mcherry-nmd3-BSD plasmid (~650 bp) showing episomal presence in NF54-*0105800*-2xFKBP-GFP-2xFKBP parasites.

3.6.4. Plasma membrane mislocalisation of PF3D7_0105800

Asexual proliferation of rapalog- (rapamycin) treated and untreated NF54-*0105800*-2xFKBP-GFP-2xFKBP/Lyn-FRB-mcherry parasites was not altered, as before (Figure 3-31).
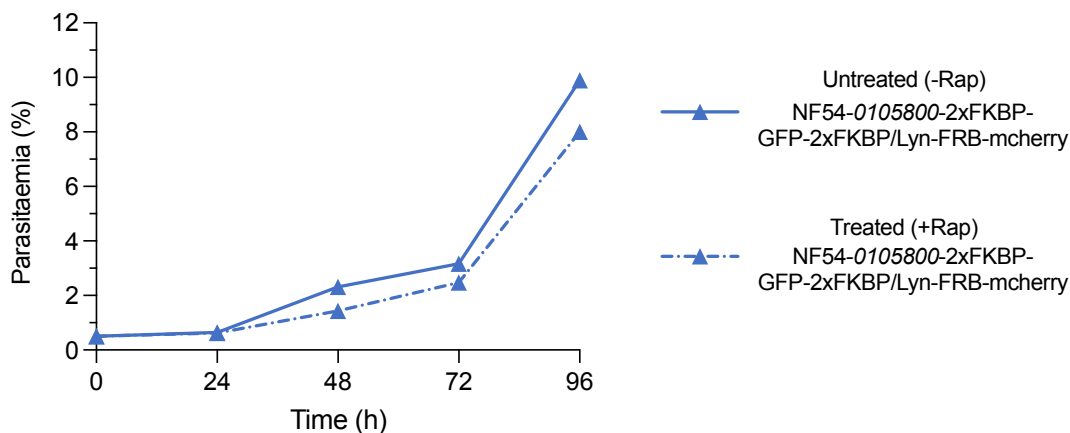
Figure 3–31: Growth rate of untreated and rapalog-treated NF54-*0105800*-2xFKBP-GFP-2xFKBP/Lyn-FRB-mcherry parasite lines. Proliferation of synchronised NF54-*0105800*-2xFKBP-GFP-2xFKBP/Lyn-FRB-mcherry parasites was determined for 96 h. Parasites were treated with rapalog every 24 h. Parasitaemia was calculated every day by counting >1000 erythrocytes for each sample. Figure was generated using GraphPad Prism version 9.2.0.

As before, confocal microscopy was used to confirm membrane mislocalisation of PF3D7_0105800 (Figure 3-32). The GFP (green) signal and mCherry (red) signal overlap was seemingly identical in the untreated sample. However, this occurrence was also observed in the rapalog-treated sample, without any increase in the GFP signal to the periphery of the parasite (Figure 3-32). These results can be confirmed with future Z-stacking to observe depth in signal throughout the parasite. The inability to observe a shift in mCherry signal upon induction in either the nuclear or membrane mislocalisation systems, indicates that the knock sideways system may be compromised. Therefore, alternative inducible systems that does not rely on cellular localisation to affect protein function was investigated. The *glmS* conditional knockdown system was used to functionally study the putative kinase proteins.
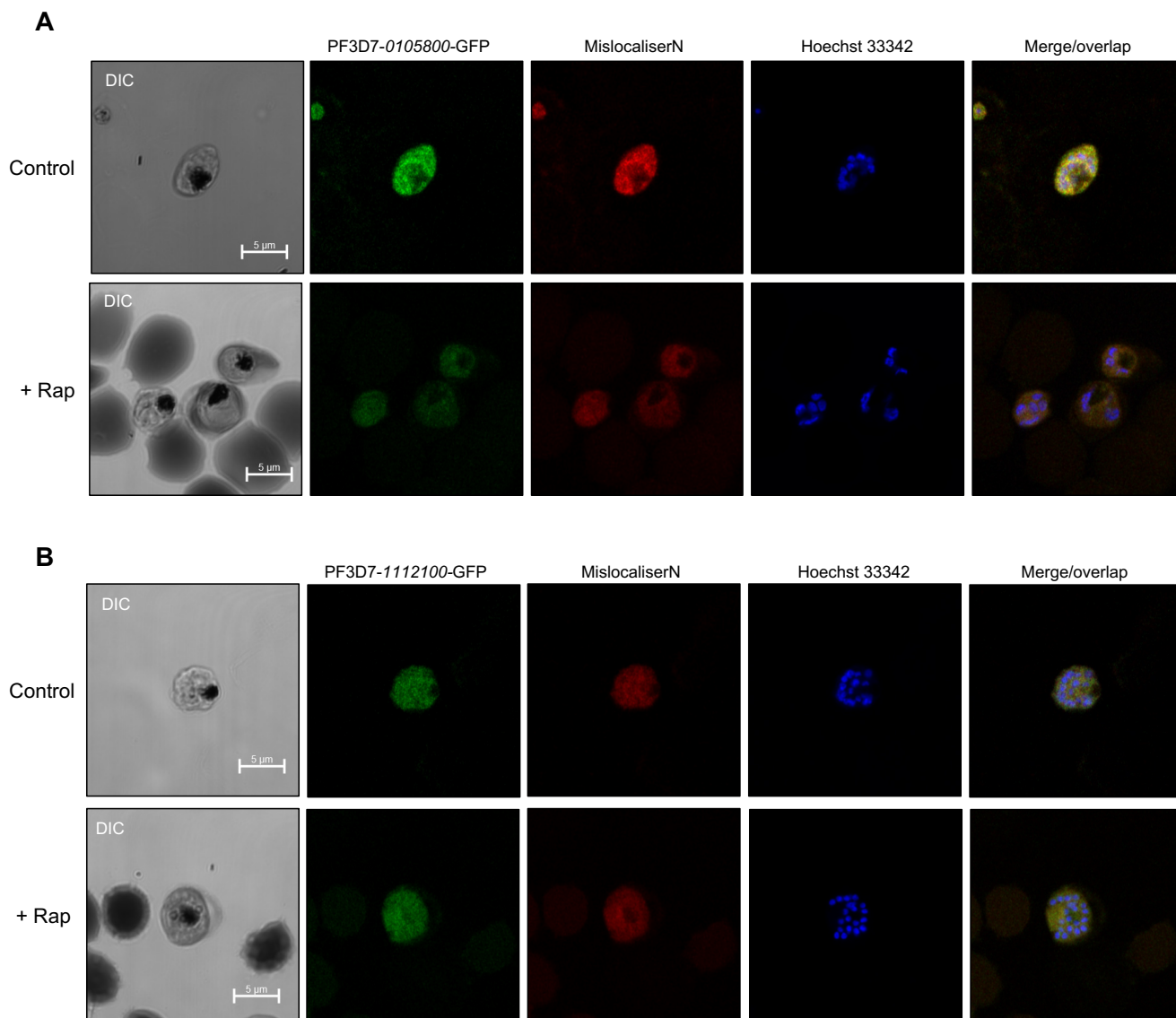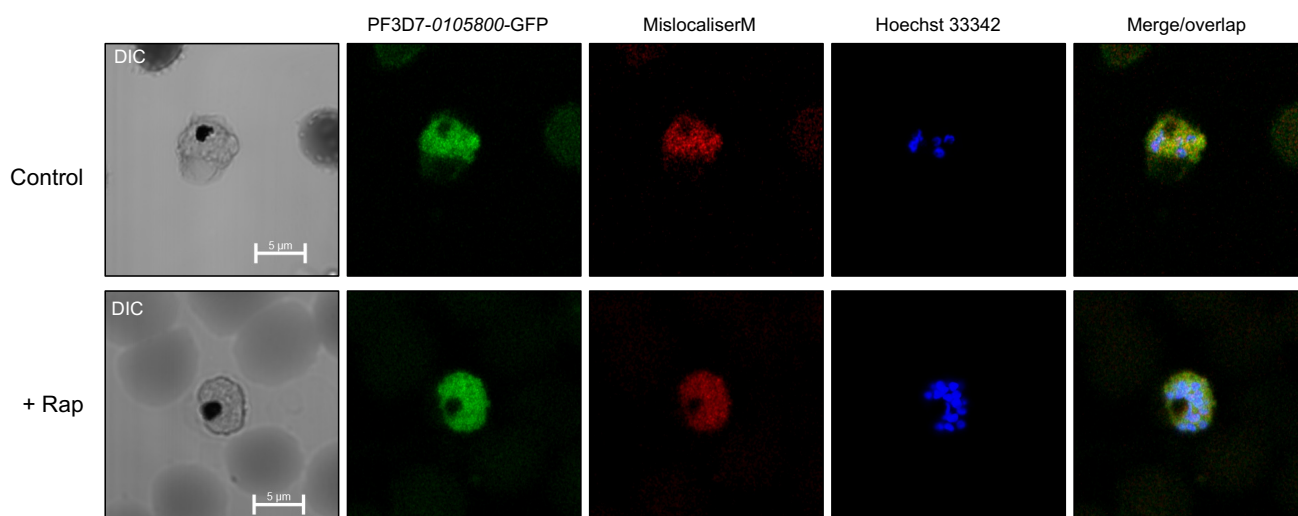

Figure 3–32: Fluorescent evaluation of plasma membrane knock sideways of NF54-*0105800*-2xFKBP-GFP-2xFKBP/Lyn-FRB-mcherry parasite line via confocal microscopy. Synchronised untreated (control) and 1h rapalog treated (+Rap) NF54-*0105800*-2xFKBP-GFP-2xFKBP/Lyn-FRB-mcherry parasites were examined using a Zeiss LSM 880 Confocal Laser Scanning Microscope (LSM). DIC: differential interference contrast. Target protein kinase associated with GFP-tag (green); Hoechst 33342: parasite nuclear stain (blue); MislocaliserM: Plasma membrane mislocaliser, with mCherry-tag indicated in red. Scale bars represent a5 µm distance.

3.7. Cloning of a 3'-gene fragment from each selected kinase encoding gene into the SLI-*glmS* system

Gene-specific 3'-gene fragments were successfully amplified for all of the selected kinase genes (*pf3d7_0105800, pf3d7_1112100* and *pf3d7_1364400*) with PCR amplicons corresponding to the expected fragment sizes: ~1050 bp, ~640 bp and ~940 bp (Figure 3-33). All the PCR products of the correct sizes were extracted from the gel and purified, with total DNA yields of 600–750 ng and with acceptable purity indicators.
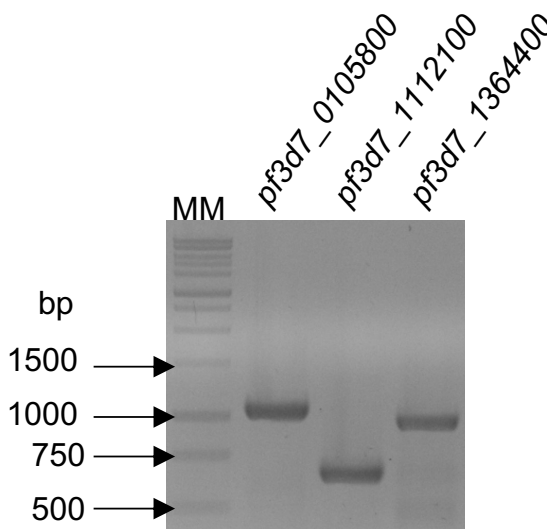
Figure 3–33: PCR amplification of gene specific 3'-gene fragments to be cloned into the SLI-*glmS* and SLI-*glmS*-mut plasmids. Amplified PCR products were analysed on a 2 % (w/v) agarose gel post stained with EtBr (0.4 mg/mL). Molecular marker (MM): 1 kb ladder (Promega, USA). The expected amplicon band sizes were obtained of ~1050 bp (*pf3d7_0105800* 3'-gene fragment), ~640 bp (*pf3d7_1112100* 3'-gene fragment), ~940 bp (*pf3d7_1364400* 3'-gene fragment).

A saturated bacterial culture was cultivated from bacterial stock cultures containing the original SLI-*glmS* and SLI-*glmS*-mut plasmids. This plasmid DNA was isolated and digested with *Not*I-HF and *Mlu*I-HF to verify the plasmid identity (Figure 3-34A), yielding two bands, of which the larger (~6.9 kb) corresponds to the expected size of the plasmid backbone and the smaller (~860 bp) corresponds to the expected size of the original insert (*pf3d7_1406300*) (Figure 3-34B
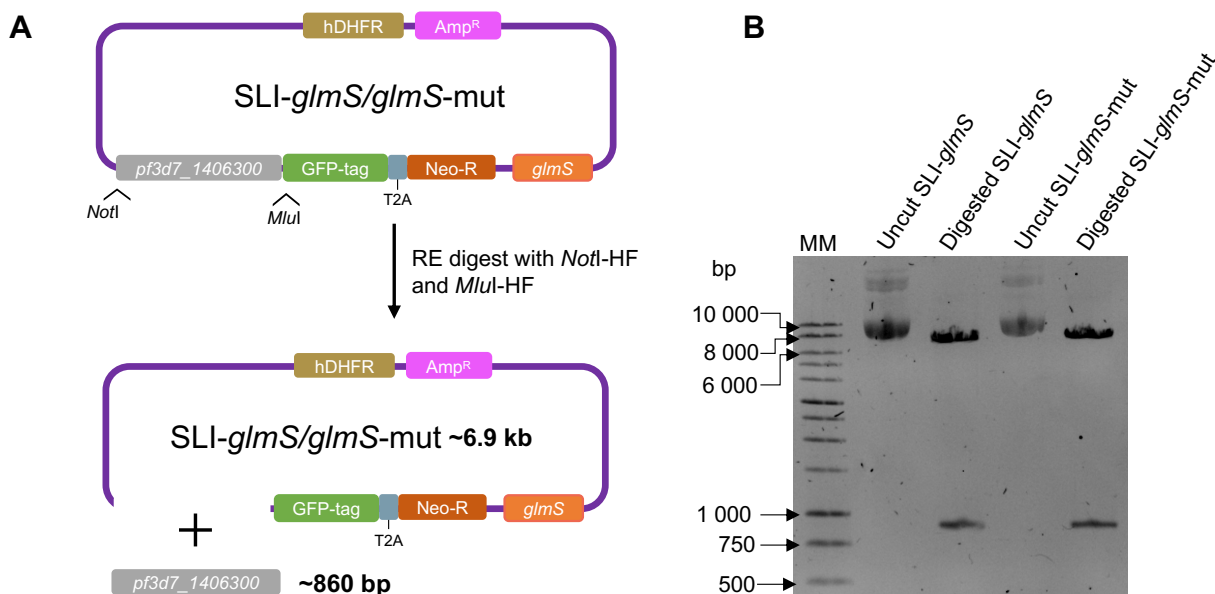
Figure 3–34: Restriction enzyme digest of the original SLI-*glmS* and SLI-*glmS*-mut plasmids. **(A)** Schematic representation of RE mapping of the original SLI-*glmS* and SLI-*glmS*-mut plasmids with the expected sized plasmid backbone and insert indicated. **(B)** Plasmid DNA (550 ng) was analysed on 1 % (w/v) agarose gel post stained with EtBr (0.4 mg/mL) after RE digestion for 3 h at 37 °C. Molecular marker (MM): 1 kb ladder (Promega, USA). Complete digestion of the original SLI-*glmS* and SLI-*glmS*-mut plasmids with *Not*I-HF and *Mlu*I-HF yielded two bands with the larger bands corresponding to the expected size of the plasmid backbone and the smaller bands to original insert**.**

The plasmids were prepared for ligation by digestion with *Not*I-HF and *Mlu*I-HF to allow for sticky-end cloning. After ligation, colony PCR screening was performed to confirm the presence of recombinant clones with ~1200 bp (SLI-*glmS-0105800*), ~770 bp (SLI-*glmS-1112100*) and ~1100 bp (SLI-*glmS-1364400*) insert sizes (Figure 3-35B, Supplementary figure S3 and S4), all of which were verified with additional RE mapping (Figure 3-35C, supplementary Figure S3 and S4), yielding the expected sizes for each insert.
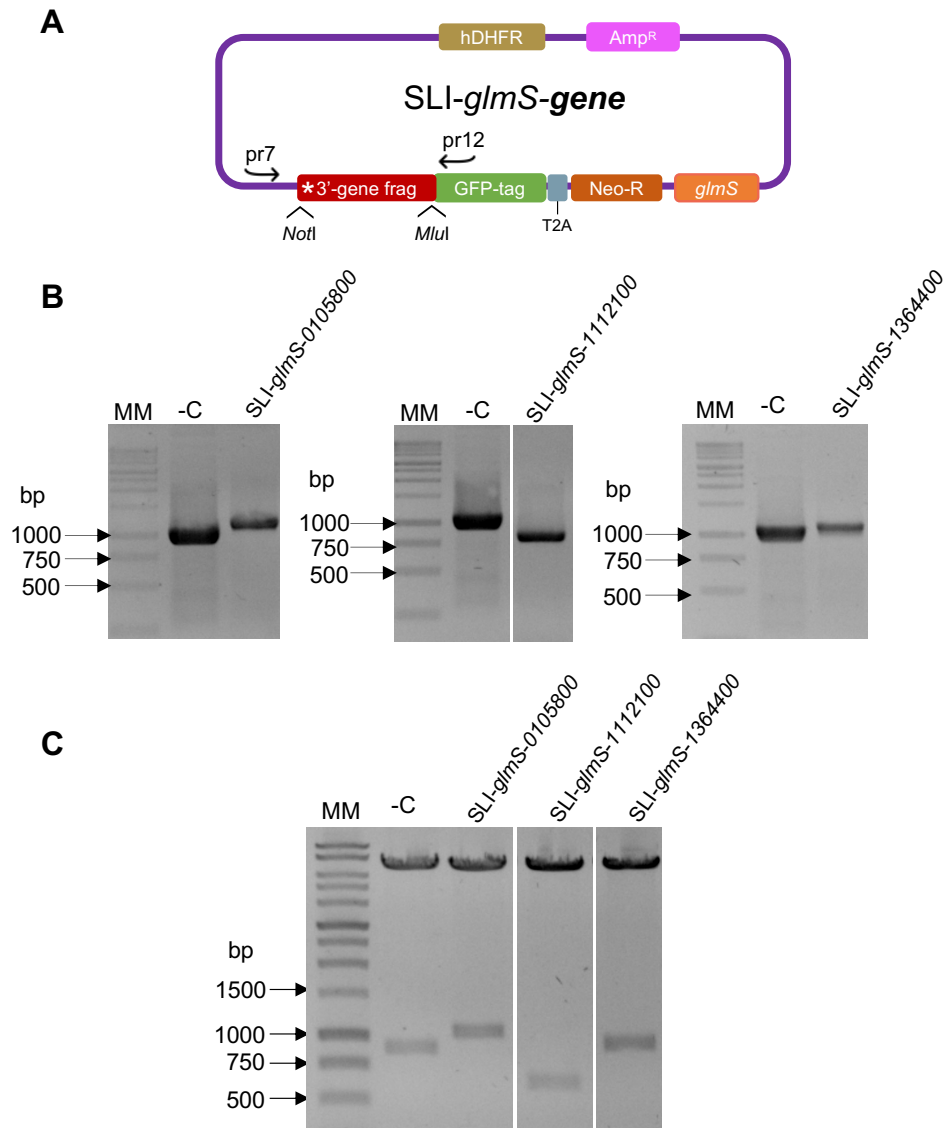
Figure 3–35: Validation of SLI-*glmS*-0105800, SLI-*glmS*-1112100 and SLI-*glmS*-1364400 recombinant plasmids. DNA samples were analysed on 1.5 % (w/v) agarose gel, post stained with EtBr (0.4 mg/mL). Molecular marker (MM): 1 kb ladder (Promega, USA). **(A)** A schematic representation showing the primer pair (pr7 and pr12) used during the screening PCR, listed in Table 4. The primers (pr7 and pr12) bind upstream and downstream respectively on the SLI-*glmS* backbone flanking the insert region. **(B)** Negative control (-C) containing the amplification of the original insert region (~1100 bp). Colony screening PCR of the *pf3d7_0105800, pf3d7_1112100* and *pf3d7_1364400* 3'-gene fragments cloned into the SLI-*glmS* plasmid. The expected regions were amplified for all of the 3'-gene fragments with PCR products of ~1200 bp (SLI-*glmS*-0105800), ~770 bp (SLI-*glmS*-1112100) and ~1100 bp (SLI-*glmS*-1364400). **(C)** Negative control (-C) containing the digestion of the original SLI-*glmS*-mut plasmid containing the original insert (~860 bp). Restriction enzyme mapping of isolated plasmid DNA form SLI-*glmS*-0105800, SLI-*glmS*-1112100 and SLI-*glmS*-1364400 positive screening clones using *Not*I-HF and *Mlu*I-HF. The insert regions, indicated by bands of ~1050 bp (SLI-*glmS*-0105800), ~640 bp (SLI-*glmS*-1112100) and ~940 bp (SLI-*glmS*-1364400), were excised.

In addition to generating recombinant SLI-*glmS* plasmids containing the 3'-gene fragment of each selected putative kinase gene, recombinant SLI-*glmS*-mut plasmids had to be generated. Therefore, the same 3'-gene fragment isolated, and purified and prepared earlier was ligated into the SLI-*glmS*-mut vector, with transformed positive colonies selected by colony PCR screening and RE mapping (Figure 3-36B, C) and retained.
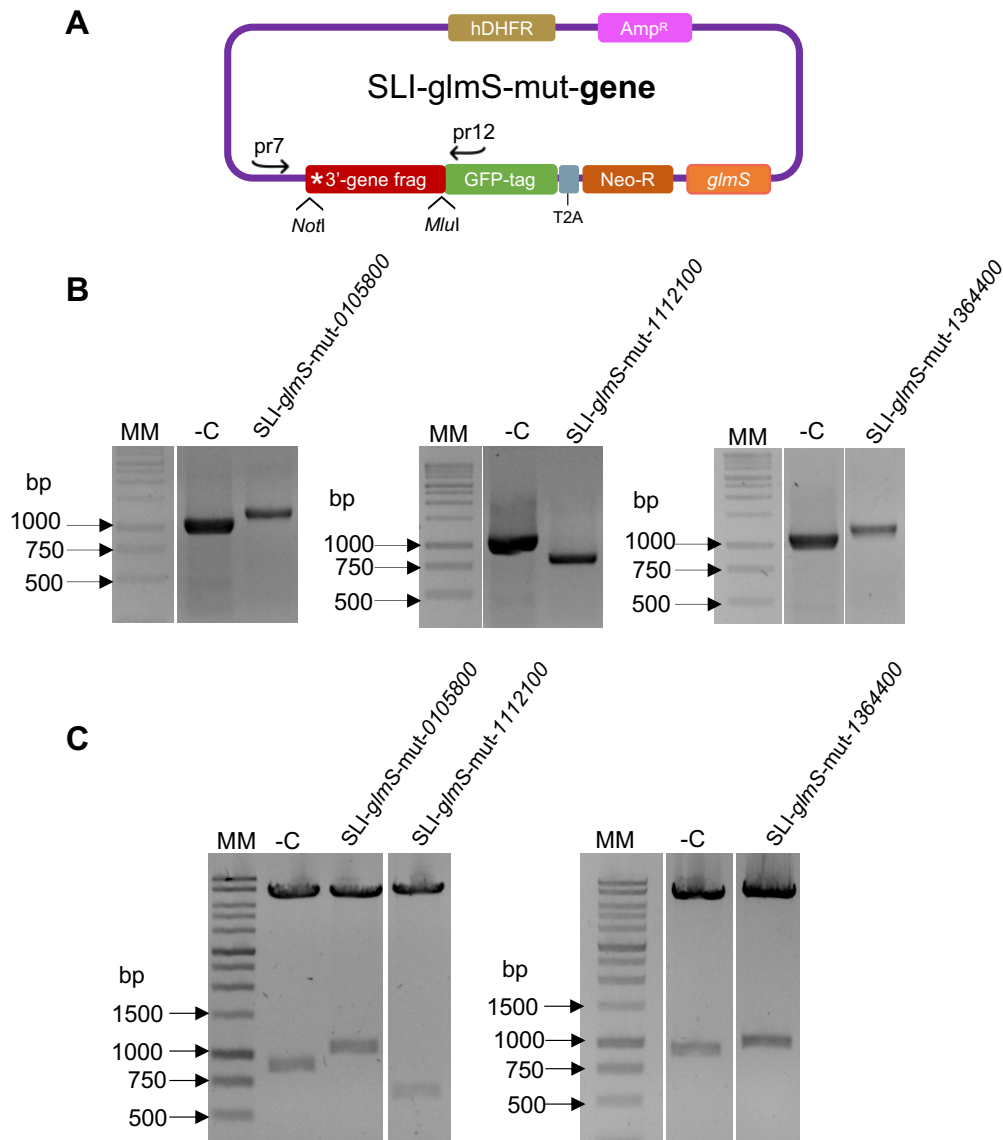
Figure 3–36: Validation of SLI-*glmS*-mut-*0105800*, SLI-*glmS*-mut-*1112100* and SLI-*glmS*-mut-*1364400* recombinant plasmids. DNA samples were analysed on 1.5 % (w/v) agarose gel, post stained with EtBr (0.4 mg/mL). Molecular marker (MM): 1 kb ladder (Promega, USA). **(A)** A schematic representation showing the primer pair (pr7 and pr12) used during the screening PCR, listed in Table 4. The primers (pr7 and pr12) bind upstream and downstream respectively on the SLI-*glmS*-mut backbone flanking the insert region. **(B)** Negative control (-C) containing the amplification of the original insert region (~1100 bp). Colony screening PCR of the *pf3d7_0105800, pf3d7_1112100* and *pf3d7_1364400* 3'-gene fragments cloned into the SLI-*glmS*-mut plasmid. The expected regions were amplified for all of the 3'-gene fragments with PCR products of ~1200 bp (SLI-*glmS*-mut-*0105800*), ~770 bp (SLI-*glmS*-mut-*1112100*) and ~1100 bp (SLI-*glmS*-mut-*1364400*). **(C)** Negative control (-C) containing the digestion of the original SLI-*glmS*-mut plasmid containing the original insert (~860 bp). Restriction enzyme mapping of isolated plasmid DNA form SLI-*glmS*-mut-*0105800*, SLI-*glmS*-mut-*1112100* and SLI-*glmS*-mut-*1364400* positive screening clones using *Not*I-HF and *Mlu*I-HF. The insert regions, indicated by bands of the expected sizes, with bands of ~1050 bp (SLI-*glmS*-mut-*0105800*), ~640 bp (SLI-*glmS*-mut-*1112100*) and ~940 bp (SLI-*glmS*-mut-*1364400*) were excised.

Sanger sequencing confirmed the insert and orientation in SLI-*glmS*-*0105800,* SLI-*glmS*-*1112100* and SLI-*glmS*-*1364400* (Figure 3-37), as well as the *glmS*-mut forms of each gene (Figure 3-38). The sequencing alignment further revealed that no missense or nonsense mutations were present.
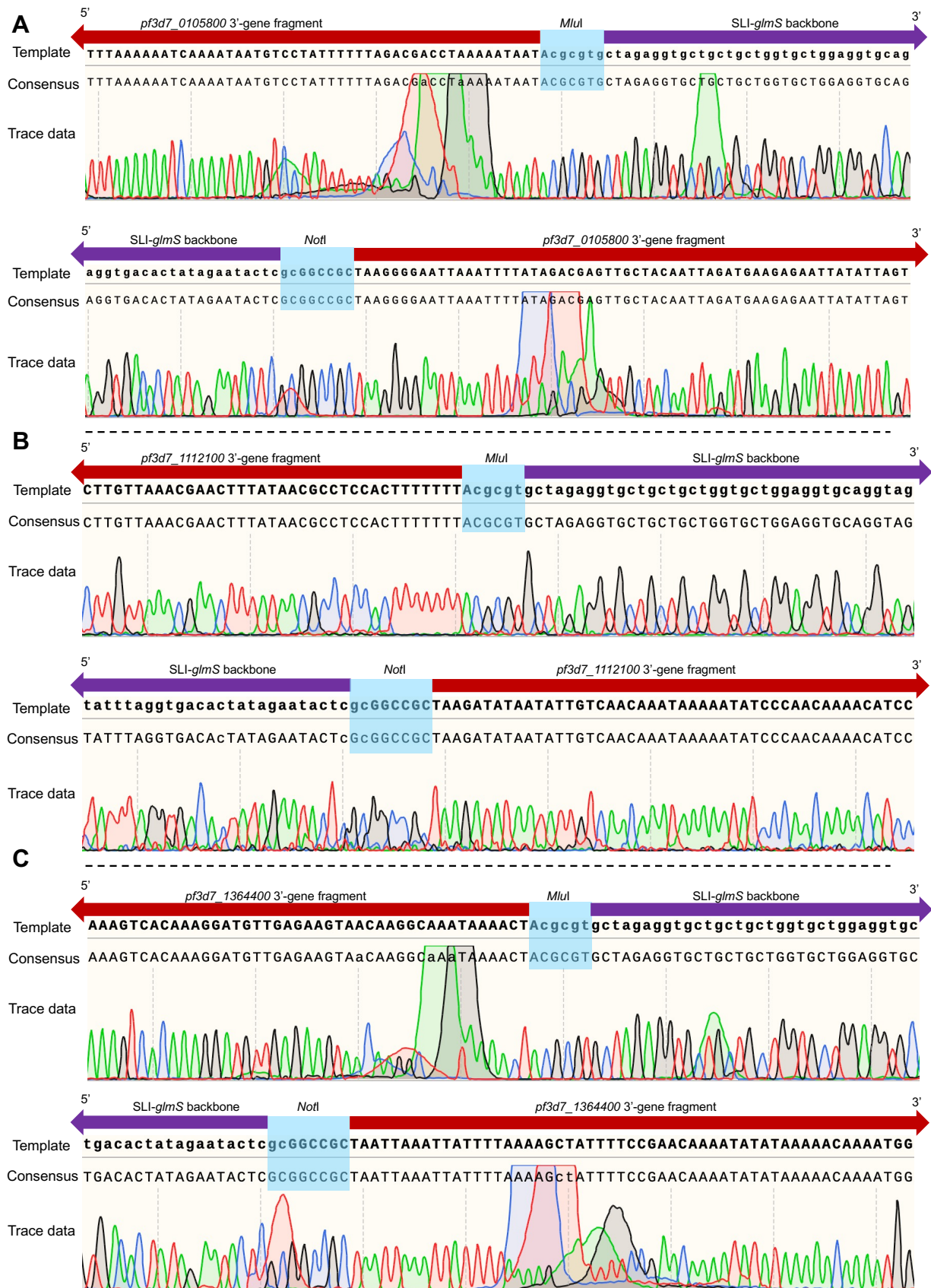
Figure 3–37: Sanger sequencing alignment of SLI-*glmS-0105800*, SLI-*glmS*-1112100 and SLI-*glmS-1364400* 3'-gene fragments. Only the sequencing information surrounding the cloning sites is indicated including a section of aligned plasmid backbone (purple), 3'-gene fragment (red), and the restriction enzyme cleavage sites indicated in light blue. DNA fragments in schematics not drawn to scale. A representative forward or reverse chromatogram (trace data) is shown below the consensus sequence. **(A)** Sequence alignment confirming the identity of the *pf3d7_0105800* 3'-gene fragment. **(B)** Sequence alignment confirming the identity of the *pf3d7_1112100* 3'-gene fragment. **(C)** Sequence alignment confirming the identity of the *pf3d7_1364400* 3'-gene fragment. Chromatogram obtained from SnapGene alignment. Images were designed using SnapGene V 5.3.2.

Figure 3–38: Sanger sequencing alignment of SLI-*glmS*-mut-*0105800*, SLI-*glmS*-mut-*1112100* and SLI-*glmS*-mut-*1364400* 3'-gene fragments. Only the sequencing information surrounding the cloning sites is indicated including a section of aligned plasmid backbone (purple), 3'-gene fragment (red), and the restriction enzyme cleavage sites indicated in light blue. DNA fragments in schematics not drawn to scale. A representative forward or reverse chromatogram (trace data) is shown below the consensus sequence. **(A)** Sequence alignment confirming the identity of the *pf3d7_0105800* 3'-gene fragment. **(B)** Sequence alignment confirming the identity of the *pf3d7_1112100* 3'-gene fragment. **(C)** Sequence alignment confirming the identity of the *pf3d7_1364400* 3'-gene fragment. Chromatogram obtained from SnapGene alignment. Images were designed using SnapGene V 5.3.2.

3.8. Generation of transgenic knockdown *P. falciparum* lines using recombinant SLI-*glmS/glmS*-mut-*gene* plasmids

As in section 3.2, satisfactory yields (0.72-1 mg) of recombinant SLI-*glmS/glmS*-mut-*0105800*, SLI-*glmS/glmS*-mut-*1112100* and SLI-*glmS/glmS*-mut-*1364400* plasmids were obtained and successfully RE mapped (Figure 3-39).
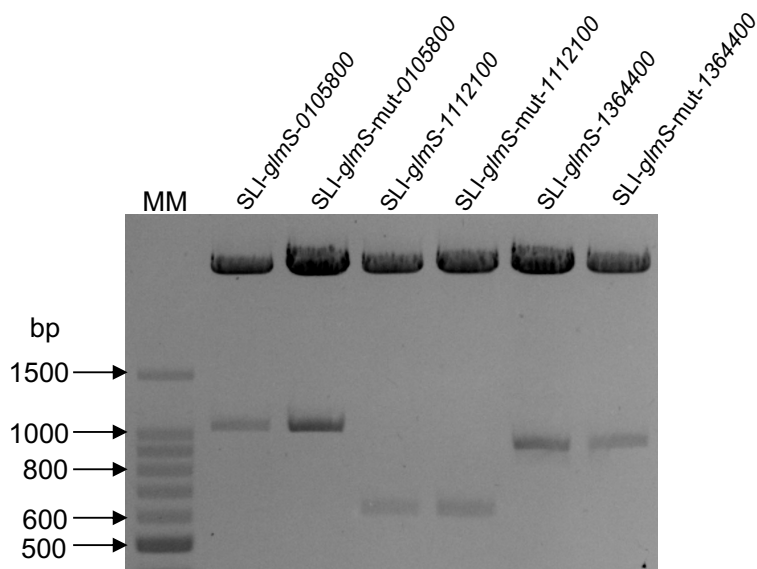
Figure 3–39: Restriction enzyme mapping of isolated SLI-*glmS/glmS*-mut-*0105800*, SLI-*glmS/glmS*-mut-*1112100* and SLI-*glmS/glmS*-mut-*1364400* plasmid. Plasmid DNA (~2 µg) was digested for 3 h at 37 °C. Digested DNA samples were analysed on 1.5 % (w/v) agarose gel post stained with EtBr (0.4 mg/mL). Molecular marker (MM): 100 bp ladder (Promega, USA). Complete digestion of SLI-*glmS/glmS*-mut-*0105800*, SLI-*glmS/glmS*-mut-*1112100* and SLI- *glmS/glmS*-mut-*1364400* was accomplished using *Not*I-HF and *Mlu*I-HF. Each digested recombinant SLI- *glmS/glmS*-mut plasmid yielded two bands where each of the smaller bands corresponded to the expected 3'-gene fragment sizes, ~1050 bp (*pf3d7_0105800*), ~630 bp (*pf3d7_1112100*), and ~940 bp (*pf3d7_1364400*).

Asexual NF54 *P. falciparum* parasites were transfected with the respective recombinant SLI-*glmS/glmS*-mut plasmids and subjected to WR22910 drug selection for episomal uptake. A sharp decrease in parasitaemia was seen following electroporation, whereafter the parasitaemia further decreased until no parasites were observed (Figure 3-40). NF54-epi(SLI-*glmS/glmS*-mut-*0105800*), NF54-epi(SLI-*glmS/glmS*-mut-*1112100*) and NF54-epi(SLI-*glmS/glmS*-mut-*1364400*) parasites reappeared 9–12 days after WR99210 drug selection was removed (Figure 3-40).
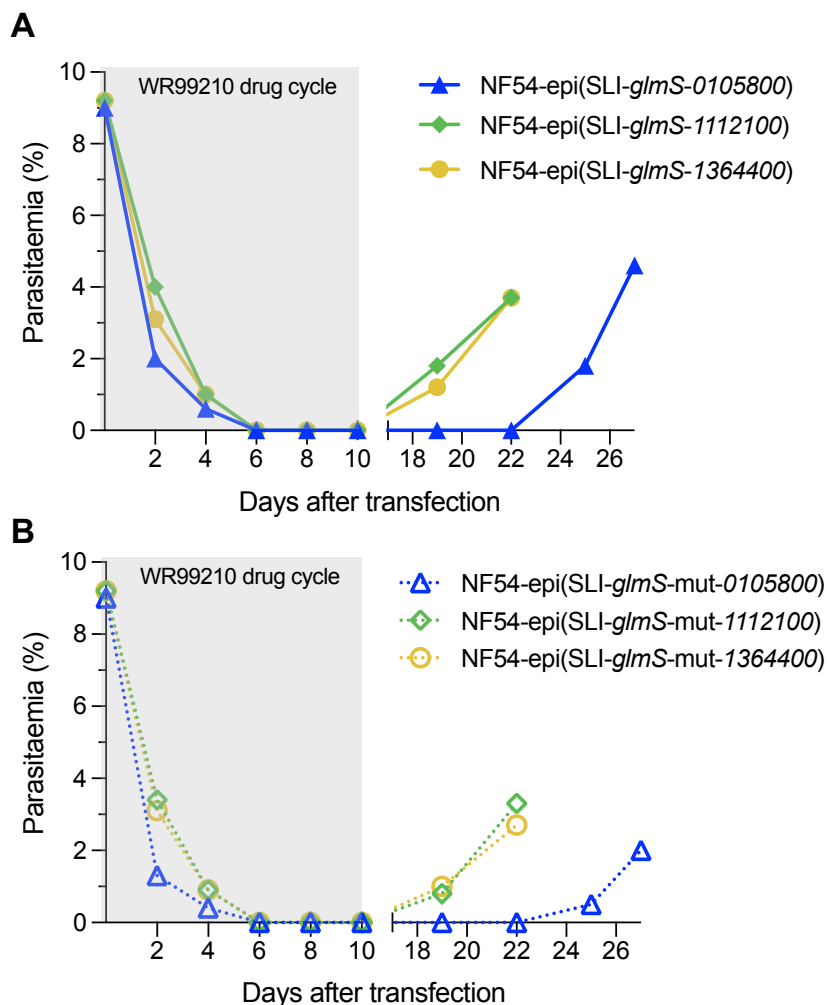
Figure 3–40: Selection and recovery of *P. falciparum* parasites transfected with recombinant SLI-*glmS/glmS*-mut-*0105800*, SLI-*glmS/glmS*-mut-*1112100* and SLI-*glmS/glmS*-mut-*1364400* plasmid DNA. (A) The line graph displays the parasitaemia of the transfected NF54 *P. falciparum* parasites with SLI-*glmS-0105800*, SLI-*glmS-1112100* and SLI-*glmS-1364400* plasmids while **(B)** displays the parasitaemia of the transfected NF54 *P. falciparum* parasites with SLI-*glmS*-mut-*0105800*, SLI-*glmS*-mut-*1112100* and SLI-*glmS*-mut-*1364400* plasmids The parasitaemia was determined before transfection (day 0) and every second day post-transfection up to 27 days by Rapi-Diff-stained thin blood smears. Figure was generated using GraphPad Prism version 9.2.0.

Successful episomal uptake was confirmed for recovered parasites using screening PCRs on recovered parasites (Figure 3-41B, expected sizes ~1140 bp (SLI-*glmS/glmS*-mut-*0105800*), ~720 bp (SLI-*glmS/glmS*-mut-*1112100*) and ~1030 bp (SLI-*glmS/glmS*-mut-*1364400*)). The NF54-epi(SLI-*glmS/glmS*-mut-*0105800*), NF54-epi(SLI-*glmS/glmS*-mut-*1112100*) and NF54-epi(SLI-*glmS/glmS*-mut-*1364400*) lines were therefore successfully generated and could be used to select for integration of the *glmS-gene* constructs into the *P. falciparum* genomes. Although this was not performed in the current study as it requires another 3-4 month cultivation, selection, and validation process, the episomal lines generated will facilitate future work aiming to generate inducible knockdown transgenic parasite lines.
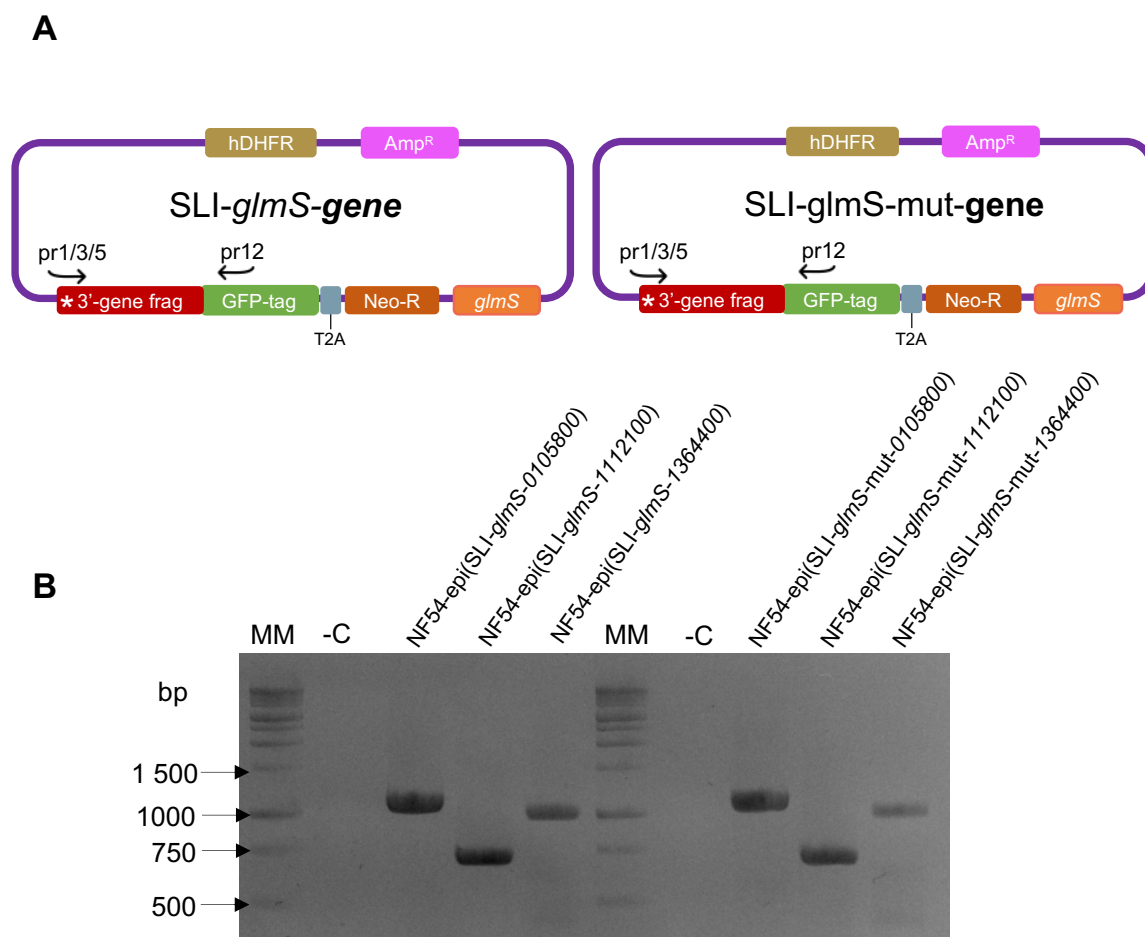
Figure 3–41: Validation of episomal uptake of recombinant SLI-*glmS* and SLI-*glmS*-mut plasmids after transfection. (A) Schematic representation showing the primer pair (pr1/3/5 and pr12) used during the screening PCR, listed in Tables 3 and 4 respectively. The forward primers used (pr1/3/5) bind to the 5' end of the gene fragment while the reverse primer (pr12) binds downstream of the gene fragment on the SLI-*glmS* plasmid backbone. **(B)** Negative control (-C) containing no template DNA. Episomal screening PCR results were analysed on 1.5 % (w/v) agarose gel post stained with EtBr (0.4 mg/mL). Molecular marker (MM): 1 kb ladder (Promega, USA). The expected insert regions were amplified for all of the 3'-gene fragments with PCR products of ~1140 bp (SLI-*glmS*/*glmS*-mut-*0105800*), ~720 bp (SLI-*glmS*/*glmS*-mut-*1112100*), and ~1030 bp (SLI-*glmS*/*glmS*-mut-*1364400*) observed.

Chapter 4: Discussion

The *P. falciparum* parasite is extraordinary in that, in the space of 48 h, a single merozoite that has invaded an erythrocyte is able to produce up to 32 new viable daughter merozoites. The rapid and successful developmental process occurring throughout the IDC implies strict regulatory mechanisms in place, governed by specialised regulatory elements, which are characteristics commonly associated with the cell cycle. However, it has been revealed that the hypothesised cell cycle model of *Plasmodium* parasites is divergent from the canonical mammalian cell cycle model, with the unusual occurrence of alternating DNA synthesis and mitosis events during endocyclic schizogony [3, 52]. Despite the presence of known canonical cell cycle phases and regulators, the exact mechanisms and regulator elements governing the cell cycle of *Plasmodium* parasites has yet to be uncovered [3]. Therefore, this study aimed to elucidate the essential nature of three uncharacterised putative kinase proteins (PF3D7_0105800, PF3D7_1112100 and PF3D7_1364400) during the multistage parasite asexual intraerythrocytic life cycle, and implied cell cycle. To achieve this aim, recombinant SLI-TGD, SLI-sandwich and SLI-*glmS*/*glmS*-mut plasmids containing the 5'- and 3'-gene fragment of each selected putative kinase gene respectively were constructed. The recombinant SLI-TGD and SLI-sandwich plasmids were subsequently used to generate transgenic lines to uncover the function of the selected kinase proteins.

In this study NF54_*0105800*_2xFKBP-GFP_2xFKBP and NF54_*1112100*_2xFKBP-GFP_2xFKBP transgenic lines were successfully generated and used in determining cytosolic localisation of both PF3D7_0105800 and PF3D7_1112100 proteins, in addition to knock sideways studies, to gain a better understanding of the function and role these putative kinase proteins play. However, attempts to mislocalise both PF3D7_0105800 and PF3D7_1112100 target proteins to the nucleus of the parasite and PF3D7_0105800 to the plasma membrane were unsuccessful, as no change in localisation of the target proteins was observed once the knock sideways system was induced. Additionally, no phenotypic effect was observed on asexual parasite proliferation consequent to knock sideways induction. It is possible that the mislocaliser protein (FRB) was inaccessible to the FKBP-proteins associated with the target proteins. Alternatively, it may be that the FKBP-proteins did not retain their function. These have previously been described as possible limitations, in some instances, of the knock sideways system [67]. Therefore, although an integrated recombinant SLI-*glms*/*glmS*-mut line was not generated in the present study for conditional knockdown experiments, episomal uptake of this plasmid was confirmed, and future studies will attempt to use this system to functionally characterise these proteins.

Utilising the GFP-tagged fusion proteins generated using the SLI system, cytosolic localisation of both PF3D7_0105800, a supposed CDK-like kinase protein, and PF3D7_1112100, a supposed member of the Bub1/Mad3 kinase family, was established. Another CDK-like protein, *Pf*PK5, which is the most well-characterised member of the *P. falciparum* CDK family, has also been found to localise to the cytosol prior to initiation of DNA replication during the S phase, whereupon it is relocated to the DNA

periphery [124]. Similarly, within mammalian cells, the CDK-cyclin D1 complex is exported to the cytoplasm for proteolysis once its function has been completed within the cell cycle [125]. This relocation and degradation is also observed during the M checkpoint of the mammalian cell cycle where, once the checkpoint is satisfied by attachment of the final kinetochore, the MCC is released and exported to the cytoplasm for ubiquitination and proteolysis [49, 126].

Thus, further evaluation of PF3D7_0105800 and PF3D7_1112100 localisation throughout asexual IDC progression and equivalent cell cycle transition phases within asexual *P. falciparum* parasites are required. Additional studies evaluating the progression and equivalent cell cycle transition phases during and after cell cycle arrest due to mitogen depletion would provide valuable information on the possible function of PF3D7_0105800 and PF3D7_1112100. Future studies, including enzymatic assays, will allow evaluation of whether PF3D7_0105800 and PF3D7_1112100 have phosphorylation activity on target proteins. Future fluorescence-based studies will provide further evidence as to whether PF3D7_1112100 localises to the spindle bodies during kinetochore attachment validation, as is seen in other *P. falciparum* CDK-like proteins as well as other organisms like yeast, mammals, and *Toxoplasma gondii* [14, 46, 125-127]. A greater sensitivity may be achieved through the application of immunofluorescence to determine localisation of these proteins by targeting the GFP tag expressed with these proteins in the transgenic line.

The essentiality of the selected putative kinase proteins was established using the SLI-TGD system and, consequently, PF3D7_0105800, PF3D7_1112100 and PF3D7_1364400 were all indicated to be essential to asexual parasite proliferation due to the production of non-functional proteins. The loss in functionality of each PF3D7_0105800, PF3D7_1112100 and PF3D7_1364400 protein is supported when considering the locations of the predicted InterPro domains, which were all situated at the C-terminal end of the selected putative kinase proteins and, once integration occurred, were truncated. The prolonged ring/early trophozoite stage observed upon gene knockout of PF3D7_0105800 and PF3D7_1364400 implied an importance of these proteins in transition through the G_1/S transition phase, with a possible role during early cell cycle progression. Standing in support of this, PF3D7_0105800 is predicted to contain a CKS subunit, while PF3D7_1364400 is a predicted member of the cyclin-like superfamily. Additionally, transcriptomic data during cell cycle arrest and re-entry, wherein *pf3d7_0105800* was found to be upregulated during cell cycle re-entry, supports a function during early cell cycle transition [8].

Furthermore, PF3D7_1227500 (SOC2), a cyclin-related protein, was shown by STRING analysis to be co-expressed with PF3D7_0105800, which further supports the notion that PF3D7_0105800 is a CDK-like protein. Recently it has been found that the homologue of PF3D7_1227500 within *Plasmodium bergei*, PBANKA_1442200, binds to the CDK-like protein *Pb*CRK5 (PBANKA_1230200), which is implicated in the initiation of DNA replication [128] forming an atypical cyclin/CDK complex. Additionally, PF3D7_0105800 was found to be co-expressed with other proteins that have been

connected to membrane-associated functions, such as PF3D7_0105300 (CAP). Homologues of this protein in other eukaryotes have been found to play an important role in cytoskeleton development [129, 130]. This provides further support that PF3D7_0105800 is implicated in the G_1/S transition, as this phase corresponds to the transition from ring to trophozoite stage, where growth and morphological changes to the cytoskeleton occur. It is therefore proposed that PF3D7_0105800 may be involved in a signalling cascade promoting this transition, a possibility that may be explored in subsequent studies. Similar studies done on *Pf*PKG and some *Pf*CDPKs have successfully been completed to identify their kinase activity and the subsequent involvement in various signalling pathways [1, 74, 106, 131, 132].

Comparably, PF3D7_1364400 may also be involved in cell cycle regulation early on in cell-cycle progression, based on the similar phenotypic stage distribution profile observed. However, when looking at the transcriptomic data obtained during cell cycle arrest and re-entry, an inverse profile was seen compared to that of PF3D7_0105800, where *pf3d7_1364400* was found to upregulated during arrest and decreased during re-entry [8]. This could suggest that PF3D7_1364400 has a complementary function to that of PF3D7_0105800, with a possible repressive function like a CKI protein. Therefore, it is speculated that, in the absence of mitogens within the parasite environment, PF3D7_1364400 could be part of a signalling cascade, or may prevent one from occurring, ultimately leading to a halt in cell-cycle progression. This would be similar to what is found within mammalian and *S. cerevisiae* cells, where MAPK signalling cascades modulate cell-cycle progression by affecting the levels and activity of transcription factors, promoting CDK/cyc gene expression, and synthesis of CKI members [46, 133, 134]. Interestingly, *Pf*PK5/*Pf*cyc-1 and *Pf*mrk/*Pf*cyc-1 CDK/cyc complexes have been reported to interact with, and be inhibited by mammalian CKI members p21 and p16 *in vitro* suggesting CDK inhibitor-like proteins are present within the parasite, performing a similar function [135, 136].

Furthermore, the co-expression and experimental determination connections illustrated by STRING analysis highlighted PF3D7_1323400, a 60S ribosomal protein L23 that, within mammals cells, inhibits E3 ubiquitin-protein ligase Mdm2, leading to the activation of p53 [121]. The latter further supports the notion that PF3D7_1364400 could perform a repressive role or modulate other target proteins to perform a repressive function, leading to cell cycle arrest within the parasite. However, sequence-based searches of the *P. falciparum* genome have not yet identified any putative *P. falciparum* proteins with significant sequence homology to any canonical CDK inhibitor homologues [2, 61, 135], indicating that PF3D7_1364400 could possibly be the first CKI-like member identified within *P. falciparum.* This will be explored in future to better understand the role PF3D7_1364400 plays within the parasite.

In contrast to the delayed ring/early trophozoite phenotype observed for PF3D7_0105800 and PF3D7_1364400, a delayed death response was observed for PF3D7_1112100, where parasites were only affected during the second replication cycle. Based on its membership of the Bub1/Mad3 superfamily, it is expected that parasites are not phenotypically affected during early IDC stages, but

rather during later schizont stages where a final round of synchronous nuclear division and mitosis occurs, followed by subsequent segmentation and a single cytokinesis event resulting in daughter parasites, as is be predicted that this protein is involved in kinetochore attachment. Therefore, if PF3D7_1112100 function is disrupted, this will possibly lead to uneven distribution of chromosomes between daughter cells which could explain the observed delayed death response. Similarly, within yeast cells it was found that disruption of BUB1 function caused the chromosomes to lag on the anaphase spindle and increase the frequency of chromosome loss [137]. The notion that PF3D7_1112100 plays a role during cell cycle stages is supported to some extent when considering the transcriptomic data obtained during cell cycle arrest and re-entry. PF3D7_1112100 expression initially decreases as the parasite re-enters the cell cycle, but as the parasite progresses through the cell cycle, expression increases [8]. This prolife is similar to that observed in yeast and mammal cells, as Bub1 and BubR1 levels are decreased during the G_1 phase [126].

Furthermore, STRING analysis identified PF3D7_1227600 (SPC24), a kinetochore protein, as a co-expression connection, supporting the predicted Bub1/Mad3 function in spindle attachment. Known centrosomal cycle regulators, such as ARKs, NEK kinases along with four APC/C components, APC10, APC11 and APC3 and CDC20 have been identified within *Plasmodium spp.*, with the latter only being described in male gametogenesis and not in the asexual IDC [96, 97, 100, 138]. However, the specific molecular signalling networks that regulate mitosis and associated mechanisms that govern chromosome segregation with *P. falciparum* parasites are largely unknown, with few proteins identified with similarity to the canonical MCC components (Mad2, BubR1/ Mad3, Bub3), kinetochore scaffolds (Mad1, Knl1), and kinases (Bub1, Mps1) [14, 49]. Therefore, further investigation into the potential role PF3D7_1112100 performs during spindle development and chromosome segregation is required.

A limitation of the TGD system employed in the present study was that, as all the targeted genes were essential to asexual proliferation, no further functional evaluation was possible and evaluation of the essentiality of these proteins in other parasite life cycle stages, particularly the sexual stages (gametocytes and gametes), was precluded. Therefore, inducible systems are required to overcome this obstacle and allow for further interrogation and functional evaluation of the selected putative kinase proteins using a conditional knock sideways and knockdown approach.

In conclusion, the three novel uncharacterized kinase proteins were indicated to play an essential role in asexual proliferation coupled with a proposed role at the G1/S transition for CDK/cyclin-like kinases (PF3D7_0105800 and PF3D7_1364400) and mitotic regulation (PF3D7_1112100). By highlighting the essential nature of these kinase proteins within asexual proliferation, this has introduced these putative kinase proteins as potential new drug targets in the kinase inhibitory space.

Chapter 5: Conclusion

Malaria remains a global health threat, constituting a major health burden and severely impacting the socio-economic status of various countries worldwide, especially developing countries which bear the brunt of the disease burden, adding strain on the already struggling healthcare systems of these countries [9]. However, the emergence of parasite strains resistant to the current frontline antimalarials, ACTs, stresses the need for new antimalarial drugs against *P. falciparum* parasites [37]. One avenue being used to uncover and identify new antimalarial drugs is to find novel drug targets. Within these unexplored biological avenues of the parasite, unique and essential proteins can be identified and studied as potential drug targets. One such biology is the extraordinary kinome, consisting of unique protein kinases which have not been fully exploited, especially with respect to mechanisms and kinase protein regulators of the atypical cell cycle of *P. falciparum* parasites.

This study aimed to functionally validate the essential nature of three uncharacterized kinase proteins (PF3D7_0105800, PF3D7_1112100 and PF3D7_1364400) within the parasite life cycle, exposing potential novel targets in the kinase inhibitory space. By using a targeted gene disruption (TGD) system to determine the essentiality of all three of the selected kinase proteins it was revealed that all three are essential for asexual parasite proliferation. Additionally, it was discovered that both PF3D7_0105800 and PF3D7_1364400 could potentially be involved in processes governing the G_1/S transition phase, while PF3D7_1112100 could be involved later during cell cycle progression.

To gain a more in-depth understanding of the functions these putative kinase proteins play during the parasite life cycle, and especially cell cycle progression, an inducible knock sideways system was used. NF54-*0105800*-2xFKBP-GFP-2xFKBP and NF54-*1112100*-2xFKBP-GFP-2xFKBP transgenic parasites were successfully generated, although a homogenous NF54-*1364400*-2xFKBP-GFP-2xFKBP transgenic line was not obtained. Using the GFP-tag associated with the target proteins under investigation, both PF3D7_0105800 and PF3D7_1112100 were found to localise to the cytosol of the parasite. Additionally, the knock sideways system was used to mislocalise PF3D7_0105800 and PF3D7_1112100 from their predicted sites of action. Both proteins, however proved refractory to mislocalisation. In this MSc project, NF54-epi(SLI-*glmS/glmS*-mut-*0105800*), NF54-epi(SLI-*glmS/glmS*-mut-*1112100*) and NF54-epi(SLI-*glmS/glmS*-mut-*1364400*) transgenic parasite lines were successfully generated.

Altogether, the work presented in this dissertation revealed novel kinases that may be exploitable within the kinase inhibitory space, and which may be implicated in cell cycle regulatory mechanisms.

References

1   Solyakov, L., Halbert, J., Alam, M. M., Semblat, J.-P., Dorin-Semblat, D., Reininger, L., Bottrill, A. R., Mistry, S., Abdi, A. and Fennell, C. (2011) Global kinomic and phospho-proteomic analyses of the human malaria parasite *Plasmodium falciparum*. Nature communications. **2**, 565

2   Adderley, J., Williamson, T. and Doerig, C. (2021) Parasite and host erythrocyte kinomics of *Plasmodium* infection. Trends in Parasitology

3   Matthews, H., Duffy, C. W. and Merrick, C. J. (2018) Checks and balances? DNA replication and the cell cycle in *Plasmodium*. Parasites & vectors. **11**, 216

4   Brochet, M., Tobin, A., Billker, O. and Doerig, C. (2015) The kinomics of malaria.

5   Miranda-Saavedra, D., Gabaldón, T., Barton, G. J., Langsley, G. and Doerig, C. (2012) The kinomes of apicomplexan parasites. Microbes and infection. **14**, 796-810

6   Baker, D. A., Drought, L. G., Flueck, C., Nofal, S. D., Patel, A., Penzo, M. and Walker, E. M. (2017) Cyclic nucleotide signalling in malaria parasites. Open biology. **7**, 170213

7   Kern, S., Agarwal, S., Huber, K., Gehring, A. P., Strödke, B., Wirth, C. C., Brügl, T., Abodo, L. O., Dandekar, T. and Doerig, C. (2014) Inhibition of the SR protein-phosphorylating CLK kinases of *Plasmodium* falciparum impairs blood stage replication and malaria transmission. PloS one. **9**, e105732

8   van Biljon, R., Niemand, J., van Wyk, R., Clark, K., Verlinden, B., Abrie, C., von Grüning, H., Smidt, W., Smit, A. and Reader, J. (2018) Inducing controlled cell cycle arrest and re-entry during asexual proliferation of *Plasmodium falciparum* malaria parasites. Scientific reports. **8**, 16581

9   Organization, W. H. (2020) World malaria report 2020: 20 years of global progress and challenges. In World malaria report 2020: 20 years of global progress and challenges ed.)^eds.)

10   Tangpukdee, N., Duangdee, C., Wilairatana, P. and Krudsood, S. (2009) Malaria diagnosis: a brief review. The Korean journal of parasitology. **47**, 93

11   Trampuz, A., Jereb, M., Muzlovic, I. and Prabhu, R. M. (2003) Clinical review: Severe malaria. Critical care. **7**, 315

12   Girard, M. P., Reed, Z. H., Friede, M. and Kieny, M. P. (2007) A review of human vaccine research and development: malaria. Vaccine. **25**, 1567-1580

13   Birkholtz, L.-M., Bornman, R., Focke, W., Mutero, C. and De Jager, C. (2012) Sustainable malaria control: transdisciplinary approaches for translational applications. Malaria journal. **11**, 431

14   Gerald, N., Mahajan, B. and Kumar, S. (2011) Mitosis in the human malaria parasite *Plasmodium falciparum*. Eukaryotic cell. **10**, 474-482

15   Garcia, C. R., de Azevedo, M. F., Wunderlich, G., Budu, A., Young, J. A. and Bannister, L. (2008) *Plasmodium* in the postgenomic era: new insights into the molecular cell biology of malaria parasites. International review of cell and molecular biology. **266**, 85-156

16   Kirk, K. (2001) Membrane transport in the malaria-infected erythrocyte. Physiological reviews. **81**, 495-537

17   Bannister, L. and Mitchell, G. (2003) The ins, outs and roundabouts of malaria. Trends in parasitology. **19**, 209-213

18   Francis, S. E., Sullivan Jr, D. J., Goldberg and E, D. (1997) Hemoglobin metabolism in the malaria parasite *Plasmodium falciparum*. Annual Reviews in Microbiology. **51**, 97-123

19   Sherman, I. (1977) Amino acid metabolism and protein synthesis in malarial parasites. Bulletin of the World Health Organization. **55**, 265

20   Rudlaff, R. M., Kraemer, S., Marshman, J. and Dvorin, J. D. (2020) Three-dimensional ultrastructure of *Plasmodium falciparum* throughout cytokinesis. PLoS pathogens. **16**, e1008587

21   Baker, D. A. (2010) Malaria gametocytogenesis. Molecular and biochemical parasitology. **172**, 57-65

22   Dixon, M. W. and Tilley, L. (2021) *Plasmodium falciparum* goes bananas for sex. Molecular and Biochemical Parasitology, 111385

23   Dearnley, M. K., Yeoman, J. A., Hanssen, E., Kenny, S., Turnbull, L., Whitchurch, C. B., Tilley, L. and Dixon, M. W. (2012) Origin, composition, organization and function of the inner membrane complex of *Plasmodium falciparum* gametocytes. Journal of cell science. **125**, 2053-2063

24   Josling, G. A. and Llinas, M. (2015) Sexual development in *Plasmodium* parasites: knowing when it's time to commit. Nature Reviews Microbiology. **13**, 573

25   Vlachou, D., Schlegelmilch, T., Runn, E., Mendes, A. and Kafatos, F. C. (2006) The developmental migration of *Plasmodium* in mosquitoes. Current opinion in genetics & development. **16**, 384-391

26   Raghavendra, K., Barik, T. K., Reddy, B. N., Sharma, P. and Dash, A. P. (2011) Malaria vector control: from past to future. Parasitology research. **108**, 757-779
27   Kleinschmidt, I., Bradley, J., Knox, T. B., Mnzava, A. P., Kafy, H. T., Mbogo, C., Ismail, B. A., Bigoga, J. D., Adechoubou, A. and Raghavendra, K. (2018) Implications of insecticide resistance for malaria vector control with long-lasting insecticidal nets: a WHO-coordinated, prospective, international, observational cohort study. The Lancet infectious diseases. **18**, 640-649
28   Laurens, M. B. (2018) The Promise of a Malaria Vaccine—Are We Closer? Annual review of microbiology. **72**, 273-292
29   Hott, A., Casandra, D., Sparks, K. N., Morton, L. C., Castanares, G.-G., Rutter, A. and Kyle, D. E. (2015) Artemisinin-resistant *Plasmodium falciparum* parasites exhibit altered patterns of development in infected erythrocytes. Antimicrobial agents and chemotherapy. **59**, 3156-3167
30   Bunditvorapoom, D., Kochakarn, T., Kotanan, N., Modchang, C., Kümpornsin, K., Loesbanluechai, D., Krasae, T., Cui, L., Chotivanich, K. and White, N. J. (2018) Fitness loss under amino acid starvation in artemisinin-resistant *Plasmodium falciparum* isolates from Cambodia. Scientific reports. **8**, 12622
31   Hassett, M. R. and Roepe, P. D. (2019) Origin and Spread of Evolving Artemisinin-Resistant *Plasmodium falciparum* Malarial Parasites in Southeast Asia. The American Journal of Tropical Medicine and Hygiene, tpmd190379
32   Ariey, F. (2014) Nature. **505**
33   Balikagala, B. (2021) N. Engl. J. Med. **385**
34   Mwakingwe-Omari, A. (2021) Nature. **595**
35   Uwimana, A. (2020) Nature Med. **26**
36   Uwimana, A. (2021) Lancet Infect. Dis. **21**
37   Alonso, P. and Noor, A. M. (2017) The global fight against malaria is at crossroads. The Lancet. **390**, 2532-2534
38   Voet, D. V. J. G. P. C. W. (2016) Fundamentals of biochemistry : life at the molecular level.
39   Dong, P., Zhang, C., Parker, B.-T., You, L. and Mathey-Prevot, B. (2018) Cyclin D/CDK4/6 activity controls G1 length in mammalian cells. PloS one. **13**, e0185637
40   Harashima, H., Dissmeyer, N. and Schnittger, A. (2013) Cell cycle control across the eukaryotic kingdom. Trends in cell biology. **23**, 345-356
41   Lodish, H., Berk, A., Kaiser, C. A., Krieger, M., Bretscher, A., Ploegh, H., Amon, A. and Martin, K. C. (2016) Loose-leaf Version for Molecular Cell Biology. Macmillan Higher Education
42   Murray, A. W. (2004) Recycling the cell cycle: cyclins revisited. Cell. **116**, 221-234
43   Jorgensen, P., Nishikawa, J. L., Breitkreutz, B.-J. and Tyers, M. (2002) Systematic identification of pathways that couple cell growth and division in yeast. Science. **297**, 395-400
44   Lavia, P. and Jansen-Dürr, P. (1999) E2F target genes and cell-cycle checkpoint control. Bioessays. **21**, 221-230
45   Abraham, R. T. (2001) Cell cycle checkpoint signaling through the ATM and ATR kinases. Genes & development. **15**, 2177-2196
46   Barnum, K. J. and O'Connell, M. J. (2014) Cell cycle regulation by checkpoints. In Cell Cycle Control. pp. 29-40, Springer
47   Lara-Gonzalez, P., Westhorpe, F. G. and Taylor, S. S. (2012) The spindle assembly checkpoint. Current biology. **22**, R966-R980
48   Alfieri, C., Chang, L., Zhang, Z., Yang, J., Maslen, S., Skehel, M. and Barford, D. (2016) Molecular basis of APC/C regulation by the spindle assembly checkpoint. Nature. **536**, 431-436
49   Vleugel, M., Hoogendoorn, E., Snel, B. and Kops, G. J. (2012) Evolution and function of the mitotic checkpoint. Developmental cell. **23**, 239-250
50   Jacobberger, J., Horan, P. and Hare, J. (1992) Cell cycle analysis of asexual stages of erythrocytic malaria parasites. Cell proliferation. **25**, 431-445
51   By, D. and Manchester, A. (1998) The *Plasmodium* cell-cycle: facts and questions. Annals of Tropical Medicine & Parasitology. **92**, 361-365
52   Arnot, D. E., Ronander, E. and Bengtsson, D. C. (2011) The progression of the intra-erythrocytic cell cycle of *Plasmodium falciparum* and the role of the centriolar plaques in asynchronous mitotic division during schizogony. International journal for parasitology. **41**, 71-80
53   Francia, M. E. and Striepen, B. (2014) Cell division in apicomplexan parasites. Nature Reviews Microbiology. **12**, 125-136
54   Dubremetz, J. (1973) Ultrastructural study of schizogonic mitosis in the coccidian, Eimeria necatrix (Johnson 1930). Journal of ultrastructure research. **42**, 354-376

55   Gray, K.-A., Gresty, K. J., Chen, N., Zhang, V., Gutteridge, C. E., Peatey, C. L., Chavchich, M., Waters, N. C. and Cheng, Q. (2016) Correlation between cyclin dependent kinases and artemisinin-induced dormancy in *Plasmodium falciparum* in vitro. PloS one. **11**, e0157906

56   Sinden, R. (2015) The cell biology of malaria infection of mosquito: advances and opportunities. Cellular microbiology. **17**, 451-466

57   Babbitt, S. E., Altenhofen, L., Cobbold, S. A., Istvan, E. S., Fennell, C., Doerig, C., Llinás, M. and Goldberg, D. E. (2012) *Plasmodium falciparum* responds to amino acid starvation by entering into a hibernatory state. Proceedings of the National Academy of Sciences. **109**, E3278-E3287

58   Oredsson, S. (2003) Polyamine dependence of normal cell-cycle progression. Biochemical Society Transactions. **31**, 366-370

59   Hanks, S. K. (2003) Genomic analysis of the eukaryotic protein kinase superfamily: a perspective. Genome biology. **4**, 1-7

60   Talevich, E., Tobin, A. B., Kannan, N. and Doerig, C. (2012) An evolutionary perspective on the kinome of malaria parasites. Philosophical Transactions of the Royal Society B: Biological Sciences. **367**, 2607-2618

61   Srinivasan, N. and Krupa, A. (2005) A genomic perspective of protein kinases in *Plasmodium* falciparum. Proteins: Structure, Function, and Bioinformatics. **58**, 180-189

62   Ward, P., Equinet, L., Packer, J. and Doerig, C. (2004) Protein kinases of the human malaria parasite *Plasmodium* falciparum: the kinome of a divergent eukaryote. BMC genomics. **5**, 79

63   Doerig, C. and Meijer, L. (2007) Antimalarial drug discovery: targeting protein kinases. Expert opinion on therapeutic targets. **11**, 279-290

64   Nunes, M. C., Goldring, J. D., Doerig, C. and Scherf, A. (2007) A novel protein kinase family in *Plasmodium falciparum* is differentially transcribed and secreted to various cellular compartments of the host cell. Molecular microbiology. **63**, 391-403

65   Nunes, M. C., Okada, M., Scheidig-Benatar, C., Cooke, B. M. and Scherf, A. (2010) *Plasmodium falciparum* FIKK kinase members target distinct components of the erythrocyte membrane. PloS one. **5**

66   Doerig, C., Billker, O., Haystead, T., Sharma, P., Tobin, A. B. and Waters, N. C. (2008) Protein kinases of malaria parasites: an update. Trends in parasitology. **24**, 570-577

67   Briquet, S., Gissot, M. and Silvie, O. (2021) A toolbox for conditional control of gene expression in apicomplexan parasites. Mol Microbiol

68   Wilde, M.-L., Triglia, T., Marapana, D., Thompson, J. K., Kouzmitchev, A. A., Bullen, H. E., Gilson, P. R., Cowman, A. F. and Tonkin, C. J. (2019) Protein kinase A is essential for invasion of *Plasmodium falciparum* into human erythrocytes. mBio. **10**, e01972-01919

69   Vaid, A., Thomas, D. C. and Sharma, P. (2008) Role of Ca2+/calmodulin-PfPKB signaling pathway in erythrocyte invasion by *Plasmodium* falciparum. Journal of Biological Chemistry. **283**, 5589-5597

70   Taylor, H. M., McRobert, L., Grainger, M., Sicard, A., Dluzewski, A. R., Hopp, C. S., Holder, A. A. and Baker, D. A. (2010) The malaria parasite cyclic GMP-dependent protein kinase plays a central role in blood-stage schizogony. Eukaryotic cell. **9**, 37-45

71   Alam, M. M., Solyakov, L., Bottrill, A. R., Flueck, C., Siddiqui, F. A., Singh, S., Mistry, S., Viskaduraki, M., Lee, K. and Hopp, C. S. (2015) Phosphoproteomics reveals malaria parasite Protein Kinase G as a signalling hub regulating egress and invasion. Nature communications. **6**, 1-15

72   Fang, H., Gomes, A. R., Klages, N., Pino, P., Maco, B., Walker, E. M., Zenonos, Z. A., Angrisano, F., Baum, J. and Doerig, C. (2018) Epistasis studies reveal redundancy among calcium-dependent protein kinases in motility and invasion of malaria parasites. Nature communications. **9**, 1-14

73   Kadian, K., Gupta, Y., Kempaiah, P., Gupta, N., Sharma, A. and Rawat, M. (2017) Calcium dependent protein kinases (CDPKs): key to malaria eradication. Current topics in medicinal chemistry. **17**, 2215-2220

74   Bansal, A., Singh, S., More, K. R., Hans, D., Nangalia, K., Yogavel, M., Sharma, A. and Chitnis, C. E. (2013) Characterization of *Plasmodium falciparum* calcium-dependent protein kinase 1 (PfCDPK1) and its role in microneme secretion during erythrocyte invasion. Journal of Biological Chemistry. **288**, 1590-1602

75   Bansal, A., Molina-Cruz, A., Brzostowski, J., Liu, P., Luo, Y., Gunalan, K., Li, Y., Ribeiro, J. M. and Miller, L. H. (2018) PfCDPK1 is critical for malaria parasite gametogenesis and mosquito infection. Proceedings of the National Academy of Sciences. **115**, 774-779

76   Blomqvist, K., Helmel, M., Wang, C., Absalon, S., Labunska, T., Rudlaff, R. M., Adapa, S., Jiang, R., Steen, H. and Dvorin, J. D. (2020) Influence of *Plasmodium falciparum* Calcium-Dependent Protein Kinase 5 (PfCDPK5) on the Late Schizont Stage Phosphoproteome. mSphere. **5**

77   Kumar, P., Tripathi, A., Ranjan, R., Halbert, J., Gilberger, T., Doerig, C. and Sharma, P. (2014) Regulation of *Plasmodium falciparum* development by calcium-dependent protein kinase 7 (PfCDPK7). Journal of Biological Chemistry. **289**, 20386-20395

78   Roques, M., Wall, R. J., Douglass, A. P., Ramaprasad, A., Ferguson, D. J., Kaindama, M. L., Brusini, L., Joshi, N., Rchiad, Z. and Brady, D. (2015) *Plasmodium* P-type cyclin CYC3 modulates endomitotic growth during oocyst development in mosquitoes. PLoS pathogens. **11**, e1005273

79   Deshmukh, A. S., Agarwal, M. and Dhar, S. K. (2016) Regulation of DNA replication proteins in parasitic protozoans: possible role of CDK-like kinases. Current genetics. **62**, 481-486

80   Le Roch, K., Sestier, C., Dorin, D., Waters, N., Kappes, B., Chakrabarti, D., Meijer, L. and Doerig, C. (2000) Activation of a *Plasmodium falciparum* cdc2-related kinase by heterologous p25 and cyclin H: functional characterization of a P. falciparum cyclin homologue. Journal of Biological Chemistry. **275**, 8952-8958

81   Dorin-Semblat, D., Carvalho, T. G., Nivez, M.-P., Halbert, J., Poullet, P., Semblat, J.-P., Goldring, D., Chakrabarti, D., Mehra, P. and Dhar, S. (2013) An atypical cyclin-dependent kinase controls *Plasmodium falciparum* proliferation rate. Kinome. **1**, 4-16

82   Bracchi-Ricard, V., BARIK, S., DELVECCHIO, C., DOERIG, C., CHAKRABARTI, R. and CHAKRABARTI, D. (2000) PfPK6, a novel cyclin-dependent kinase/mitogen-activated protein kinase-related protein kinase from *Plasmodium* falciparum. Biochemical Journal. **347**, 255-263

83   Deshmukh, A. S., Agarwal, M., Mehra, P., Gupta, A., Gupta, N., Doerig, C. D. and Dhar, S. K. (2015) Regulation of P lasmodium falciparum O rigin R ecognition C omplex subunit 1 (PfORC 1) function through phosphorylation mediated by CDK-like kinase PK 5. Molecular microbiology. **98**, 17-33

84   Robbins, J. A., Absalon, S., Streva, V. A. and Dvorin, J. D. (2017) The malaria parasite cyclin H homolog PfCyc1 is required for efficient cytokinesis in blood-stage *Plasmodium* falciparum. MBio. **8**, e00605-00617

85   Agarwal, S., Kern, S., Halbert, J., Przyborski, J. M., Baumeister, S., Dandekar, T., Doerig, C. and Pradel, G. (2011) Two nucleus-localized CDK-like kinases with crucial roles for malaria parasite erythrocytic replication are involved in phosphorylation of splicing factor. Journal of cellular biochemistry. **112**, 1295-1310

86   Alam, M. M., Sanchez-Azqueta, A., Janha, O., Flannery, E. L., Mahindra, A., Mapesa, K., Char, A. B., Sriranganadane, D., Brancucci, N. M. and Antonova-Koch, Y. (2019) Validation of the protein kinase PfCLK3 as a multistage cross-species malarial drug target. Science. **365**

87   Leroy, D. and Doerig, C. (2008) Drugging the *Plasmodium* kinome: The benefits of academia–industry synergy. Trends in pharmacological sciences. **29**, 241-249

88   Carvalho, T. G., Doerig, C. and Reininger, L. (2013) Nima-and Aurora-related kinases of malaria parasites. Biochimica et Biophysica Acta (BBA)-Proteins and Proteomics. **1834**, 1336-1345

89   Dorin-Semblat, D., Quashie, N., Halbert, J., Sicard, A., Doerig, C., Peat, E., Ranford-Cartwright, L. and Doerig, C. (2007) Functional characterization of both MAP kinases of the human malaria parasite *Plasmodium falciparum* by reverse genetics. Molecular microbiology. **65**, 1170-1180

90   Tewari, R., Dorin, D., Moon, R., Doerig, C. and Billker, O. (2005) An atypical mitogen-activated protein kinase controls cytokinesis and flagellar motility during male gamete formation in a malaria parasite. Molecular microbiology. **58**, 1253-1263

91   Abdi, A., Eschenlauer, S., Reininger, L. and Doerig, C. (2010) SAM domain-dependent activity of PfTKL3, an essential tyrosine kinase-like kinase of the human malaria parasite *Plasmodium* falciparum. Cellular and molecular life sciences. **67**, 3355-3369

92   Lye, Y. M., Chan, M. and Sim, T.-S. (2006) Pfnek3: an atypical activator of a MAP kinase in *Plasmodium* falciparum. FEBS letters. **580**, 6083-6092

93   O'connell, M. J., Krien, M. J. and Hunter, T. (2003) Never say never. The NIMA-related protein kinases in mitotic control. Trends in cell biology. **13**, 221-228

94   O'regan, L., Blot, J. and Fry, A. M. (2007) Mitotic regulation by NIMA-related kinases. Cell division. **2**, 1-12

95   Le Roch, K. G., Zhou, Y., Blair, P. L., Grainger, M., Moch, J. K., Haynes, J. D., De la Vega, P., Holder, A. A., Batalov, S. and Carucci, D. J. (2003) Discovery of gene function by expression profiling of the malaria parasite life cycle. Science. **301**, 1503-1508

96   Dorin-Semblat, D., Schmitt, S., Semblat, J.-P., Sicard, A., Reininger, L., Goldring, D., Patterson, S., Quashie, N., Chakrabarti, D. and Meijer, L. (2011) *Plasmodium falciparum* NIMA-related kinase Pfnek-1: sex specificity and assessment of essentiality for the erythrocytic asexual cycle. Microbiology. **157**, 2785

97   Morahan, B. J., Abrie, C., Al-Hasani, K., Batty, M. B., Corey, V., Cowell, A. N., Niemand, J., Winzeler, E. A., Birkholtz, L.-M. and Doerig, C. (2020) Human Aurora kinase inhibitor Hesperadin reveals epistatic interaction between *Plasmodium falciparum* PfArk1 and PfNek1 kinases. Communications biology. **3**, 1-10

98   Reininger, L., Tewari, R., Fennell, C., Holland, Z., Goldring, D., Ranford-Cartwright, L., Billker, O. and Doerig, C. (2009) An essential role for the *Plasmodium* Nek-2 Nima-related protein kinase in the sexual development of malaria parasites. Journal of Biological Chemistry. **284**, 20858-20868

99   Reininger, L., Garcia, M., Tomlins, A., Müller, S. and Doerig, C. (2012) The *Plasmodium falciparum*, Nima-related kinase Pfnek-4: a marker for asexual parasites committed to sexual differentiation. Malaria journal. **11**, 1-11

100   Dorin, D., Le Roch, K., Sallicandro, P., Alano, P., Parzy, D., Poullet, P., Meijer, L. and Doerig, C. (2001) Pfnek-1, a NIMA-related kinase from the human malaria parasite *Plasmodium* falciparum: Biochemical properties and possible involvement in MAPK regulation. European journal of Biochemistry. **268**, 2600-2608

101   Reininger, L., Billker, O., Tewari, R., Mukhopadhyay, A., Fennell, C., Dorin-Semblat, D., Doerig, C., Goldring, D., Harmse, L. and Ranford-Cartwright, L. (2005) A NIMA-related protein kinase is essential for completion of the sexual cycle of malaria parasites. Journal of Biological Chemistry. **280**, 31957-31964

102   Read, M., Sherwin, T., Holloway, S., Gull, K. and Hyde, J. (1993) Microtubular organization visualized by immunofluorescence microscopy during erythrocytic schizogony in *Plasmodium falciparum* and investigation of post-translational modifications of parasite tubulin. Parasitology. **106**, 223-232

103   Jones, M. L., Das, S., Belda, H., Collins, C. R., Blackman, M. J. and Treeck, M. (2016) A versatile strategy for rapid conditional genome engineering using loxP sites in a small synthetic intron in *Plasmodium* falciparum. Scientific reports. **6**, 1-9

104   Ganesan, S. M., Falla, A., Goldfless, S. J., Nasamu, A. S. and Niles, J. C. (2016) Synthetic RNA–protein modules integrated with native translation mechanisms to control gene expression in malaria parasites. Nature communications. **7**, 1-10

105   de Koning-Ward, T. F., Gilson, P. R. and Crabb, B. S. (2015) Advances in molecular genetic systems in malaria. Nature Reviews Microbiology. **13**, 373-387

106   Birnbaum, J., Flemming, S., Reichard, N., Soares, A. B., Mesén-Ramírez, P., Jonscher, E., Bergmann, B. and Spielmann, T. (2017) A genetic system to study *Plasmodium falciparum* protein function. Nature Methods. **14**, 450-456

107   Radfar, A., Méndez, D., Moneriz, C., Linares, M., Marín-García, P., Puyet, A., Diez, A. and Bautista, J. M. (2009) Synchronous culture of *Plasmodium falciparum* at high parasitemia levels. Nature protocols. **4**, 1899

108   Lambros, C. and Vanderberg, J. P. (1979) Synchronization of *Plasmodium falciparum* erythrocytic stages in culture. The Journal of parasitology, 418-420

109   Rug, M. and Maier, A. G. (2013) Transfection of *Plasmodium* falciparum. Methods Mol Biol. **923**, 75-98

110   Birkholtz, L.-M., Blatch, G., Coetzer, T. L., Hoppe, H. C., Human, E., Morris, E. J., Ngcete, Z., Oldfield, L., Roth, R. and Shonhai, A. (2008) Heterologous expression of plasmodial proteins for structural studies and functional annotation. Malaria journal. **7**, 1-20

111   Bolanos-Garcia, V. M. and Blundell, T. L. (2011) BUB1 and BUBR1: multifaceted kinases of the cell cycle. Trends in biochemical sciences. **36**, 141-150

112   Choi, C. H., Hiromura, M. and Usheva, A. (2003) Transcription factor IIB acetylates itself to regulate transcription. Nature. **424**, 965-969

113   Classon, M. and Harlow, E. (2002) The retinoblastoma tumour suppressor in development and cancer. Nature Reviews Cancer. **2**, 910-917

114   Saini, E., Zeeshan, M., Brady, D., Pandey, R., Kaiser, G., Koreny, L., Kumar, P., Thakur, V., Tatiya, S., Katris, N. J., Limenitakis, R. S., Kaur, I., Green, J. L., Bottrill, A. R., Guttery, D. S., Waller, R. F., Heussler, V., Holder, A. A., Mohmmed, A., Malhotra, P. and Tewari, R. (2017) Photosensitized INA-Labelled protein 1 (PhIL1) is novel component of the inner membrane complex and is required for *Plasmodium* parasite development. Scientific Reports. **7**, 15577

115   Parkyn Schneider, M., Liu, B., Glock, P., Suttie, A., McHugh, E., Andrew, D., Batinovic, S., Williamson, N., Hanssen, E. and McMillan, P. (2017) Disrupting assembly of the inner membrane complex blocks *Plasmodium falciparum* sexual stage development. PLoS pathogens. **13**, e1006659

116   Lenne, A., De Witte, C., Tellier, G., Hollin, T., Aliouat, E. M., Martoriati, A., Cailliau, K., Saliou, J.-M., Khalife, J. and Pierrot, C. (2018) Characterization of a Protein Phosphatase Type-1 and a Kinase Anchoring Protein in *Plasmodium* falciparum. Frontiers in Microbiology. **9**

117   Fang, H., Klages, N., Baechler, B., Hillner, E., Yu, L., Pardo, M., Choudhary, J. and Brochet, M. (2017) Multiple short windows of calcium-dependent protein kinase 4 activity coordinate distinct cell cycle events during *Plasmodium* gametogenesis. Elife. **6**, e26524

118   Arredondo, S. A. and Kappe, S. H. (2017) The s48/45 six-cysteine proteins: mediators of interaction throughout the *Plasmodium* life cycle. International journal for parasitology. **47**, 409-423

119   Painter, H. J., Campbell, T. L. and Llinás, M. (2011) The Apicomplexan AP2 family: integral factors regulating *Plasmodium* development. Molecular and biochemical parasitology. **176**, 1-7

120   Samarsky, D. A. and Fournier, M. J. (1998) Functional Mapping of the U3 Small Nucleolar RNA from the Yeast *Saccharomyces cerevisiae*. Molecular and Cellular Biology. **18**, 3431-3444

121   Dai, M.-S., Zeng, S. X., Jin, Y., Sun, X.-X., David, L. and Lu, H. (2004) Ribosomal protein L23 activates p53 by inhibiting MDM2 function in response to ribosomal perturbation but not to translation inhibition. Molecular and cellular biology. **24**, 7654-7668

122   Rabie, T. (2021) Genetic manipulation of histone deacetylases SAP18 and SIR2A in *Plasmodium* falciparum. In Biochemistry (BGM) ed.)^eds.). p. 104, University of Pretoria

123   Wichers, J. S., Scholz, J. A., Strauss, J., Witt, S., Lill, A., Ehnold, L.-I., Neupert, N., Liffner, B., Lühken, R. and Petter, M. (2019) Dissecting the gene expression, localization, membrane topology, and function of the *Plasmodium falciparum* STEVOR Protein Family. MBio. **10**, e01500-01519

124   Graeser, R., Wernli, B., Franklin, R. M. and Kappes, B. (1996) *Plasmodium falciparum* protein kinase 5 and the malarial nuclear division cycles. Molecular and biochemical parasitology. **82**, 37-49

125   Yang, J. and Kornbluth, S. (1999) All aboard the cyclin train: subcellular trafficking of cyclins and their CDK partners. Trends in cell biology. **9**, 207-210

126   Taylor, S. S., Hussein, D., Wang, Y., Elderkin, S. and Morrow, C. J. (2001) Kinetochore localisation and phosphorylation of the mitotic checkpoint components Bub1 and BubR1 are differentially regulated by spindle events in human cells. Journal of cell science. **114**, 4385-4395

127   Gubbels, M.-J., White, M. and Szatanek, T. (2008) The cell cycle and Toxoplasma gondii cell division: tightly knit or loosely stitched? International journal for parasitology. **38**, 1343-1358

128   Balestra, A. C., Zeeshan, M., Rea, E., Pasquarello, C., Brusini, L., Mourier, T., Subudhi, A. K., Klages, N., Arboit, P. and Pandey, R. (2020) A divergent cyclin/cyclin-dependent kinase complex controls the atypical replication of a malaria parasite during gametogony and transmission. Elife. **9**, e56474

129   Makkonen, M., Bertling, E., Chebotareva, N. A., Baum, J. and Lappalainen, P. (2013) Mammalian and malaria parasite cyclase-associated proteins catalyze nucleotide exchange on G-actin through a conserved mechanism. Journal of biological chemistry. **288**, 984-994

130   Hliscs, M., Sattler, J. M., Tempel, W., Artz, J. D., Dong, A., Hui, R., Matuschewski, K. and Schüler, H. (2010) Structure and function of a G-actin sequestering protein with a vital role in malaria oocyst development inside the mosquito vector. Journal of Biological Chemistry. **285**, 11572-11583

131   Absalon, S., Blomqvist, K., Rudlaff, R. M., DeLano, T. J., Pollastri, M. P. and Dvorin, J. D. (2018) Calcium-dependent protein kinase 5 is required for release of egress-specific organelles in *Plasmodium* falciparum. MBio. **9**, e00130-00118

132   Soni, R., Sharma, D., Rai, P., Sharma, B. and Bhatt, T. K. (2017) Signaling strategies of malaria parasite for its survival, proliferation, and infection during erythrocytic stage. Frontiers in immunology. **8**, 349

133   Wilkinson, M. G. and Millar, J. B. (2000) Control of the eukaryotic cell cycle by MAP kinase signaling pathways. The FASEB Journal. **14**, 2147-2157

134   Foijer, F., Wolthuis, R. M., Doodeman, V., Medema, R. H. and te Riele, H. (2005) Mitogen requirement for cell cycle progression in the absence of pocket protein activity. Cancer cell. **8**, 455-466

135   Doerig, C., Endicott, J. and Chakrabarti, D. (2002) Cyclin-dependent kinase homologues of *Plasmodium* falciparum. International journal for parasitology. **32**, 1575-1585

136   Li, Z., Le Roch, K., Geyer, J. A., Woodard, C. L., Prigge, S. T., Koh, J., Doerig, C. and Waters, N. C. (2001) Influence of human p16INK4 and p21CIP1 on the in vitro activity of recombinant *Plasmodium falciparum* cyclin-dependent protein kinases. Biochemical and biophysical research communications. **288**, 1207-1211

137   Bernard, P., Hardwick, K. and Javerzat, J.-P. (1998) Fission yeast bub1 is a mitotic centromere protein essential for the spindle checkpoint and the preservation of correct ploidy through mitosis. The Journal of cell biology. **143**, 1775-1787

138   Wall, R. J., Ferguson, D. J., Freville, A., Franke-Fayard, B., Brady, D., Zeeshan, M., Bottrill, A. R., Wheatley, S., Fry, A. M. and Janse, C. J. (2018) *Plasmodium* APC3 mediates chromosome condensation and cytokinesis during atypical mitosis in male gametogenesis. Scientific reports. **8**, 1-10

Supplementary information

Figure S1 shows the entire agarose gels of Figure 3-15B in the main text. The clones shown in Figure-15B in the main text are indicated in red boxes.
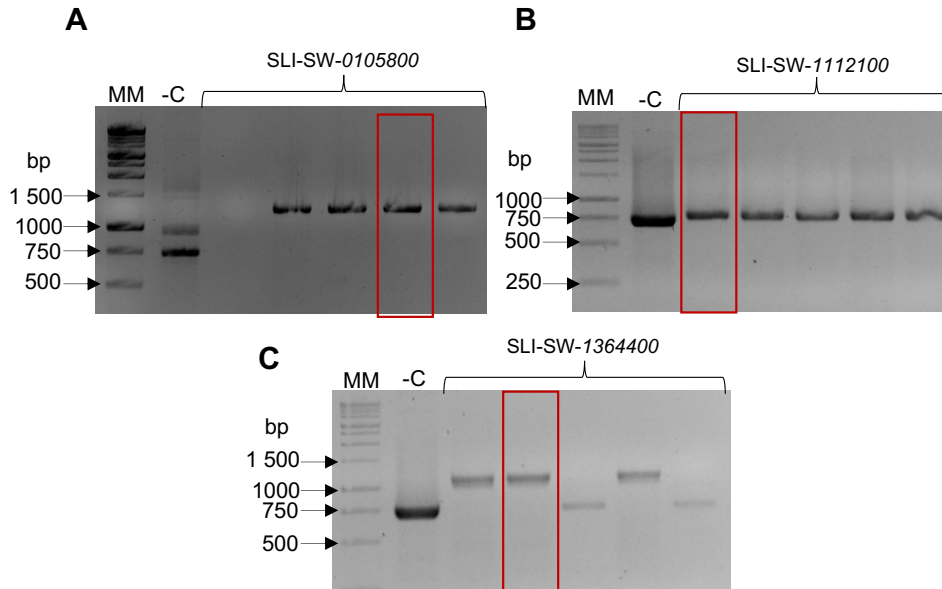

Figure S 1: Representative image of colony screening PCR for recombinant SLI-sandwich clones. DNA was analysed on 1.5 % (w/v) agarose gel post stained with EtBr (0.4 mg/ml). Molecular marker (MM): 1 kb ladder (Promega, USA). Negative control (-C) contains the amplification of the SLI-sandwich original insert (~740 bp) **(A)** Colony screening PCR for *pf3d7_0105800* SLI-sandwich clones Amplification of the *pf3d7_0105800* 3'-gene fragments of expected size, ~1200 bp. **(B)** Colony screening PCR for *pf3d7_1112100* SLI-sandwich clones. Amplification of the *pf3d7_1112100* 3'-gene fragments of expected size, ~770 bp. **(C)** Colony screening PCR for *pf3d7_1364400* SLI-sandwich clones. Amplification of the *pf3d7_1364400* 3'-gene fragments of expected size, ~1100 bp.

Figure S2 shows the entire agarose gels of Figure 3-15C in the main text. The clones shown in Figure 3-15C in the main text are indicated in red boxes.
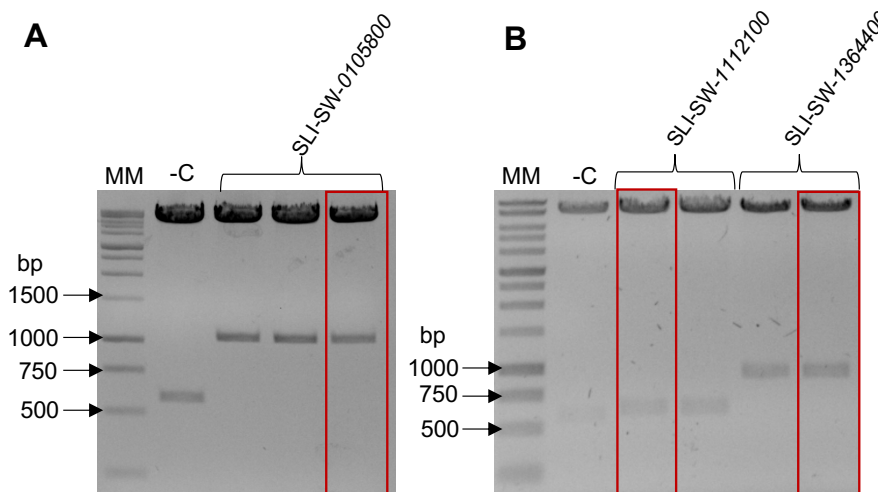

Figure S 2: Restriction enzyme digest of positive recombinant SLI-sandwich plasmids. Plasmid DNA (1 µg) was analysed on 1.5 % (w/v) agarose gel post stained with EtBr (0.4 mg/ml) after RE digestion for 3 h at 37 °C. Molecular marker (MM): 1 kb ladder (Promega, USA). Negative control (-C) contains the digested product of the original SLI-sandwich plasmid with the original insert (~600 bp). **(A)** Digested products of the recombinant plasmid DNA containing the 3'fragments of interest for *pf3d7_0105800* (~1050 bp). **(B)** Digested products of the recombinant plasmid DNA containing the 3'fragments of interest for *pf3d7_1112100* (~640 bp) and *pf3d7_1364400* (~940 bp) respectively.

Figure S4 shows the entire agarose gels of Figure 3-35C and Figure 3-36C in the main text respectively. The clones shown in Figure 3-35C and 3-36C in the main text are indicated in red boxes.
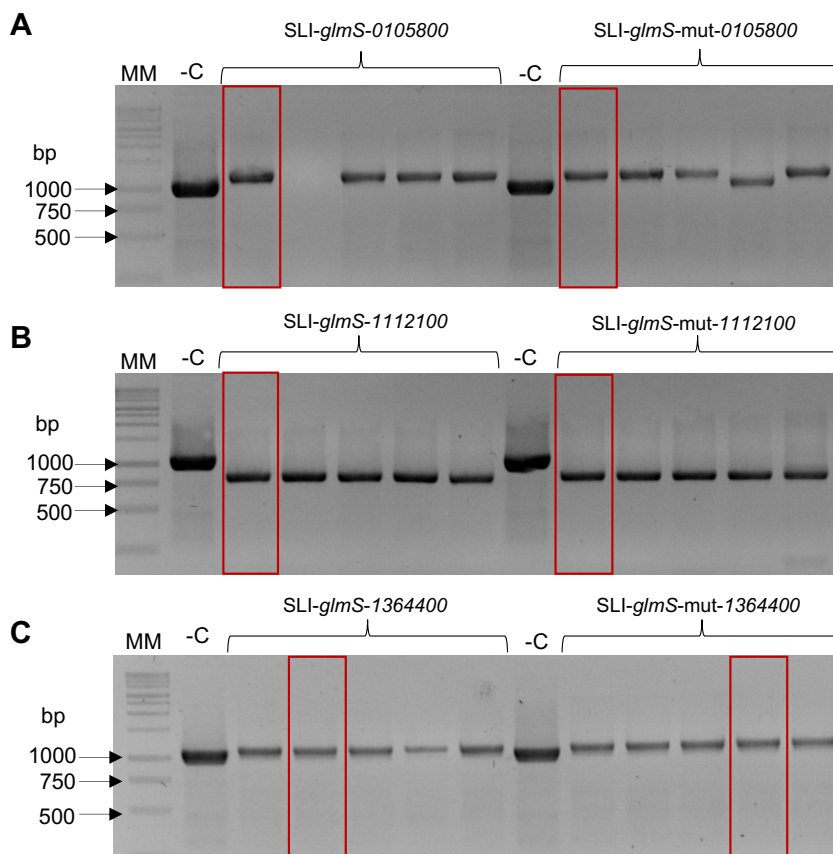

Figure S 3: Representative image of colony screening PCR for recombinant SLI-*glmS* and SLI-*glmS*-mut clones. DNA was analysed on 1.5 % (w/v) agarose gel post stained with EtBr (0.4 mg/ml). Molecular marker (MM): 1 kb ladder (Promega, USA). Negative control (-C) contains the amplification of the SLI-*glmS* and SLI-*glmS*-mut original insert (~1100 bp) **(A)** Colony screening PCR for *pf3d7_0105800* SLI-*glmS*/*glmS*-mut clones Amplification of the *pf3d7_010580* 3'-gene fragments of expected size, ~1200 bp. **(B)** Colony screening PCR for *pf3d7_1112100* SLI-*glmS*/*glmS*-mut clones. Amplification of the *pf3d7_1112100* 3'-gene fragments of expected size, ~770 bp. **(C)** Colony screening PCR for *pf3d7_1364400* SLI-*glmS*/*glmS*-mut clones. Amplification of the *pf3d7_1364400* 3'-gene fragments of expected size, ~1100 bp.

Figure S4 shows the entire agarose gels of Figure 3-35C and Figure 3-36C in the main text respectively. The clones shown in Figure 3-35C and 3-36C in the main text are indicated in red boxes.
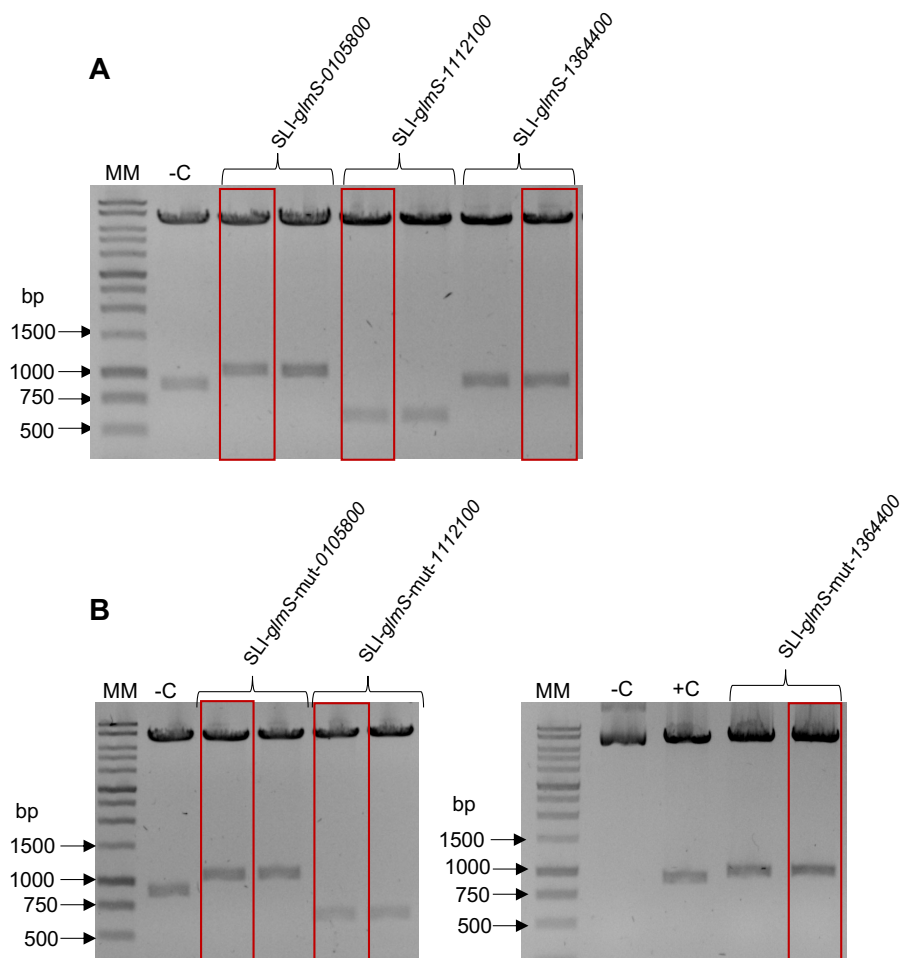

Figure S 4: Restriction enzyme digest of positive recombinant SLI-*glmS* and SLI-*glmS*-mut plasmids. Plasmid DNA (1 µg) was analysed on 1.5 % (w/v) agarose gel post stained with EtBr (0.4 mg/ml) after RE digestion for 3 h at 37 °C. Molecular marker (MM): 1 kb ladder (Promega, USA). Negative control (-C) contains the digested product of the original SLI-*glmS* and SLI-*glmS*-mut plasmid with the original insert (~870 bp). **(A)** Digested products of the recombinant SLI-*glmS* plasmid DNA containing the 3'fragments of interest for *pf3d7_0105800* (~1050 bp), *pf3d7_1112100* (~640 bp) and *pf3d7_1364400* (~940 bp) respectively. **(B)** Digested products of the recombinant SLI-*glmS*-mut plasmid DNA containing the 3'fragments of interest for *pf3d7_0105800* (~1050 bp), *pf3d7_1112100* (~640 bp) and *pf3d7_1364400* (~940 bp) respectively.

If you give up today...
You'll never know how far you could've gotten.